

A Unified Study of LoRA Variants: Taxonomy, Review, Codebase, and Empirical Evaluation

Haonan He^{1,2†}, Jingqi Ye^{1,2†}, Minglei Li^{1,3†}, Zhengbo Wang^{2,5}, Mengqi Li⁶,
Tao Chen³, Lei Bai¹, Peng Ye^{1,3,4*}

¹Shanghai Artificial Intelligence Laboratory, Shanghai 200233, China

²University of Science and Technology of China, Hefei 230026, China

³Fudan University, Shanghai 200433, China

⁴The Chinese University of Hong Kong, Hong Kong SAR 999077, China

⁵Institute of Automation, Chinese Academy of Sciences, Beijing 100190, China

⁶The Chinese University of Hong Kong, Shenzhen, Shenzhen 518172, China

Abstract—Low-Rank Adaptation (LoRA) is a fundamental parameter-efficient fine-tuning method that balances efficiency and performance in large-scale neural networks. However, the proliferation of LoRA variants has led to fragmentation in methodology, theory, code, and evaluation. To this end, this work presents the first unified study of LoRA variants, offering a systematic taxonomy, unified theoretical review, structured codebase, and standardized empirical assessment. First, we categorize LoRA variants along four principal axes: rank, optimization dynamics, initialization, and integration with Mixture-of-Experts. Then, we review their relationships and evolution within a common theoretical framework focused on low-rank update dynamics. Further, we introduce LoRAFactory, a modular codebase that implements variants through a unified interface, supporting plug-and-play experimentation and fine-grained analysis. Last, using this codebase, we conduct a large-scale evaluation across natural language generation, natural language understanding, and image classification tasks, systematically exploring key hyperparameters. Our results uncover several findings, notably: LoRA and its variants exhibit pronounced sensitivity to the choices of learning rate compared to other hyperparameters; moreover, with proper hyperparameter configurations, LoRA consistently matches or surpasses the performance of most of its variants. All code and configurations are publicly available at this link.

Index Terms—PEFT, LoRA, LLMs, Optimization.

I. INTRODUCTION

LARGE-SCALE models with billions of parameters, such as large language models (LLMs), which are pretrained on massive corpora, have demonstrated remarkable performance across diverse tasks, transforming fields ranging from natural language processing to multimodal reasoning [1]–[3]. However, full fine-tuning large-scale models is highly resource-intensive, primarily due to the substantial GPU memory required to store optimizer states. To alleviate this burden, numerous parameter-efficient fine-tuning (PEFT) methods have been proposed [4]–[8]. These approaches drastically reduce memory usage by either minimizing the number of trainable parameters or optimizing the management of optimizer states, especially for adaptive optimizers [9], [10]. Consequently, PEFT methods also enhance the training efficiency under distributed frameworks, such as ZeRO [11] and FSDP [12], by reducing communication overhead.

Low-Rank Adaptation (LoRA) [8] has emerged as one of the most widely adopted PEFT methods. Its popularity stems

from strong empirical performance, implementation simplicity, and broad generalization across domains, including parametric knowledge memory [13], [14], multimodal learning [15], [16], and federated learning [17], [18]. Despite its efficiency and effectiveness, such as fine-tuning 32B-scale models on a consumer-level GPU through quantization methods [19], [20], LoRA still exhibits limitations, such as the low-rank structure, which often results in a performance gap compared to full fine-tuning, particularly on complex downstream tasks.

To bridge this gap, numerous variants of LoRA have been developed, which can be broadly classified as follows: *Rank Adjustment Based Variants* (Section II-B) include methods such as RELORA [21], which composes multiple low-rank update subspaces; ADALORA [22], which dynamically masks less important ranks; and RANDLORA [23], which enables high-rank training via rank-sharing strategies. *Optimization Process Adjustment Based Variants* (Section II-C) cover approaches like LoRA+ [24], which decouples the learning rates of low-rank weights for optimization stability; LORA-PRO [25], which reduces the discrepancy with full fine-tuning via parameter update space alignment. *Initialization Adjustment Based Variants* (Section II-D) comprise techniques such as PiSSA [26], which applies Singular Value Decomposition (SVD) on pretrained weights to extract dominant features for initializing low-rank weights, and LORA-GA [27], which performs SVD on the gradients of pretrained weights for initialization. Lastly, *Mixture-of-Experts (MoE) Integration Based Variants* (Section II-E) combine LoRA with MoE mechanisms to enable adaptive parameter activation, as exemplified by MIXTURE-OF-LORAS [28], which distributes low-rank updates across multiple conditionally activated experts. Despite the rapid development, critical gaps remain in the field.

First, existing taxonomies in the general field of PEFT or LoRA outline broad and superficial organization, and thus fail to render a fine-grained and systematic framework focused on LoRA variants based on their principal operational axes. **Second**, there is a lack of an in-depth review. Surveys on LoRA do not provide a thorough review of the theoretical foundations, design principles, and operational mechanisms that distinguish LoRA variants. This limitation, combined with the mathematical sophistication of many proposals, impedes accessibility, especially for non-specialists. **Third**, code support is fragmented and unwieldy. While the popular PEFT library [29] provides a basic LoRA implementation with useful features (e.g., multi-LoRA serving), it supports only

† Equal contribution.

* Correspondence: yepeng@pjlab.org.cn.

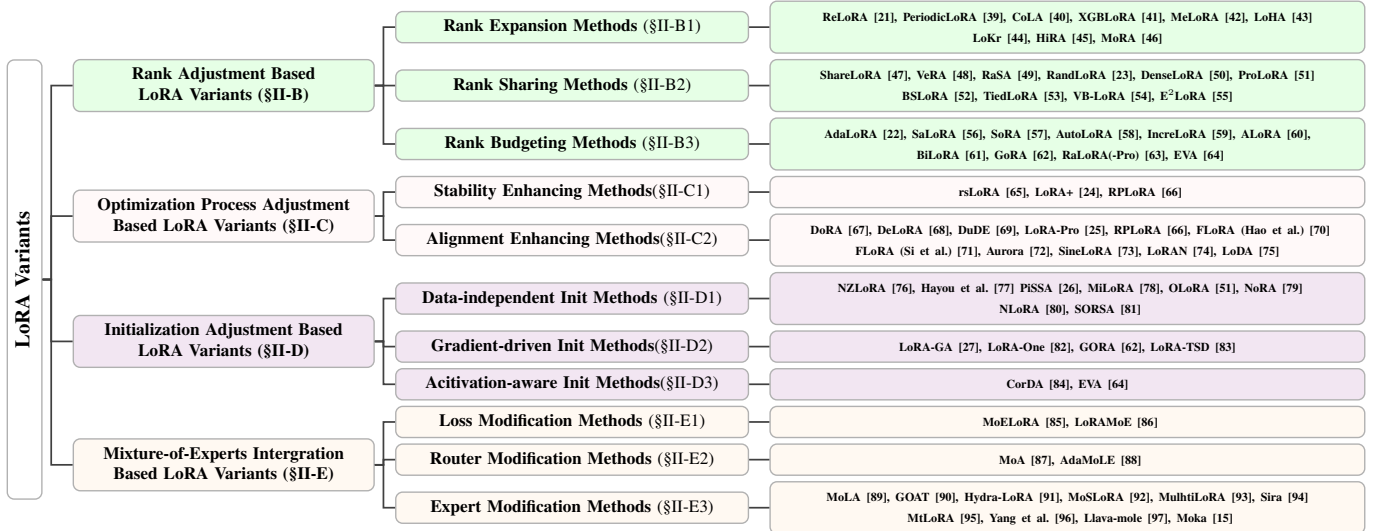


Fig. 1. Hierarchical taxonomy of LoRA variants based on four core principle operational axes.

a limited set of variants. Worse, its codebase has become cluttered with deeply nested logic and tight interdependencies, making it difficult to read and extend. **Fourth**, evaluations are inconsistent and limited in scope. The original LORA paper conducts the evaluation using models like ROBERTa [30] (GLUE [31]), GPT-2 [32] (E2E NLG [33]), and GPT-3 [34] (WikiSQL [35], MNLI [31], SAMSum [36]). Recent works now use large models such as LLaMA3 [37] and Qwen3 [38] for evaluation, creating a comparison gap. Moreover, evaluations remain largely confined to language tasks, despite the growing use of LORA in various domains.

To address these challenges, this work presents the **first** unified study of LORA variants: (1) We propose a structured and fine-grained taxonomy (Figure 1) focused on LORA variants according to their operational principles; (2) Building upon the taxonomy, we conduct an in-depth review in Section II grounded in a unified theoretical framework; (3) Further, we provide a clean, modular codebase detailed in Section III that implements variants as subclasses of a LORA base class, thereby significantly enhancing readability and extensibility; (4) Building on these infrastructures, we launch a large-scale empirical study across three domains: natural language generation, natural language understanding, and image classification, evaluating 20 representative variants that have been accepted in top AI/ML venues under extensive hyperparameter sweeping. We discover several important key findings as shown in Section IV, especially, LORA can match or outperform most of its variants with appropriate hyperparameter configurations. Our work provides a solid foundation for future research. The contributions are summarized as follows:

- 1) We formulate a structured taxonomy of LORA variants, providing a **fine-grained systematic framework** based on the principal operational axes of LORA variants.
- 2) We present a theoretical review of LORA variants, which establishes a **unified foundation** rooted in low-rank adaptation dynamics to promote understanding.
- 3) We introduce **LoRAFactory**, which implements over 50 LORA variants and functions beyond a toolkit by enabling standardized and extensible evaluations.

- 4) We conduct **large-scale evaluations** with over 3,000 experiments across 3 model architectures and 22 tasks, spanning natural language generation, natural language understanding, and image classification.
- 5) We uncover several **key findings**, with two being particularly noteworthy: (1) LORA and its variants are highly sensitive to the learning rate compared to other hyperparameters; (2) LORA can match or outperform its most variants with proper hyperparameter configurations.

II. REVIEW OF LORA AND ITS VARIANTS

In this section, we conduct a theoretical review; details of the notations we used can be found in the Appendix B.

A. Overview of LORA

1) Mechanism of LORA: LORA is grounded in the hypothesis that the updates to pretrained weights during fine-tuning possess *low intrinsic ranks*, aligning with observations that over-parameterized models often reside on a low intrinsic dimension [98]. Specifically, at each fine-tuning step t , for a pretrained weight matrix $\tilde{W} \in \mathbb{R}^{m \times n}$, LORA approximates the corresponding update ΔW_t using low-rank matrices $A_t \in \mathbb{R}^{m \times r}$ and $B_t \in \mathbb{R}^{r \times n}$, with $r \ll \min(m, n)$. Formally:

$$W_t = \tilde{W} + \Delta W_t = \tilde{W} + \frac{\alpha}{r} A_t B_t. \quad (1)$$

Here, the product $A_t B_t$ is normalized by the rank r and scaled by a hyperparameter α . This design ensures that the magnitude of ΔW_t depends primarily on α rather than the rank r , allowing for more controllable fine-tuning. However, empirical studies [99], [100] suggest setting α to $2r$, as a constant α may lead LoRA to converge to low-rank solutions even under large- r settings.

2) Comparison between LORA and Full Fine-tuning: LORA is fundamentally related to full fine-tuning, though still demonstrates differences in both optimization dynamics and final performance. Mathematically, the gradients of a low-rank adapter at the t -th step are expressed as:

$$\nabla A_t = \frac{\alpha}{r} \nabla \tilde{W}_t B_t^\top, \quad \nabla B_t = \frac{\alpha}{r} A_t^\top \nabla \tilde{W}_t. \quad (2)$$

As demonstrated in prior research [62], [70], under standard LORA initialization with either small learning rates or a frozen A matrix (as in LORA-FA [101], [102]), the update can be approximated, with exact simplification for frozen A or approximate simplification under small learning rates as:

$$\Delta W_t = A_t B_t = -\eta \frac{\alpha}{r} \sum_{i=0}^{t-1} A_0 A_0^\top \nabla \widetilde{W}_i. \quad (3)$$

Moreover, the step-wise update obtained from the low-rank adapter can be expressed as:

$$\begin{aligned} \Delta W_{t+1} - \Delta W_t &= (A_{t+1} - \eta \nabla A_t)(B_{t+1} - \eta \nabla B_t) - A_t B_t \\ &= -\eta A_t \nabla B_t - \eta \nabla A_t B_t + \eta^2 \nabla A_t \nabla B_t \\ &\approx -\frac{\eta \alpha}{r} (A_t A_t^\top \nabla \widetilde{W}_t + \nabla \widetilde{W}_t B_t^\top B_t), \end{aligned} \quad (4)$$

where the approximation holds under the assumption of a small learning rate, such that the $\mathcal{O}(\eta^2)$ term is negligible.

Eqs. (3)-(4) uncover the relationship between LORA adapters and the gradients of pretrained weights. Especially, Eq. (3) reveals that a LORA adapter essentially functions as a gradient compressor, which first compresses the gradient of the corresponding pretrained weight through A^\top , and then decompresses it via A .

Despite the connection, LoRA differs in its optimization dynamics, final performance, and applicable use cases. Ghosh et al. [103] empirically show that during instruction tuning, models fine-tuned with LORA retain closer alignment with the pretrained knowledge, whereas full fine-tuning tends to fit the instruction data closer. Specifically, LORA results in a reduced token-level distribution shift compared to full fine-tuning. It learns localized adaptations, such as sentence initiation, leading to a more concentrated distribution shift. As further validated by Biderman et al. [99] and Shuttleworth et al. [100], LoRA better mitigates catastrophic forgetting [104]. Additionally, Biderman et al. [99], and Schulman et al. [105] find that LORA is more sensitive to hyperparameters than full fine-tuning, especially to the learning rate.

3) *Advantages of LORA*: LORA’s primary benefit lies in its ability to significantly reduce the memory footprint of optimizer states—particularly in mixed-precision training, where stateful optimizers [9], [10], [106] require storing states in 32-bit precision. Contrary to popular belief, LORA introduces additional FLOPs in both training and inference (without merging). This overhead is especially noticeable in single-GPU and non-offload setups. However, in distributed training settings, LORA can reduce communication costs between devices and nodes, especially for optimizer offloading strategies such as ZERO-OFFLOAD [107] and data parallelism strategies such as ZERO [11] and FSDP [12], leading to faster overall training processes.

B. Rank Adjustment Based LORA Variants

Vanilla LORA applies a uniform small rank to all adapters for simplicity, though this design can hinder both expressiveness and parameter efficiency. Since different modules and layers contribute unevenly to downstream performance, a fixed small-rank allocation can be inherently suboptimal.

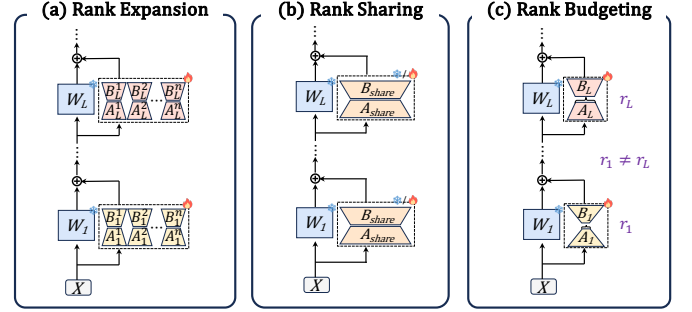


Fig. 2. Illustration of rank adjustment based LoRA variants.

As shown in Figure 2, recent research investigates three approaches: (a) Rank Expansion Methods, which composite low-rank matrices through linear algebraic principles; (b) Rank Sharing Methods, which share low-rank parameters across adapters to enable larger rank configurations; (c) Rank Budgeting Methods, which dynamically allocate rank across modules during or before training.

1) *Rank Expansion Methods*: Rank expansion methods share a common objective: to preserve the parameter efficiency (not equal to computational efficiency) of LORA while expanding the effective ranks. At their core, several well-known rank inequalities and identities from linear algebra provide theoretical justification for their effectiveness. These include:

$$\mathcal{R}(M_1 + M_2) \leq \mathcal{R}(M_1) + \mathcal{R}(M_2), \quad (5)$$

$$\mathcal{R}(M_1 \odot M_2) \leq \mathcal{R}(M_1) \cdot \mathcal{R}(M_2), \quad (6)$$

$$\mathcal{R}(M_1 \otimes M_2) = \mathcal{R}(M_1) \cdot \mathcal{R}(M_2), \quad (7)$$

$$\mathcal{R}(M_1 M_2) \leq \min(\mathcal{R}(M_1), \mathcal{R}(M_2)), \quad (8)$$

$$\max(\mathcal{R}(M_1), \mathcal{R}(M_2)) \leq \mathcal{R}([M_1 | M_2]) \quad (9)$$

$$\mathcal{R}([M_1 | M_2]) \leq \mathcal{R}(M_1) + \mathcal{R}(M_2), \quad (10)$$

$$\mathcal{R}\left(\bigoplus_{i=0}^{k-1} M_i\right) = \sum_{i=1}^n \mathcal{R}(M_i), \quad (11)$$

where $\mathcal{R}(M)$ denotes the rank of matrix M , \odot the Hadamard product, \otimes the Kronecker product, and \bigoplus represents block-diagonal concatenation. These guide the construction of composite structures, enabling richer representations without a proportional increase in trainable parameters.

Inspired by Eq. (5), **RELORA** [21] introduces a *merge-and-reinit* strategy to construct higher-rank updates by accumulating low-rank subspaces.

Training is divided into N phases, each consisting of T steps. At step t , the current phase index is defined as $\tau = \lfloor (t-1)/T \rfloor + 1$. Let $t_\tau := \tau T$ denote the final step of phase τ , with $t_0 := 0$. At the end of phase τ , the low-rank update is merged into the base weight:

$$W_{t_\tau} = \begin{cases} \widetilde{W}, & \tau = 0, \\ W_{t_{\tau-1}} + \frac{\alpha}{r} A_{t_\tau} B_{t_\tau}, & \tau = 1, 2, \dots, N, \end{cases} \quad (12)$$

Within phase τ (i.e., for $t_{\tau-1} < t \leq t_\tau$), the model weight is:

$$W_t = W_{t_{\tau-1}} + \frac{\alpha}{r} A_t B_t. \quad (13)$$

After merging, low-rank matrices are reinitialized, and their optimizer states are reset, enabling the exploration of a new

low-rank subspace. To mitigate instability from optimizer resets, a jagged learning rate schedule, which re-warmups the learning rate from zero at the next phase, is adopted.

PERIODICLORA [39] implements a method similar to RELORA but introduces a momentum-based merging mechanism to enhance training stability. Additionally, **COLA** [40] also proposes a similar approach with a motivation from the Frank Wolfe algorithm [108]. Moreover, the *merge-and-reinit* method can also be viewed as a gradient boosting (GB) method. From this perspective, Zhang et al. [41] draw inspiration from GB algorithms such as GBDT [109], proposing **XGBLORA**, which randomly selects 2 layers to be trained by rank-one adapters at each *merge-and-reinit* phase.

However, the method of RELORA lacks a lower bound of effective rank. Furthermore, as the *merge-and-reinit* process directly modifies the pretrained weights, these weights must be saved after training, leading to substantial storage requirements compared to LORA. To address these issues, **MELORA** [42] draws inspiration from Eq. (11). Specifically, it partitions both A_t and B_t into k mini blocks and stacks them along the diagonal to form the overall update:

$$\Delta W_t = \left(\bigoplus_{i=1}^k A_t^i \right) \left(\bigoplus_{i=1}^k B_t^i \right), \quad (14)$$

$$A_t^i \in \mathbb{R}^{\frac{m}{k} \times r'}, \quad B_t^i \in \mathbb{R}^{r' \times \frac{n}{k}}. \quad (15)$$

This construction ensures that the effective rank is equal to kr' . When $r' = r$, MELORA increases the rank from r to kr without increasing the trainable parameter count. Conversely, when $r' = \frac{r}{k}$, MELORA reduces the trainable parameter count by a factor of k , while preserving the rank of r .

Hyeon-Woo et al. [43] draw inspiration from the Hadamard product to enhance the expressiveness of LORA, proposing **FEDPARA** (also known as **LOHA** [44]). Specifically, a LOHA adapter reparameterizes the update to a pretrained weight matrix via the Hadamard product of two low-rank matrix pairs: $A_t^1 \in \mathbb{R}^{m \times r}$, $A_t^2 \in \mathbb{R}^{m \times r}$ and $B_t^1 \in \mathbb{R}^{r \times n}$, $B_t^2 \in \mathbb{R}^{r \times n}$. The adaptation update can be formally expressed as:

$$\Delta W_t = \frac{\alpha}{r} (A_t^1 B_t^1 \odot A_t^2 B_t^2). \quad (16)$$

As shown in Eq. (6), LOHA enables an upper effective rank bound of r^2 , while only doubling the trainable parameter count compared to LORA with the same hyperparameter r .

To approximate even higher-rank updates, **HIRA** [45] constructs the update to a pretrained weight via the Hadamard product between the pretrained weight and the low-rank update. This update is formally expressed as:

$$\Delta W_t = \widetilde{W} \odot \frac{\alpha}{r} A_t B_t. \quad (17)$$

By leveraging the multiplicative interaction, HIRA allows potential high-rank update bounding by the product of the rank of the pretrained weight and the rank of the low-rank update.

Inspired by LOHA and **KRONA** [110], which employ Kronecker products for matrix decomposition, Yeh et al. [44] propose **LOKR**, which can be formally expressed as:

$$m_d = \max(u \leq \min(k, \sqrt{m}) | m \bmod u = 0), \quad (18)$$

$$n_d = \max(u \leq \min(k, \sqrt{n}) | n \bmod u = 0), \quad (19)$$

$$A_t \in \mathbb{R}^{m_d \times r}, \quad B_t \in \mathbb{R}^{r \times n_d}, \quad C_t \in \mathbb{R}^{m/m_d \times n/n_d}, \quad (20)$$

$$\Delta W_t = \frac{\alpha}{r} A_t B_t \otimes C_t, \quad (21)$$

where k is a hyperparameter. LOKR maintains comparable parameter counts to LORA while significantly increasing effective ranks.

2) *Rank Sharing Methods*: Parameter sharing is a widely adopted strategy for neural networks [111], [112]. Recently, it has also become prevalent for improving the parameter efficiency of LORA, as it allows for sharing low-rank weights across modules, thereby reducing the number of trainable parameters [47], [48], [54], [55]. For example, **VB-LORA** [54] implements an extreme parameter efficiency method using a shared vector bank strategy to composite low-rank matrices. In this paper, we focus on another function of parameter sharing, i.e., increasing the overall rank of adapters by sharing, and we refer to this as *rank sharing strategies*.

An intuitive parameter sharing strategy is to share the trainable low-rank matrices across all modules. Following this idea, **SHARELORA** [47] investigates the performance of sharing different components of the low-rank matrices, namely, matrix A , matrix B , or both, across modules. Empirical results show that sharing both A and B significantly reduces the trainable parameter count but incurs a noticeable performance drop. In contrast, sharing matrix A achieves performance on par with vanilla LORA while halving the trainable parameter count.

This observation suggests a practical strategy: by sharing matrix A and doubling the rank r , one can **potentially** surpass the performance of standard LORA with the same trainable parameter count. Formally, when both low-rank matrices A and B are shared across targeted modules, the update of a SHARELORA adapter is defined as:

$$A_t^S \in \mathbb{R}^{m_{\max} \times r}, \quad B_t^S \in \mathbb{R}^{r \times n_{\max}}, \quad (22)$$

$$\Delta W_t = \frac{\alpha}{r} A_t^S[:, m, :] B_t^S[:, :, n], \quad \Delta W_t \in \mathbb{R}^{m \times n}, \quad (23)$$

where A_t^S, B_t^S are shared low-rank matrices at step t , m_{\max} and n_{\max} denote the maximum input and output dimensions across all adapted modules.

Building upon shared low-rank matrices, **VERA** [48] proposes a vector-based fine-tuning approach. It shares and fixes randomly initialized low-rank matrices across modules, while introducing trainable scaling vectors to modulate the adaptation. This design is motivated by findings that tuning small, strategically chosen parts of randomly initialized models can yield surprisingly strong performance [113]–[115]. Formally, the adaptation in VERA is expressed as:

$$A^S \in \mathbb{R}^{m_{\max} \times r}, \quad B^S \in \mathbb{R}^{r \times n_{\max}}, \quad (24)$$

$$\Lambda_t^d \in \mathbb{R}^{r \times r}, \quad \Lambda_t^b \in \mathbb{R}^{n \times n}, \quad (25)$$

$$\Delta W_t = \frac{\alpha}{r} A^S[:, m, :] \Lambda_t^d B^S[:, :, n] \Lambda_t^b, \quad \Delta W_t \in \mathbb{R}^{m \times n}, \quad (26)$$

where Λ_t^d and Λ_t^b are diagonal matrices constructed at the t -th step from the trainable vectors $d_t \in \mathbb{R}^r$ and $b_t \in \mathbb{R}^n$.

TIED-LORA [53] further investigates the performance of freezing different parts of shared low-rank matrices and scaling

vectors upon the architecture of VERA. This vector-based formulation shifts the optimization focus to the scaling vectors, enabling a substantial increase in rank while maintaining a trainable parameter count smaller than that of vanilla LORA.

RASA [49] decomposes low-rank adaptation matrices into shared and module-specific (local) components. For a low-rank adapter of rank r , RASA allocates k ranks to be shared across all modules of the same type (e.g., query projection modules). Since these shared components have consistent shapes, no slicing operations are required during computation. The remaining $r - k$ ranks are kept specific to each module. In a model with L layers, the effective rank of each RASA adapter becomes $(r - k) + L \times k$, while the total number of trainable parameters remains identical to a LORA adapter of rank r . Formally, the update ΔW_t computed by a RASA adapter is given by:

$$\Delta W_t = [B_t^L \ B_t^S] D_t^L \begin{bmatrix} A_t^L \\ A_t^S \end{bmatrix}, \quad (27)$$

where A_t^L and B_t^L are the local low-rank weights, and D_t^L is a trainable diagonal scaling matrix.

Similar to RASA, **BSLORA** [52] decomposes low-rank adapters into three parts: *inter-layer shared parts*, *intra-layer shared parts*, and *local parts*. This stems from an entropy-based analysis [116] on fine-tuned low-rank adapters, revealing high similarity of adapters within and between adjacent layers, indicating redundancy and sharing potential. Formally, the update ΔW_t of BSLORA is:

$$\Delta W_t = 2 \times (A_t^L B_t^L + \mathcal{T}(A_t^{S_1} B_t^{S_1}) + \mathcal{T}(A_t^{S_2} B_t^{S_2})), \quad (28)$$

where $\mathcal{T}(\cdot)$ enables shape-flexible parameter sharing, and 2 is a fixed scaling factor (adopted in the official implementation). Here, $A_t^{S_1}, B_t^{S_1}$ are shared within a layer, and $A_t^{S_2}, B_t^{S_2}$ are shared across layers. As slicing (Eq. (23)) requires shared weights to be initialized at the maximum module dimension, BSLORA introduces two compact transformations $\mathcal{T}(AB)$ as:

$$\mathcal{T}_g(AB) = G_{id} G_{od} A B G_{od} G_{ou}, \quad AB \in \mathbb{R}^{k \times d}, \quad (29)$$

$$\mathcal{T}_k(AB) = (K_A \otimes A)(K_B \otimes B), \quad (30)$$

where $G_{id} \in \mathbb{R}^{1 \times k}$, $G_{od} \in \mathbb{R}^{d \times 1}$, $G_{iu} \in \mathbb{R}^{m \times 1}$, $G_{ou} \in \mathbb{R}^{1 \times n}$ are gating matrices, and $K_A \in \mathbb{R}^{m/k \times 1}$, $K_B \in \mathbb{R}^{1 \times n/d}$ are Kronecker kernels. These allow shared weights of an arbitrary size $k \times d$ to be efficiently transformed to target dimensions $m \times n$, enabling flexible, efficient, and adaptive sharing.

RANDLORA [23] performs full-rank weight updates by decomposing a weight update $\Delta W_t \in \mathbb{R}^{m \times n}$ into a sum of products involving shared, fixed, randomly initialized low-rank bases and trainable scaling coefficients:

$$n_b = \lceil \min(d_s, U) / r \rceil, \quad (31)$$

$$\Delta W_t = \frac{2}{\sqrt{n_b}} \sum_{i=1}^{n_b} \Gamma_t^i A_t^S[:, m, :] \Lambda_t^i B_t^{S_i}[:, n], \quad (32)$$

where d_s denotes the smaller dimension of the module with the largest output dimension among all target modules. (adopted in the PEFT implementation), U is an additional hyperparameter introduced in LoRAFactory to balance computational

efficiency of RANDLORA, and $\frac{2}{\sqrt{n_b}}$ is a scaling factor. Here, $A_t^S \in \mathbb{R}^{\min(d, k) \times r}$ and $B_t^{S_i} \in \mathbb{R}^{r \times \max(d, k)}$ are shared random basis matrices (A_t^S is further shared across random bases), and $\Gamma_t^i \in \mathbb{R}^{m \times m}$, $\Lambda_t^i \in \mathbb{R}^{r \times r}$ are module-specific trainable scaling coefficients. For compatibility between adapted layers with distinct input and output dimensions and the fixed random bases, RANDLORA swaps A_t^S and $B_t^{S_i}$ with $B_t^{S_i \top}$ and $A_t^S \top$ when the largest dimension of an adapted module is not its output dimension.

DENSELORA [50] proposes a strategy that additionally refines the low-rank hidden states rather than only fine-tuning the low-rank weights. Specifically, DENSELORA shares low-rank weights A_t^S and B_t^S across modules of the same type and introduces an intermediate module-specific trainable matrix $C_t \in \mathbb{R}^{r \times r}$ to refine the hidden states. Formally, the adaptation form of DENSELORA can be expressed as:

$$\Delta W_t = \frac{\alpha}{r} A_t^S C_t B_t^S. \quad (33)$$

By sharing low-rank matrices, DenseLoRA sharply reduces the trainable parameters, enabling high-rank configurations with smaller or comparable parameter counts compared with LoRA.

The aforementioned sharing-based methods share ranks across modules. In contrast, **PROLORA** [51] shares ranks intra low-rank matrices. The computation of a PROLORA adapter can be expressed as:

$$\Delta W_t = A_t B_t = [A_t^L \ | \ A_t^{S_1} \ | \ \dots \ | \ A_t^{S_{P-1}}] [B_t^L \ | \ B_t^{S_1} \ | \ \dots \ | \ B_t^{S_{P-1}}]^\top, \quad (34)$$

where A_t^L, B_t^L are local (rank-specific) low-rank matrices, and $A_t^{S_i}, B_t^{S_i}$ are components obtained by applying a row-wise cyclic shift to a shared base matrix: $A_t^{S_i} = \text{Roll}(A_t^{S_0}, i \cdot \delta_A)$, $B_t^{S_i} = \text{Roll}(B_t^{S_0}, i \cdot \delta_B)$. Here, δ_A and δ_B are the **strides** that control the shift offset. This share and shift strategy allows parameters to be reused between ranks, enabling a larger effective rank.

3) *Rank Budgeting Methods*: As we mentioned before, LORA neglects different modules contribute unequally to task-specific adaptation [22], [117]–[119]. Allocating overmuch ranks to less critical modules may waste parameter budgets and potentially lead to overfitting, while assigning insufficient ranks to pivotal modules could constrain their ability to learn task-specific information. Consequently, the core challenge of such methods lies in intelligently and adaptively allocating the ranks of low-rank adapters with a predefined budget.

To facilitate masking ranks to a budget, **ADALORA** [22] parameterizes a low-rank adapter as $\Delta W_t = A_t D_t B_t^\top$, factorized form analogous to truncated SVD, where $A_t \in \mathbb{R}^{m \times r}$ and $B_t \in \mathbb{R}^{n \times r}$ are matrices containing vectors simulating singular vectors, and $D_t \in \mathbb{R}^{r \times r}$ is a diagonal matrix containing values simulating singular values. To simulate the orthogonality of SVD during training, an auxiliary regularization term \mathcal{L}_{reg} is added to the training loss with a hyperparameter λ :

$$R_{\text{orth}}(A, B) = \|A^\top A - I\|_{\text{F}}^2 + \|B^\top B - I\|_{\text{F}}^2, \quad (35)$$

$$\mathcal{L}_{\text{reg}} = \lambda \cdot \sum_{i=1}^k R_{\text{orth}}(A_t^i, B_t^i) \quad (36)$$

where k is the number of ADALORA adapters in the model.

ADALORA incorporates an importance scoring mechanism to mask less critical ranks. At each training step t , the i -th diagonal value of D_t is masked to zero or retained after each backpropagation update, according to the importance score S_t^i of the i -th triplet of the adapter, comprising the i -th columns $a_t^i \in \mathbb{R}^m$ and $b_t^i \in \mathbb{R}^n$ of A_t and B_t , and the i -th diagonal value d_t^i of D_t , as follows:

$$d_t^i \leftarrow m_t^i \cdot d_t^i, \quad \text{where } m_t^i = \begin{cases} 1 & \text{if } S_t^i \geq \theta_t, \\ 0 & \text{otherwise.} \end{cases} \quad (37)$$

Here, the threshold θ_t is set to the b_t -th largest value of importance scores of all triplets in the model, such that exactly b_t singular values remain masked. The budget b_t , which controls the number of active singular values at each step t , follows a piecewise schedule across T total steps:

$$b_t = \begin{cases} b_0, & 0 \leq t < t_i, \\ b_t^{\text{anneal}}, & t_i \leq t < T - t_f, \\ b_T, & \text{otherwise,} \end{cases} \quad (38)$$

where b_0 and b_T are the initial and final budgets, respectively. During the annealing phase, b_t^{anneal} decreases cubically from b_0 to b_T over the interval $[t_i, T - t_f]$, following:

$$b_t^{\text{anneal}} = b_T + (b_0 - b_T) \left(1 - \frac{t - t_i}{T - t_i - t_f} \right)^3. \quad (39)$$

One of the metrics for accurately estimating importance scores is a sensitivity measurement, defined below to capture the influence of parameter w on the loss across update steps:

$$I(w) = |w \cdot g|, \quad (40)$$

$$\bar{I}_t(w) = \beta_1 \bar{I}_{t-1}(w) + (1 - \beta_1) I_t(w), \quad (41)$$

$$\bar{U}_t = \beta_2 \bar{U}_{t-1}(w) + (1 - \beta_2) |I(w) - \bar{I}_{t-1}(w)|, \quad (42)$$

$$s_t(w) = \bar{I}_t(w) \cdot \bar{U}_t(w), \quad (43)$$

where g is the gradient of w , β_1 and β_2 are hyperparameters that are smaller than 1. The importance score of ADALORA is therefore defined as:

$$S_t^i = s_t(d_t^i) + \frac{1}{m} \sum_{j=1}^m s_t(a_t^{ij}) + \frac{1}{n} \sum_{j=1}^n s_t(b_t^{ij}) \quad (44)$$

These designs enable ADALORA to adaptively allocate representational capacity during training, pruning less informative directions while preserving those critical for performance.

However, due to the masking mechanism, ADALORA initializes low-rank adapters with a uniform initial rank slightly larger than the final average rank (e.g., 1.5 times), leading to parameter redundancy, and the maximum rank of each adapter is bounded by the initial rank, limiting the model's capacity to expand its representational budget. To address this issue, **INCRELORA** [59] adopts an incremental rank allocation strategy. It first views the parameterization $A_t D_t B_t^\top$ with the sum of the product of rank-one components a, b , and d :

$$\Delta W_t = A_t D_t B_t^\top = \sum_{i=1}^r d_t^i \cdot a_t^i b_t^{i\top}. \quad (45)$$

During fine-tuning, additional rank-one components with randomly initialized a, b (d will be initialized with a small value) are allocated every t_n steps to the top- h most important modules at that interval. Both h and t_n are hyperparameters. A separate learning rate warmup and decay schedule is applied for newly added rank-one components. As a result, the ranks of modules with high importance are incrementally increased at every t_n steps until the total rank budget is exhausted. The importance score used by INCRELORA adopts the same smoothing strategy as ADALORA; the raw (unsmoothed) module-wise importance is computed by averaging all sensitivity scores in the corresponding update matrix. The orthogonality regularization (Eq. 36) is also applied by INCRELORA.

SALORA [56] extends ADALORA with a distinct masking strategy that formulates rank budgeting as an optimizable objective via L_0 regularization on simulated singular values. This is achieved through two techniques: (1) a differentiable surrogate R_{L_0} approximating the non-differentiable L_0 norm, and (2) Lagrangian relaxation to embed the rank budget constraint b into the loss for automatic budget control.

SALORA maps the diagonal entries of matrix D to $[0, 1]$ using a Hard-Concrete (HC) distribution with $u \sim \mathcal{U}(0, 1)$:

$$\tilde{d}_t^i = \sigma \left(\frac{\log \left(\frac{u}{1-u} \right) + \log(d_t^i)}{\tau} \right) \cdot (\zeta - \gamma) + \gamma, \quad (46)$$

$$\Delta W_t = \sum_{i=1}^r \min(1, \max(0, \tilde{d}_t^i)) \cdot a_t^i b_t^{i\top}, \quad (47)$$

where σ is the sigmoid function, τ is its temperature, and $\gamma < 0, \zeta > 1$ are HC hyperparameters that push most values outside $[0, 1]$ toward $(-\infty, 0)$ or $(1, \infty)$. The surrogate R_{L_0} has a closed-form expression based on the HC distribution:

$$R_{L_0}(D) = \mathbb{P}(\tilde{d}_t^i > 0) = \sum_{i=1}^r \sigma \left(\log(d_i) - \tau \log \left(\frac{-\gamma}{\zeta} \right) \right). \quad (48)$$

Given a target rank budget b , **SALORA** combines R_{L_0} with orthogonality regularization R_{orth} in Eq. 35 via Lagrangian relaxation, yielding the following regulation loss with hyperparameters λ and β :

$$\mathcal{L}_{\text{reg}} = \lambda \cdot \sum_{i=1}^k R_{\text{orth}}(A_t^i, B_t^i) + \beta \cdot \left(\frac{1}{r} \sum_{i=1}^k R_{L_0}(D_t^i) - b \right)^2. \quad (49)$$

ALORA [60] introduces a rank reallocation strategy based on a train-evaluate-reallocate-retrain loop. At its core lies Ablation-based LoRA (AB-LORA), an importance estimation method designed to guide rank reallocation. For a given rank component r_i , its importance score is computed as:

$$\text{IS}(r_i) = S(M) - S(M_{\setminus r_i}) + S(M_{r_i}), \quad (50)$$

where $S(M)$ denotes the performance of the fully fine-tuned model, $S(M_{\setminus r_i})$ is the performance after removing the component with rank r_i , and $S(M_{r_i})$ is the performance of the model when only rank r_i is retained. Based on these scores, the least important ranks are removed from their respective modules and reallocated to more critical ones. The model is then further fine-tuned to adapt to the updated rank configuration.

The core idea of **GOR**A [62] is to perform a one-off gradient computation on a small subset of training data before training, jointly achieving adaptive rank allocation and gradient-driven weight initialization (detailed in Section II-D2). By initializing low-rank matrices with allocated ranks, GORA adaptively assigns more parameters to modules that have a greater impact on final performance, avoiding parameter redundancy and maintaining training stability. Specifically, GORA first measures the advantage of each weight on k pretrained weights to be adapted $\{\widetilde{W}_i\}_{i=0}^k$ with corresponding gradients $\{G_i\}_{i=0}^k$ based on loss sensitivity:

$$I_i = \text{avg}(|\widetilde{W}_i \odot G_i|), \quad \alpha_i = \frac{I_i}{\sum_{i=1}^k I_i}. \quad (51)$$

The rank for the i -th low-rank adapter is determined by:

$$P_{\text{total}} = \sum_{i=1}^k (m_i + n_i) \cdot r_{\text{ref}} \quad (52)$$

$$r_i = \text{round}\left(\frac{P_{\text{total}} \cdot \alpha_i}{\sqrt{m_i + n_i}}\right), \quad \text{s.t. } r_{\min} \leq r_i \leq r_{\max}, \quad (53)$$

Where $\text{round}(\cdot)$ denotes rounding to the nearest integer, and r_{ref} is a reference rank to control the parameter budget, and r_{\min}, r_{\max} are predefined bounds of rank allocation.

Building upon the framework of GORA, **RALORA(-PRO)** [63] further introduces an entropy-based effective rank estimator to measure the intrinsic dimensionality of gradient matrices $\{G_i\}_{i=0}^k$:

$$\text{erank}(G_i) = \exp\left(-\sum_{i=1}^n p_i \log p_i\right), \quad p_i = \frac{\sigma_i}{\sum_{j=1}^n \sigma_j}, \quad (54)$$

where p_i denotes the normalized singular value distribution. The core insight of RALORA(-PRO) is revealing the substantial gap between the fixed small rank of the low-rank adapter (typically 8) and the gradient's intrinsic dimensionality (GID), which can be up to 300. Building on this observation, using the block-diagonal structure in Eq. (14), RaLoRA aligns each low-rank adapter's effective rank to the corresponding GID by adaptively increasing the number of diagonal blocks without increasing the total parameter count. RaLoRA-Pro further incorporates the parameter allocation strategy of GORA, achieving dual adaptive alignment at both intra-layer and inter-layer levels with a manual parameter budget.

EVA [64] performs incremental SVD on downstream activation vectors and selects the top- r right singular vectors to initialize the low-rank matrix A , thereby capturing the highest-variance directions in activation space and theoretically maximizing the initial gradient signal (in this section, we focus solely on EVA's adaptive rank allocation; initialization is discussed in Section II-D3). Specifically, EVA computes the explained variance ratio for each singular vector:

$$\xi_j^i = \frac{\sigma_j^{i^2}}{(M-1)\|\boldsymbol{\sigma}^i\|_1}, \quad (55)$$

and globally redistributes the rank budget by prioritizing directions with the largest explained variance, effectively reducing redundancy while preserving the most informative subspaces.

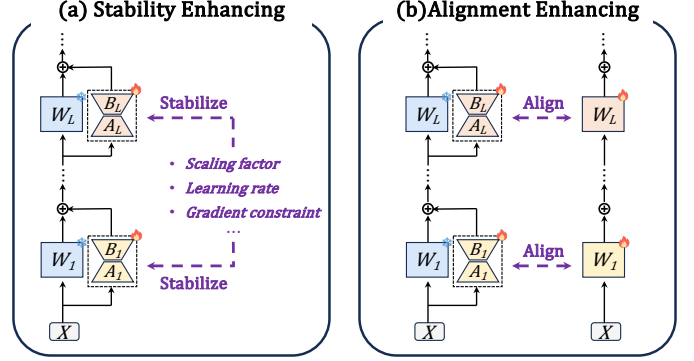


Fig. 3. Illustration of optimization process adjustment based LORA variants.

C. Optimization Process Adjustment Based LORA Variants

As shown in Figure 3, this section introduces LORA variants that directly adjust the optimization process of LORA, including: (a) Stability Enhancement Methods focus on regulating training dynamics to prevent collapse or instability. (b) Update Alignment Methods aim to bridge the gap between low-rank adaptation and full fine-tuning.

1) *Stability Enhancing Methods*: **RsLORA** [65] introduces an optimized scaling factor for LORA to achieve a rank-stabilized optimization process, ensuring two key rank-stability properties: (1) **Forward Stability**: If the input $X \in \mathbb{R}^{bs \times m}$ to the low-rank adapter is i.i.d. with an m 'th moment of $\Theta_r(1)$ per entry, then the m 'th moment of the adapter's outputs remains $\Theta_r(1)$ per entry. (2) **Backward Stability**: If the gradients of the loss with respect to the adapter outputs are $\Theta_r(1)$ per entry, then the gradients propagated back to the adapter's inputs also maintain $\Theta_r(1)$ per entry. Consider the scaling factor to be optimized $\gamma_r \in \mathbb{R}$ with $\gamma_r \xrightarrow{r \rightarrow \infty} 0$, which constrains the product of low-rank matrices as the rank r increases. For any training step $t > 1$, the low-rank matrices evolve according to the gradient formula in Eq (2) and the inductive derivation:

$$A_t = (I + \mathcal{O}_r(\gamma_r^2))A_0, \quad (56)$$

$$B_t = A_0^\top \left(-\eta \gamma_r \sum_{i=0}^{t-1} \nabla \widetilde{W}_i + \mathcal{O}_r(\gamma_r^2) \right), \quad (57)$$

$$\gamma_r A_t B_t = -\eta \gamma_r^2 \sum_{i=0}^{t-1} A_0 A_0^\top \nabla \widetilde{W}_i + A_0 A_0^\top \mathcal{O}_r(\gamma_r^3). \quad (58)$$

Assuming the entries of A_0 are i.i.d. with mean 0, variance σ_A ($\mathbb{E}_{A_0}[A_0 A_0^\top] = r \sigma_A I$), the expectation of Eq. (58) becomes:

$$\mathbb{E}_{A_0}[\gamma_r A_t B_t] = -\gamma_r^2 r \sigma_A \eta \sum_{i=0}^{t-1} \nabla \widetilde{W}_i + \mathcal{O}_r(\gamma_r^3 r), \quad (59)$$

For an adapted linear model where $Y = X(\widetilde{W} + AB)$, the gradient G and output O of the adapter satisfy:

$$G = -\gamma_r^2 r \sigma_A \eta \sum_{i=0}^{t-1} \nabla X_t Y_i^\top X_i + \mathcal{O}_r(\gamma_r^3 r), \quad (60)$$

$$\mathbb{E}_{X, A_0}[O] = -\gamma_r^2 r \sigma_A \eta \sum_{i=0}^{t-1} \nabla \mathbb{E}_X[X_t X_i^\top] Y_i + \mathcal{O}_r(\gamma_r^3 r), \quad (61)$$

where $G \in \mathcal{O}_r(\gamma_r^2 r)$ and $\mathbb{E}_{X,A_0}[O] \in \mathcal{O}_r(\gamma_r^2 r)$. To maintain both forward and backward stability, we require $\mathcal{O}_r(\gamma_r^2 r) = \mathcal{O}_r(1)$, implying $\gamma_r \in \mathcal{O}_r(1/\sqrt{r})$. Therefore, RSLORA recommends setting the scaling factor from $\frac{\alpha}{r}$ to $\frac{\alpha}{\sqrt{r}}$.

Hayou et al. [24] analyze the optimization dynamics of models adapted via low-rank adapters in the limit as the model width $m \rightarrow \infty$ increases and propose **LORA+** which sets the learning rate of matrix B 2^4 times that of matrix A . In the wide-network regime, one expects the change in model predictions at any training step t to remain stable—specifically, that the prediction increment $\Delta f_t(x) = f_t(x) - f_{t-1}(x)$ scales as $\Theta(1)$, meaning it neither vanishes nor diverges.

To investigate this behavior, Hayou et al. consider a simplified, analytically tractable model defined as $f(x) = x^\top(\tilde{w} + ab)$, where $\tilde{w} \in \mathbb{R}^m$ is a fixed pretrained weight vector, $a \in \mathbb{R}^m$ and $b \in \mathbb{R}$ are trainable rank-one components, and the input $x \in \mathbb{R}^m$ satisfies $\|x\| = \Theta(1)$. Following standard LoRA initialization, the variances of the initial parameters are $\sigma_{a_0}^2 = \Theta(m^{-1})$ and $\sigma_{b_0}^2 = \Theta(1)$. In this setting, the prediction increment at step t is given by:

$$\begin{aligned} \Delta f_t(x) = & -\eta b_{t-1}^2 (f_{t-1}(x) - y) \|x\|_2^2 \\ & - \eta (a_{t-1}^\top x)^2 (f_{t-1}(x) - y) \\ & + \eta^2 (f_{t-1}(x) - y)^2 b_{t-1} (a_{t-1}^\top x) \|x\|_2^2, \end{aligned} \quad (62)$$

where y denotes the ground-truth label, the learning rate is $\eta = \Theta(m^c)$ for some constant $c \in \mathbb{R}$, and the loss function is $\frac{1}{2}(f(x) - y)^2$. For clarity, define the following terms:

$$\begin{aligned} \delta_t^1 &= \eta b_{t-1}^2 (f_{t-1}(x) - y) \|x\|_2^2, \\ \delta_t^2 &= \eta (a_{t-1}^\top x)^2 (f_{t-1}(x) - y), \\ \delta_t^3 &= \eta^2 (f_{t-1}(x) - y)^2 b_{t-1} (a_{t-1}^\top x) \|x\|_2^2. \end{aligned} \quad (63)$$

The stable optimization dynamics requires $\delta_t^1, \delta_t^2, \delta_t^3 \in \Theta(1)$, which further implies $f_t(x) \in \Theta(1)$ throughout training. Notably, $\delta_t^3 \in \Theta(1)$ is automatically satisfied if $\delta_t^1, \delta_t^2 \in \Theta(1)$, since it is a higher-order term in η .

Notation $\gamma[\cdot]$ introduced such that $\nu = \Theta(m^{\gamma[\nu]})$ captures the asymptotic scaling of any quantity ν . The conditions for stable dynamics yield the following system of constraints:

$$\begin{cases} c + 2\gamma[b_{t-1}] + 1 = 0 & (\text{for } \delta_t^1 = \Theta(1)), \\ c + 2\gamma[a_{t-1}^\top x] = 0 & (\text{for } \delta_t^2 = \Theta(1)), \\ \gamma[b_{t-1}] + \gamma[a_{t-1}^\top x] = 0 & (\text{for } f_t(x) = \Theta(1)). \end{cases} \quad (64)$$

Solving this system yields $c = -\frac{1}{2}$, implying that the learning rate should scale as $\eta \in \mathcal{O}(m^{-1/2})$. However, due to the initialization $\sigma_{b_0}^2 = \Theta(1)$ and $a_0^\top x \in \mathcal{O}(1)$ (by the *Central Limit Theorem*), one can inductively show that $b_t \in \mathcal{O}(m^{-1/2})$ and $a_t^\top x \in \mathcal{O}(m^{-1/2})$ for all $t > 0$, resulting in $f_t(x) \in \mathcal{O}(m^{-1/2})$. Consequently, the parameter updates for a_t and b_t are of order $\mathcal{O}(m^{-1})$ and $\mathcal{O}(m^{-1/2})$.

This analysis reveals that δ_t^1 and δ_t^2 cannot simultaneously be $\Theta(1)$ under standard LoRA configurations with a shared learning rate. To resolve this, Hayou et al. propose decoupling the learning rates for a and b , suggesting that $\eta_b \in \mathcal{O}(1)$ (for b) and $\eta_a \in \mathcal{O}(m^{-1})$ (for a) can restore stable training dynamics.

Zhang et al. [66] investigate another solution for stable $\Delta f_t(x)$ under $m \rightarrow \infty$ increases, leveraging Riemannian preconditioning. Specifically, their approach—**RIEMANNIAN PRECONDITIONED LORA** (which we denote as **RPLORA**)—employs a Riemannian metric derived from a regularized Lagrangian framework. This metric is grounded in the geometric optimization principles for low-rank matrices with objectives and constraints introduced by Mishra and Sepulchre [120]. Following this, RPLORA modifies the gradients of the low-rank adapter parameters according to the natural gradient flow on the manifold of fixed-rank matrices, effectively preconditioning the optimization dynamics to maintain stability:

$$\nabla A_t^* = \nabla A_t (B_t B_t^\top)^{-1}, \quad \nabla B_t^* = (A_t^\top A_t)^{-1} \nabla B_t, \quad (65)$$

where ∇A^* and ∇B^* are the modified gradients of RPLORA for a low-rank adapter. Under the modified gradients, the prediction increment shown in Eq. (62) can be rewritten as:

$$\begin{aligned} \Delta f_t(x) = & -\eta (f_{t-1}(x) - y) \|x\|_2^2 \\ & - \eta (a_{t-1}^\top x)^2 (f_{t-1}(x) - y) \|a_{t-1}\|_2^{-2} \\ & + \eta^2 (f_{t-1}(x) - y)^2 b_{t-1}^{-1} \|a_{t-1}\|_2^{-2} (a_{t-1}^\top x) \|x\|_2^2. \end{aligned} \quad (66)$$

Similar to Eq. (63), defining $\delta_t^1, \delta_t^2, \delta_t^3$ with the three terms of Eq. (66), we can rewrite the constraints shown in Eq. (64) as:

$$\begin{cases} c + 1 = 0 & (\text{for } \delta_t^1 = \Theta(1)), \\ c + 2\gamma[a_{t-1}^\top x] - \gamma[\|a_{t-1}\|_2^2] = 0 & (\text{for } \delta_t^2 = \Theta(1)), \\ \gamma[b_{t-1}] + \gamma[a_{t-1}^\top x] = 0 & (\text{for } f_t(x) = \Theta(1)), \end{cases} \quad (67)$$

where we can drive $c = -1$ and correspondingly $\eta = m^{-1}$. Under $\sigma_{b_0}^2 = \Theta(1)$ and $a_0^\top x \in \mathcal{O}(1)$, one can recursively derive $b_t, a_t^\top x, \delta_t^1, \delta_t^2, \delta_t^3 \in \mathcal{O}(1)$ for all t . Hence, the stable training dynamics are achieved.

2) *Alignment Enhancing Methods*: Liu et al. [67] perform a weight decomposition analysis on the fine-tuning updates from both LoRA and full fine-tuning, revealing an interesting contrast: while LoRA’s updates demonstrate a positive correlation between magnitude and directional changes, full fine-tuning exhibits a slightly inverse relationship. This discrepancy motivates their proposed method, **DORA**, which decouples magnitude and directional learning in LoRA, addressing the potential complexity of jointly optimizing both components and achieving an optimization pattern more closely aligning that of full fine-tuning. Formally, the adapted weight of DORA can be expressed as:

$$W_t = m_t \cdot \frac{\widetilde{W} + \gamma_r A_t B_t}{\|\widetilde{W} + \gamma_r A_t B_t\|_F}, \quad \gamma_r = \frac{\alpha}{r}, \quad (68)$$

where m_t is a learnable magnitude vector, initialized as the Frobenius norm on the input dimension of the pretrained weight.

Similarly, **DELORA** [68] introduces a strategy that decouples the directional and magnitude updates by combining

LoRA with the idea of **ETHER** [121]. Formally, the adaptation in DELORA can be expressed as:

$$\Delta W_t = A_t D_t B_t = \frac{\lambda \|\widetilde{W}\|_2}{r} \sum_{i=1}^r \frac{a_t^i b_t^i}{\|a_t^i\|_2 \|b_t^i\|_2}, \quad (69)$$

where a_t^i and b_t^i are the i -th rank-one components of the low-rank matrices, and D_t is a diagonal matrix containing the scaling factors based on the norms of these components. Here, λ is a trainable scalar that controls the upper bound on the norm of the update as:

$$\|A_t D_t B_t\|_2 = \frac{\lambda \|\widetilde{W}\|_2}{r} \left\| \sum_{i=0}^r a_t^i b_t^i \right\|_2 \leq \lambda \|\widetilde{W}\|_2. \quad (70)$$

The bounded adaptation prevents the adapted model from diverging from the pretrained model.

Hao et al. [70] also utilize inductive derivation for A_t, B_t to analyze the optimization dynamics of LoRA. Specifically, assume $\left\| \sum_{i=0}^t \nabla \widetilde{W}_i \right\|_F \leq L$ (constant L is defined as an upper bound) for every training step t , which implies that the model stays within a finite Euclidean ball. In this case, by induction:

$$A_t = (I + \eta \frac{\alpha}{r} f_A(t)) A_0, \quad B_t = \eta \frac{\alpha}{r} A_0^\top f_B(t), \quad (71)$$

where $f_A(t)$ and $f_B(t)$ are defined by induction as:

$$f_A(t) = -\eta \frac{\alpha}{r} \sum_{i=0}^{t-1} \nabla \widetilde{W} f_B^\top(i), \quad (72)$$

$$f_B(t) = -\sum_{i=0}^{t-1} (I + \eta \frac{\alpha}{r} f_A^\top(i)) \nabla \widetilde{W}. \quad (73)$$

The adapter's computation at step t can be expressed as:

$$\Delta W = \gamma_r A_t B_t = \eta \frac{\alpha^2}{r^2} A_0 A_0^\top f_A(t) + \eta^2 \frac{\alpha^3}{r^3} f_B(t) A_0 A_0^\top f_A(t). \quad (74)$$

Hao et al. further establish the upper bound at every step:

$$\|f_A(t)\|_2 \leq \frac{\eta \gamma_r L^2 (1 - (\eta^2 \gamma_r^2 L^2)^t)}{1 - \eta^2 \gamma_r^2 L^2}, \quad (75)$$

where $\gamma_r = \frac{\alpha}{r}$. This bound reveals that the second term in Eq. (74) becomes negligible when $\eta \gamma_r \ll L$, since this condition ensures $\lim_{t \rightarrow \infty} \eta \gamma_r \|f_A(t)\| \ll 1$. Consequently:

$$\Delta W = \gamma_r A_t B_t \approx \gamma_r A_0 \tilde{B}_t =: \eta \gamma_r^2 A_0 A_0^\top \tilde{f}_B(t), \quad (76)$$

where we can define $\tilde{f}_B(t) =: \tilde{f}_B(t-1) - \nabla \widetilde{W}_t = \sum_{i=0}^t \nabla \widetilde{W}_i$. Substituting this into Eq. (76), we can obtain the expression presented in Eq. (3), which implies that LoRA adapters function as gradient compressors under small learning rates.

Building upon this insight, Hao et al. propose **FLORA** [70], which employs a random low-rank projection matrix $A^\top \in \mathbb{R}^{r \times m}$ to compress the gradients of a pretrained weight of size $m \times n$. The method efficiently computes and stores optimizer states using the compressed gradient, subsequently decompressing the optimizer's updates through A , enabling an intuitive update alignment. **GALORE** [122] proposes a similar framework where the projection matrix is obtained

from the singular components of the gradient to retain gradient information as much as possible.

LORA-PRO [25] enhances the alignment between LoRA's optimization dynamics and full fine-tuning by explicitly minimizing the **step-wise discrepancy** between: the indirect updates to pretrained weights via LoRA (Eq. (4)) and the direct weight updates from full fine-tuning. LoRA-PRO's objective can be viewed as an operational extension of LoRA-GA's principle (Section II-D2), generalizing the single-step gradient alignment to step-wise matching. LoRA-PRO incorporates RSLoRA's scaling factor and optimizes:

$$\arg \min_{\nabla A_t^*, \nabla B_t^*} \left\| \frac{\alpha}{\sqrt{r}} (A_t \nabla B_t^* + \nabla A_t^* B_t) - \nabla \widetilde{W}_t \right\|_F^2, \quad (77)$$

where $\nabla A_t^*, \nabla B_t^*$ are optimized gradients of A_t, B_t , $s A_t \nabla B_t^* + s \nabla A_t^* B_t$ represents the optimized indirect update. Denoting $\mathcal{D} = \left\| s A_t \nabla B_t + s \nabla A_t B_t - \nabla \widetilde{W}_t \right\|_F^2$, we derive the following optimality conditions:

$$\frac{\partial \mathcal{D}}{\partial \nabla A_t^*} = \frac{2\alpha}{\sqrt{r}} B_t^\top (s A_t \nabla B_t^* + s \nabla A_t^* B_t - \nabla \widetilde{W}_t) = 0, \quad (78)$$

$$\frac{\partial \mathcal{D}}{\partial \nabla B_t^*} = \frac{2\alpha}{\sqrt{r}} s A_t^\top (s A_t \nabla B_t^* + s \nabla A_t^* B_t - \nabla \widetilde{W}_t) = 0. \quad (79)$$

Assuming A_t, B_t maintain full rank during training such that $A_t^\top A_t$ and $B_t B_t^\top$ are invertible, we derive ∇B^* :

$$\nabla B_t^* = \frac{\sqrt{r}}{\alpha} (A_t^\top A_t)^{-1} A_t^\top \nabla \widetilde{W}_t - (A_t^\top A_t)^{-1} A_t^\top \nabla A_t^* B_t. \quad (80)$$

Substituting Eq. (80) into Eq. (78) and solving the resulting equation yields the expression for ∇A_t^* :

$$\nabla A_t^* = \frac{\sqrt{r}}{\alpha} \nabla \widetilde{W}_t B_t^\top (B_t B_t^\top)^{-1} + A_t M_t, \quad (81)$$

where $M_t \in \mathbb{R}^{r \times r}$ is an arbitrary matrix. Substituting Eq. (81) into Eq. (80) we have:

$$\nabla B_t^* = \frac{\sqrt{r}}{\alpha} (A_t^\top A_t)^{-1} A_t^\top \nabla \widetilde{W}_t [I - B_t^\top (B_t B_t^\top)^{-1} B_t] - B_t M_t, \quad (82)$$

The final solutions to the objective of LoRA-PRO are shown in Eqs. (81)-(82). To utilize these solutions, LoRA-Pro alters the gradients of A and B , effectively aligning the indirect updates from LoRA to the direct updates from full-finetuning (LoRA-PRO only utilizes the values and gradients of low-rank matrices to compute the aligned gradients since $\nabla \widetilde{W}_t B_t^\top = \nabla A_t$ and $A_t^\top \nabla \widetilde{W}_t = \nabla B_t$).

To obtain the solution for the arbitrary matrix M , LoRA-PRO further consider the following optimization objective:

$$\arg \min_M \left\| \nabla A_t^* - \nabla A_t \right\|_F^2 + \left\| \nabla B_t^* - \nabla B_t \right\|_F^2, \quad (83)$$

which can be optimized by solving the Sylvester equation:

$$M_t B_t B_t^\top + A_t^\top A_t M_t = -\frac{r}{\alpha^2} A_t^\top \nabla A_t (B_t B_t^\top)^{-1}, \quad (84)$$

which has a unique solution provided that $B_t B_t^\top$ and $-A_t^\top A_t$ do not have any shared eigenvalues.

Integrating LoRA with intermediate nonlinear functions is also a prevalent line of research [72]–[75]. Si et al. [123]

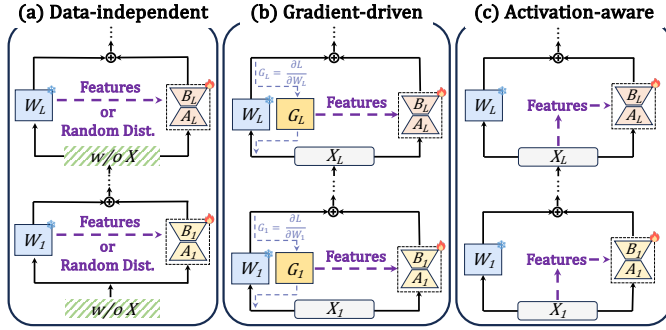


Fig. 4. Illustration of initialization adjustment based LORA variants.

argue that the linear coupling mechanism in LoRA restricts its capacity to represent arbitrary rank- r matrices; therefore, introducing an intermediate $r \times r$ matrix or nonlinearity function between A and B serves as a viable solution for a closer alignment with the learning capability of full fine-tuning. Dong et al. [72] assert that methodologies such as **MOSLoRA** [92] and **FLORA** (Si et al.) [71], which incorporate an intermediate $r \times r$ matrix, preserve the linearity of LoRA and consequently restrict the exploration of broader parameter spaces.

LoDA(+) [75] integrates LoRA with a multi-layer nonlinear activation structure to relax the low-rank linear constraint. Following the convention of PEFT methods, we denote the effective weight update induced by LoDA+ as ΔW , defined implicitly through its action on the input:

$$\frac{\alpha}{r} X \Delta W := \frac{\alpha}{r} (XAB + f_2(f_1(XAB))), \quad (85)$$

where $f_1(\cdot)$ and $f_2(\cdot)$ are parameterized nonlinear transformations (e.g., small linear layers with LeakyReLU activations). As illustrated in Figure 1 of the original paper, f_1 comprises two $r \times r$ matrices interleaved with three LeakyReLU functions, while f_2 consists of a single LeakyReLU function. ΔW in LoDA+ does not correspond to a fixed low-rank matrix but rather an input-dependent mapping, and thus cannot be explicitly materialized as a standalone weight matrix. (The original paper did not specify the use of scaling for LoDA+; therefore, scaling is omitted here.)

Similar to LoDA+, **AURORA** enhances LoRA with an adaptive nonlinear layer (ANL) that combines both fixed and learnable nonlinear components. Formally, the effective weight update in Aurora can be expressed as:

$$f_{ANL}(M) = \tanh(\tanh(M)) + V_s \cdot \mathcal{S}(M), \quad (86)$$

$$\frac{\alpha}{r} X \Delta W := \frac{\alpha}{r} f_{ANL}(XA)B, \quad (87)$$

where the first term in the ANL function $f_{ANL}(\cdot)$ represents a fixed nonlinear mapping implemented via the tanh activation function, and the second term introduces a learnable nonlinear mapping based on B-spline basis functions. Here, $C \in \mathbb{R}^{r \times r}$ is an intermediate square matrix, $\mathcal{S}(\cdot)$ is the spline basis function and $V_s \in \mathbb{R}^r$ is the spline weight vector.

D. Initialization Adjustment Based LORA Variants

In the standard LoRA implementation, the gradients of A and B depend on each other's magnitudes (i.e., as indicated by Eq (2), initializing one matrix to zero causes the gradient

of the other to vanish initially. For example, if $B_0 = 0$, then $\nabla A_0 = 0$, preventing updates to A_t until $B_t \neq 0$.

This gradient suppression results in significantly slower convergence compared to full fine-tuning, particularly when using small learning rates. As discussed in Section II-A3, LoRA does not reduce the overall computational complexity of training relative to full fine-tuning. Consequently, the slower convergence can result in substantially more FLOPs to achieve comparable performance. As shown in Figure 4, to address this limitation, while also aiming to improve performance, several advanced initialization strategies have been proposed.

1) *Data-independent Init Methods*: Typically, the initialization scheme of LoRA is defined as follows: (1) the weight matrix A is initialized using either a Gaussian distribution (reported in the original paper) or a Kaiming uniform distribution (adopted in the official implementation and the PEFT library), while (2) the weight matrix B is initialized with zeros. Formally, when employing a Kaiming uniform distribution, the initialization can be expressed as:

$$A_0 \sim \mathcal{U}\left(-\frac{1}{\sqrt{m}}, +\frac{1}{\sqrt{m}}\right), \quad B_0 = \mathbf{0}_{r \times n}. \quad (88)$$

The original paper does not explore the potential differences between initializing matrix A with zeros versus initializing matrix B with zeros. Intuitively, one might assume these two initialization schemes exhibit similar performance. However, Hayou et al. [77] verify that under Kaiming init [124] or Lecun init [125], initializing matrix B with zeros yields better performance and robustness to the learning rate.

Shiwei et al. [76] further explore a scheme where both matrices A and B are randomly initialized (referred to as **NZLoRA** in this paper). Given hyperparameters γ_A and γ_B , NZLoRA can be formally expressed as:

$$A_0 \sim \mathcal{U}\left(-\frac{\gamma_A}{\sqrt{m}}, +\frac{\gamma_A}{\sqrt{m}}\right), \quad B_0 \sim \mathcal{U}\left(-\frac{\gamma_B}{\sqrt{m}}, +\frac{\gamma_B}{\sqrt{m}}\right). \quad (89)$$

NZLoRA accelerates convergence by addressing the small gradient issue of vanilla LoRA, making it more robust to sub-optimal learning rates. A common challenge with non-zero initialization schemes is training instability. To mitigate this, existing methods typically adjust pretrained weights by subtracting the low-rank adapter's initial values—a process we term pretrained weights manipulation. However, this approach has a key limitation: since the pretrained weights must be modified again during inference, storing only the tuned low-rank adapters becomes infeasible. NZLoRA demonstrates that with carefully calibrated initialization variances (controlled by γ_A and γ_B), pretrained weights manipulation can be safely omitted without compromising final fine-tuning performance.

The strategic initialization of low-rank adapters using pretrained weight statistics has become one of the dominant paradigms in data-independent initialization schemes. This methodology enables precise fine-tuning of targeted feature subspaces within pretrained weights.

PISSA [26] laid the foundation for initialization from statistics of pretrained weights. PISSA initializes the adapter components using SVD of a pretrained weight matrix as:

$$\widetilde{W} = U_{\widetilde{W}} S_{\widetilde{W}} V_{\widetilde{W}}^\top, \quad (90)$$

$$A_0 = U_{\widetilde{W}}[:, :r] S_{\widetilde{W}}^{1/2}[:, r:], \quad (91)$$

$$B_0 = S_{\widetilde{W}}^{1/2}[:, r:] V_{\widetilde{W}}^\top[:, r:]. \quad (92)$$

Effectively capturing the most principal features of the original weight matrix according to the ECKART-YOUNG THEOREM [126], [127]. This inspired a series of subsequent works [69], [79]–[81], [128].

In contrast to this principal-component approach, **MiLORA** [78] exploits the minor components:

$$A_0 = U_{\widetilde{W}}[:, -r:] S_{\widetilde{W}}^{1/2}[-r :, -r :], \quad (93)$$

$$B_0 = S_{\widetilde{W}}^{1/2}[-r :, -r :] V_{\widetilde{W}}^\top[:, -r :]. \quad (94)$$

This preserves the primary knowledge in frozen weights while adaptively learning from the less dominant features.

OLORA [129] uses QR decomposition for initialization as:

$$\widetilde{W} = QR, A_0 = Q[:, :r], B_0 = R[:, r:], \quad (95)$$

where $Q \in \mathbb{R}^{m \times m}$ is orthonormal and $R \in \mathbb{R}^{m \times n}$ is upper triangular. This method achieves orthonormal initialization with computational efficiency.

Building upon these foundations, **SORSA** [81] enhances orthonormal preservation through a regularization scheme. The method modifies PISSA’s initialization while enforcing strict orthonormality constraints:

$$A_0 = U_{\widetilde{W}}[:, :r], B_0 = V_{\widetilde{W}}^\top[:, r:], D_0 = S_{\widetilde{W}}[r :, r :], \quad (96)$$

$$W_t = \widetilde{W} + \Delta W_t = \widetilde{W} + A_t D_t B_t, \quad (97)$$

$$\mathcal{L}_{\text{reg}} := \|A_t^\top A_t - I\|_F^2 + \|B_t B_t^\top - I\|_F^2, \quad (98)$$

where \mathcal{L}^{reg} represents the orthonormal regulation loss. This approach maintains the benefits of pretrained features while ensuring stable optimization through orthonormal constraints.

2) *Gradient-driven Init Methods*: As shown in Section II-A2, the optimization dynamics of LORA adapters are closely tied to the corresponding gradients of the pretrained weights. Motivated by this insight, multiple gradient-driven methods are proposed to enhance performance.

LORA-GA [27] introduces a gradient-based initialization strategy for low-rank adapters by effectively leveraging precomputed gradients. The central idea of LORA-GA lies in its optimization objective, which explicitly minimizes the discrepancy between the weight updates at the initial training step induced by LORA and those obtained through full fine-tuning with an arbitrary scaling factor ζ . Formally, this objective can be expressed as the following minimization problem:

$$\arg \min_{A_0, B_0} \left\| \mathcal{P}(A_0, B_0, \nabla \widetilde{W}_0) - \zeta \nabla \widetilde{W}_0 \right\|_F^2, \quad (99)$$

where the projection operator $\mathcal{P}(A_0, B_0, \nabla \widetilde{W}_0) \equiv A_0 A_0^\top \nabla \widetilde{W}_0 + \nabla \widetilde{W}_0 B_0^\top B_0$ represents the approximate gradient of \widetilde{W} as illustrated in Eq. (4). Under the assumption of a single step of stochastic gradient descent (SGD) with a learning rate η , the objective in Eq. (99) directly minimizes the difference between the updates of LoRA and full fine-tuning at the initial training step.

Assuming the gradient matrix $\nabla \widetilde{W}$ is invertible and $2r < \min(m, n)$, multiplying $A_0 A_0^\top$ or $B_0^\top B_0$ by an invertible matrix does not alter its rank. Therefore, the maximum possible rank of $\mathcal{P}(A_0, B_0, \nabla \widetilde{W}_0)$ is $2r$. In essence, LORA-GA seeks to construct the optimal rank- $2r$ approximation of the gradient matrix $\nabla \widetilde{W}$ via $\mathcal{P}(A_0, B_0, \nabla \widetilde{W}_0)$.

The solution of Eq. (99) can be derived from the truncated SVD of the pretrained weight gradient matrix as follows:

$$\nabla \widetilde{W}_0 = U_{\nabla \widetilde{W}_0} S_{\nabla \widetilde{W}_0} V_{\nabla \widetilde{W}_0}^\top, \quad (100)$$

$$A_0 = U_{\nabla \widetilde{W}_0}[:, :r], \quad B_0 = V_{\nabla \widetilde{W}_0}^\top[r + 1 : 2r, :]. \quad (101)$$

Following Eqs. (100)–(101), before the formal training phase, LORA-GA efficiently computes and offloads the gradients of the pretrained weights layer by layer, resembling the fused gradient approach proposed in LOMO [130] without performing optimization steps.

To further align with the scaling factor introduced by RSLORA [65] which we discussed in Section II-C, LORA-GA incorporates the following scaling mechanism:

$$A_0 = \frac{\sqrt[4]{m}}{\sqrt{\gamma}} U_{\nabla \widetilde{W}_0}[:, :r], \quad B_0 = \frac{\sqrt[4]{m}}{\sqrt{\gamma}} V_{\nabla \widetilde{W}_0}^\top[r + 1 : 2r, :], \quad (102)$$

where γ denotes a hyperparameter introduced by LORA-GA to control the scaling.

LORA-ONE [82] identifies several purported misconceptions in LORA-GA and proposes modifications to its SVD-based feature selection and scaling mechanisms. The authors contend that under LORA’s standard zero-initialization scheme, as shown in Eq. (88), the weight matrix B — after the first training step — naturally resides in the top- r subspace of the right singular matrix of the gradient matrix. Furthermore, they argue that the subsequent training dynamics of B remain confined to this invariant subspace, while matrix A aligns with the top- r subspace of the left singular matrix of the gradient matrix under certain requirements.

Based on this premise, LORA-ONE asserts that initializing B with $V_{\nabla \widetilde{W}_0}^\top[r + 1 : 2r, :]$ results in suboptimal alignment, trapping the optimization in an undesirable subspace. Instead, they claim B should align with $V_{\nabla \widetilde{W}_0}^\top[:, r :]$. However, since this observation hinges on LoRA’s default zero-initialization scheme, its applicability to LORA-GA — which employs a different initialization strategy — remains questionable.

Moreover, the indirect update to pretrained after the first gradient descent step of LORA-GA is given by:

$$\begin{aligned} \frac{\alpha}{\sqrt{r}} A_1 B_1 - \frac{\alpha}{\sqrt{r}} A_0 B_0 &= \frac{\alpha}{\sqrt{r}} [-\eta \nabla \widetilde{W}_0 B_0^\top B_0 \\ &\quad - \eta A_0 A_0^\top \nabla \widetilde{W}_0 + \eta^2 \nabla \widetilde{W}_0 B_0^\top A_0^\top \nabla \widetilde{W}_0]. \end{aligned} \quad (103)$$

According to Eq. (103), the optimal $2r$ -approximation of the initial gradient descent step’s update direction can be achieved when the second-order η^2 term is negligible. This approximation, however, imposes an inherent constraint on the learning rate selection using LORA-GA.

Building upon these observations, LORA-ONE introduces the following initialization:

$$-\nabla \widetilde{W}_0 = U_{\nabla \widetilde{W}_0} S_{\nabla \widetilde{W}_0} V_{\nabla \widetilde{W}_0}^\top, \quad S_{\nabla \widetilde{W}} \leftarrow S_{\nabla \widetilde{W}} / \sigma_1, \quad (104)$$

$$A_0 = \frac{1}{\sqrt{\gamma}} U_{\nabla \widetilde{W}_0}[:, :r] S_{\nabla \widetilde{W}_0}^{1/2}[:, r, :r], \quad (105)$$

$$B_0 = \frac{1}{\sqrt{\gamma}} S_{\nabla \widetilde{W}_0}^{1/2}[:, r, :r] V_{\nabla \widetilde{W}_0}^\top[:, r, :], \quad (106)$$

where γ is a hyperparameter analogous to LORA-GA's scaling factor and σ_1 is the largest singular value of $-\nabla \widetilde{W}_0$. Remarkably, LoRA-One achieves recovery of the one-step gradient updates for pretrained weights—with negligible error—while eliminating the need for explicit weight manipulation discussed in Section II-D1. **LORA-SB** [131] similarly initializes A_0 and B_0 using the top- r left and right singular vectors respectively, while introducing $D \in \mathbb{R}^{r \times r}$ initialized with the corresponding singular values. During training, while maintaining the same forward pass formulation as Eq. (97), LoRA-SB keeps A_0 and B_0 frozen and only updates D_t .

GoRA [62] observes that the compression form shown in Eq. (3) is not the optimal solution given an initialized A_0 . The best solution is given by:

$$A_0^\dagger = (A_0^\top A_0)^{-1} A_0^\top, \quad A_0 B_0 = -A_0 A_0^\dagger \nabla \widetilde{W}_0 \approx -\nabla \widetilde{W}_0, \quad (107)$$

where A^\dagger is the Moore-Penrose inverse of the matrix A . Furthermore, GoRA finds that the expected Frobenius norm of $\nabla \widetilde{W}_0$ is \sqrt{mn} , while that of AB is \sqrt{rn} under a zero-mean unit-variance distribution. Following these observations, GoRA initializes the low-rank weights by:

$$A_0 \sim \mathcal{U}\left(-\frac{1}{\sqrt{m}}, +\frac{1}{\sqrt{m}}\right), \quad B_0 = -\frac{\gamma \sqrt{m}}{\alpha} A_0^\dagger \nabla \widetilde{W}_0, \quad (108)$$

$$\frac{\alpha}{\sqrt{r}} A_0 B_0 \approx -\frac{\gamma \alpha \sqrt{rmn}}{\alpha \sqrt{rmn}} \nabla \widetilde{W}_0 \approx -\gamma \nabla \widetilde{W}_0, \quad (109)$$

where γ is a hyperparameter of GoRA that controls the scaling of initialization. With a proper γ , a lower initial loss and faster convergence speed can be achieved by GoRA.

3) *Activation-aware Init Methods*: Let $X \in \mathbb{R}^{bs \times m}$ denote the input activations of a pretrained weight matrix $\widetilde{W} \in \mathbb{R}^{m \times n}$, where b is the batch size, s is the padded sequence length. The unnormalized covariance matrix $C = X^\top X$ captures the second-order statistics of the inputs. To analyze how \widetilde{W} interacts with these input statistics, CORDA performs SVD on the matrix $C\widetilde{W} = X^\top X\widetilde{W}$, which combines the data distribution C with the learned features \widetilde{W} . Formally, the decomposition can be expressed as follows:

$$C = X^\top X, \quad C\widetilde{W} = U_{C\widetilde{W}} S_{C\widetilde{W}} V_{C\widetilde{W}}^\top, \quad (110)$$

$$\widetilde{W} = C^{-1} C\widetilde{W} = (C^{-1} U_{C\widetilde{W}}) S_{C\widetilde{W}} V_{C\widetilde{W}}^\top. \quad (111)$$

This decomposition reveals task-relevant directions in the input space that are amplified or suppressed by \widetilde{W} .

Leveraging this decomposition, **CORDA** [84] proposes two activation-based initialization schemes, namely *knowledge-preserved adaptation* and *instruction-preserved adaptation*.

The key principle behind *knowledge-preserved adaptation* is to retain the pretrained model's world knowledge as much as possible while adapting it to downstream tasks by altering minor directions. To operationalize this concept, CORDA employs the following methodology: First, it computes covariance matrices using question-answering datasets that are

specifically selected for their relevance to the model's world knowledge representation. Mathematically, after obtaining the covariance matrix, CORDA initializes the corresponding low-rank weights using the minor components of a weighted covariance matrix through the following transformation:

$$A_0 = (C^{-1} U_{C\widetilde{W}})[:, -r :] S_{C\widetilde{W}}^{-1/2}[-r :, -r :], \quad (112)$$

$$B_0 = S_{C\widetilde{W}}^{-1/2}[-r :, -r :] V_{C\widetilde{W}}^\top[-r :, :]. \quad (113)$$

In *instruction-preserved adaptation*, the primary objective is to maximize alignment with the downstream task, prioritizing task-specific performance. For this purpose, CORDA computes the covariance matrices using a subset of the training dataset and initializes the low-rank weights as:

$$A_0 = (C^{-1} U_{C\widetilde{W}})[:, :r] S_{C\widetilde{W}}^{-1/2}[:, r, :r], \quad (114)$$

$$B_0 = S_{C\widetilde{W}}^{-1/2}[:, r, :r] V_{C\widetilde{W}}^\top[:, r, :]. \quad (115)$$

As demonstrated in Section II-D, LORA faces the challenge of vanishing gradients during the initial training phases. To mitigate this issue, Paischer et al. [64] proposed **EVA** (*Explained Variance Adaptation*), which utilizes principal components derived from the activation covariance matrix $X^\top X$ to properly initialize the weights of the matrix A . The primary objective of EVA is to maximize the expected gradient signal of the matrix B during the initial training stages. Formally, this objective can be expressed as:

$$\max_{A_0 A_0^\top = I} \mathbb{E} \left[\|\nabla B_0\|_F^2 \right] = \max_{A_0 A_0^\top = I} \mathbb{E} \left[\left\| A_0^\top \nabla \widetilde{W} \right\|_F^2 \right]. \quad (116)$$

Consider the LORA forward pass in a simple linear model where the input $x \in \mathbb{R}^{1 \times m}$ and output $\hat{y} \in \mathbb{R}^{1 \times n}$:

$$\hat{y} = x(\widetilde{W} + AB), \quad \nabla B_0 = A_0^\top x^\top \nabla \hat{y}, \quad (117)$$

where $\nabla \hat{y}$ represents the gradient of the predicted label \hat{y} under the loss function $\mathcal{L}(\hat{y}, y)$. The expected squared Frobenius norm of the gradient of B_0 can then be derived as:

$$\begin{aligned} \|\nabla B_0\|_F^2 &= \text{Tr}(\nabla B_0^\top \nabla B_0) = \text{Tr}(\nabla \hat{y} \nabla \hat{y}^\top x A_0 A_0^\top x^\top) \\ &= \underbrace{\nabla \hat{y} \nabla \hat{y}^\top}_{\text{Scaler}} \cdot \text{Tr}(A_0^\top x^\top x A_0). \end{aligned} \quad (118)$$

EVA makes the key assumption that the gradient of \hat{y} is statistically independent of the input (i.e., $\nabla \hat{y} \perp x$), the gradient $\nabla \hat{y}$ depends solely on \widetilde{W} since $A_0 B_0 = 0$. Consequently, the expected covariance between the input and the gradient of \hat{y} becomes:

$$\mathbb{E} \left[(x - \mathbb{E}[x])^\top (\nabla \hat{y} - \mathbb{E}[\nabla \hat{y}]) \right] = \mathbf{0}_{m \times n}. \quad (119)$$

This leads to EVA's fundamental conclusion that the expected initial gradient magnitude of B_0 is directly proportional to the trace of the activation matrix projected by A_0 :

$$\mathbb{E} \left[\|\nabla B_0\|_F^2 \right] \propto \text{Tr}(A_0^\top \mathbb{E} [x^\top x] A_0). \quad (120)$$

Therefore, the objective in Eq. 116 can be rewritten as:

$$\max_{A_0 A_0^\top = I} \mathbb{E} \left[\|\nabla B_0\|_F^2 \right] = \max_{A_0 A_0^\top = I} \text{Tr}(A_0^\top \mathbb{E} [x^\top x] A_0). \quad (121)$$

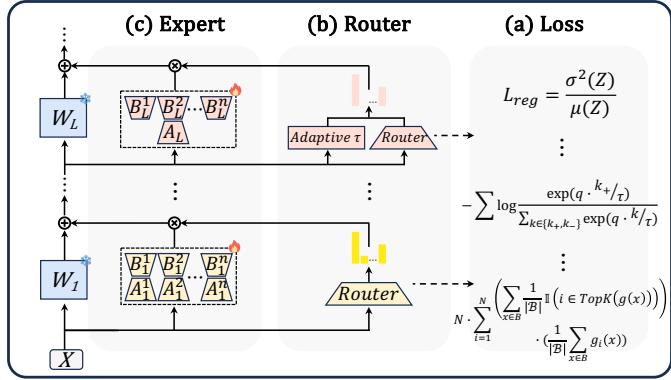


Fig. 5. Illustration of mixture of experts Integration based LORA variants.

This goal is equivalent to maximizing the variance of the down-projected activation $X_0 A_0$ and maximizing the explained variance in a rank- r approximation of the activation X_0 . The solution can be derived from the truncated SVD:

$$C = X^\top X = U_C S_C V_C^\top \quad (122)$$

$$A_0 = U_C[:, :r] S_C \in \mathbb{R}^{m \times r}, \quad B_0 = \mathbf{0}_{r \times n}, \quad (123)$$

where U_C contains the eigenvectors and S_C contains the eigenvalues of C . For computational efficiency, EVA computes the covariance matrix $X^\top X$ using a subset of training data and employs incremental SVD [132] with truncation [133] to minimize memory and time overheads during initialization. The final initialization of A_0 follows Eqs. (122)–(123).

E. Mixture-of-Experts Integration Based LORA Variants

By replacing standard LORA layers with MoE modules composed of multiple LoRA experts, Mixture-of-Experts integration based LORA variants aim to enhance model capacity and adaptability. Formally, the behavior of these variants is generally characterized by a routed combination of LORA expert outputs. The adaptation form can be defined as:

$$\Delta W = \gamma_r \cdot \sum_{i=1}^N \omega_i(x) \cdot (B_i A_i), \quad (124)$$

where x is an input vector (hidden state of a token for LLMs), N is the number of experts, and $\omega_i(x)$ is the routing weight for expert i determined by a gating network $g(x)$. Here, the foundational router activates only the top k experts based on the gating scores:

$$\omega_i(x) = \begin{cases} g_i(x) & \text{if } i \in \text{TopK}(g(x)) \\ 0 & \text{otherwise} \end{cases} \quad (125)$$

The optimization objective typically combines the primary task loss L_{task} with a regularization loss L_{reg} to regulate expert behavior. In the standard setting, L_{reg} typically serves as a load-balancing term to ensure even expert utilization. For a given batch of input tokens \mathcal{B} , this regularization loss is usually defined as the scaled dot-product between the expert selection frequency and the average gating probability:

$$L_{reg} = N \sum_{i=1}^N \left(\frac{1}{|\mathcal{B}|} \sum_{x \in \mathcal{B}} \mathbb{I}(i \in \text{TopK}(g(x))) \right) \cdot \left(\frac{1}{|\mathcal{B}|} \sum_{x \in \mathcal{B}} g_i(x) \right), \quad (126)$$

where N is the number of experts, $\mathbb{I}(\cdot)$ is the indicator function denoting whether expert i is selected for token x , and the two summation terms represent the actual fraction of tokens routed to expert i and the average predicted probability for expert i , respectively.

Recent variants have introduced innovations across three primary dimensions to this framework: modifications to the training objective (Loss), enhancements to the expert selection process (Router), and reconfigurations of the architectural design (Structure).

1) *Loss Modification Methods*: While the standard regularization term L_{reg} primarily focuses on load balancing to ensure equitable expert usage, it remains agnostic to the actual features learned by the experts. Consequently, this metric-driven constraint is insufficient for addressing the unique semantic challenges arising during fine-tuning, such as the tendency for experts to converge on identical representations or the overwriting of general world knowledge. To overcome these limitations, recent works have designed specialized auxiliary losses that go beyond simple routing statistics to actively shape expert specialization and diversity.

A key challenge in MoE training is random routing, where the gating network fails to develop strong preferences, causing different experts to converge on similar feature representations. This expert redundancy negates the capacity benefits of the MoE architecture. To address this, **MoELORA** [85] incorporates a contrastive learning objective into the loss function. The motivation is to force experts to learn distinct features by maximizing the semantic distance between their outputs. Specifically, it treats the outputs processed by the same expert as positive pairs and those from different experts as negative pairs. The expert contrastive loss L_{reg} is defined as:

$$L_{reg} = - \sum \log \frac{\exp(q \cdot k_+ / \tau)}{\sum_{k \in \{k_+, k_-\}} \exp(q \cdot k / \tau)}, \quad (127)$$

where q is the query output, k_+ represents outputs from the same expert, k_- represents outputs from other experts, and τ is the temperature. This auxiliary loss encourages high diversity among experts, ensuring that the expanded parameter space is effectively utilized for distinct feature processing.

While MoELORA focuses on general expert diversity, other approaches leverage loss functions to enforce specific functional roles, particularly to mitigate "catastrophic forgetting." Standard fine-tuning often overwrites the model's pre-trained world knowledge while learning downstream tasks. **LORAMOE** [86] addresses this by introducing a localized balancing constraint to separate experts into two groups: those preserving world knowledge and those adapting to new tasks. It utilizes an importance matrix Q and a coefficient matrix I that rewards alignment between expert types and sample types:

$$I_{n,m} = \begin{cases} 1 + \delta & \text{if } \text{Type}_e(n) = \text{Type}_s(m) \\ 1 - \delta & \text{otherwise} \end{cases} \quad (128)$$

The regularization loss is calculated based on the dispersion of the weighted importance matrix $Z = I \circ Q$:

$$L_{reg} = \frac{\sigma^2(Z)}{\mu(Z)}. \quad (129)$$

By maximizing the variance of Z , LoRAMoE effectively disentangles task-specific adaptation from general knowledge retention, thereby solving the forgetting problem through guided expert specialization.

2) *Router Modification Methods*: The routing mechanism determines how inputs are distributed among experts. Standard approaches often rely on implicit, token-level routing, where different tokens within the same sequence might be sent to different experts based on latent features. This can lead to fragmented context and interference between heterogeneous tasks. To address these limitations, **MOA** [87] diverges from the standard paradigm by adopting a sequence-level routing strategy guided by explicit domain metadata. Instead of relying on unsupervised token-wise learning, the model employs a regularization loss to penalize deviations from ground-truth domain labels. This supervision enforces precise, consistent data-to-expert assignments across all layer-wise routers, effectively mitigating task interference by prioritizing the sequence's domain identity over local token statistics.

Focusing on efficiency, **ADAMOLE** [88] challenges the static allocation of experts in Top- k methods. Motivated by the observation that tokens vary in complexity, it introduces a dynamic, context-sensitive routing strategy. Instead of a fixed k , it employs an adaptive threshold $\tau(x)$ derived from the input features. An expert is activated only if its gating score exceeds this threshold:

$$\omega_i(x) = g_i(x) \cdot \mathbb{I}(g_i(x) > \tau(x)), \quad (130)$$

$$\text{where } \tau(x) = \tau_{\max} \cdot \sigma(W_\tau x + b_\tau). \quad (131)$$

This mechanism allows the model to dynamically adjust the number of active experts based on the specific requirements of the input complexity.

3) *Expert Modification Methods*: Beyond loss functions and routing, significant research focuses on structurally optimizing how LoRA experts are constructed, initialized, and arranged within the network.

MOLA [89] is motivated by the understanding that different Transformer layers process features at varying levels of abstraction. Consequently, a uniform number of experts across all layers is suboptimal. MOLA structurally alters the MoE configuration by varying the number of experts N_l specific to each layer l . By adopting architectures such as Diamond or Inverted-Triangle patterns for expert allocation, MOLA optimizes expert redundancy where it is most needed.

Another structural challenge is bridging the performance gap between LoRA-based methods and full fine-tuning. **GOAT** [90] addresses this by structurally aligning the initialization of experts with the singular value decomposition (SVD) of the pre-trained weights. Each LoRA expert is initialized using disjoint segments of the singular vectors U and V :

$$B_i = \sqrt{\frac{1}{s}} U_i \Sigma_i^{1/2}, \quad A_i = \sqrt{\frac{1}{s}} \Sigma_i^{1/2} V_i^T. \quad (132)$$

Combined with a theoretically derived scaling factor s , this structural initialization ensures that the optimization trajectory of the MoE-LoRA model closely mimics that of full-rank fine-tuning.

In the realm of structural efficiency, **HYDRA-LoRA** [91] addresses the parameter redundancy inherent in standard MoE designs where (B_i, A_i) pairs are fully independent. Diverging from the symmetric expert structure, it proposes an asymmetric architecture consisting of a single shared A and multiple B . The shared projection matrix A captures general features across all inputs, while the set of distinct matrices $\{B_i\}$ serves as the experts. A dynamic router $g(x)$ computes input-sensitive weights to combine these heads, resulting in the update:

$$y = \widetilde{W}x + s \left(\sum_{i=1}^N \omega_i(x) B_i \right) Ax. \quad (133)$$

This design significantly reduces parameter count while maintaining the token-level adaptability of the router.

Conversely, **MOSLoRA** [92] modifies the internal structure of the LoRA module itself to introduce mixture capabilities without an external router.

III. OVERVIEW OF LoRAFACTORY

A. Core Implementations of LoRA in LoRAFactory

LoRAFactory follows a modular inheritance hierarchy with `LinearWithLoRA` as the base class, enabling efficient implementation of LoRA variants through strategic method overriding. The `LinearWithLoRA` class extends `torch.nn.Linear` class and provides the foundations of LoRA's mechanism. The core forward computation of `LinearWithLoRA` is detailed below:

$$x_{\text{out}} = x_{\widetilde{W}} + x_{\Delta W} = \text{linear}(x_{\text{in}}, \widetilde{W}^\top) + s \cdot \text{linear}(\text{linear}(\text{dropout}(x_{\text{in}}), A^\top), B^\top), \quad (134)$$

where `linear` and `dropout` are functions provided by PyTorch. Key methods of `LinearWithLoRA` are:

- `forward`: Orchestrates the forward pass as a linear layer. Conditionally applies low-rank adaptations (LoRA)—disabled either by the `DisableLoRA` context manager or when LoRA weights are inaccessible.
- `_lora_forward`: Computes the low-rank adaptation as shown in the fused forward pass of the low-rank adaptation part in Eq. (134).
- `init_lora_weights`: Initializes the low-rank weights.
- `compute_lora_weight`: Computes the effective LoRA weight ΔW .

A simple `LoRAConfig` data class is defined alongside, covering the following key configurations:

- `in_features`: int: The input dimension.
- `out_features`: int: The output dimension.
- `bias`: bool: Whether a bias term is needed.
- `lora_rank`: int: The rank of the low-rank adapter.
- `lora_scaler`: float: The scaling coefficient of the low-rank adapter (defaultly used as α).
- `lora_dropout`: float: The dropout rate of the input of the low-rank adapter.
- `weight_a_init_method`: str: The name of the initialization method for the matrix A (e.g., `kaiming`, representing the kaiming uniform distribution).

- `weight_b_init_method`: str: The name of the initialization method for the matrix B .
- `run_lora_in_fp32`: bool: Whether run low-rank computation under the FP32 precision, while keeping the pretrained weight with original precision.
- `quant`: bool: Whether quantize the pretrained weight.

The class of QLORA extends `LinearWithLoRA` by quantizing the layer’s pretrained weights to lower precision (e.g., NF4). This implementation is highly flexible: it returns the output of `LinearWithLoRA` when `LoRAConfig.quant` is `False`; otherwise, it performs computation by de-quantizing the quantized weights. Hence, the `LinearWithQLoRA` is further inherited by classes of LoRA variant methods for easy quantization.

B. Implementations of LoRA Variants in LoRAFactory

Variants such as DORA cannot directly use the forward pass of `LinearWithLoRA`; for example, DORA requires merging the low-rank weights into pretrained weights and using the weights with altered magnitudes for forward computation, making the fused computation impossible. For example, the forward pass of `LinearWithDoRA` can be expressed as:

$$x_{\text{out}} = \text{linear}(x_{\text{in}}, \text{self.}_\text{apply_dora}()^\top), \quad (135)$$

where `self._apply_dora()` follows Eq. (68).

Variants such as AURORA necessitate forward passes of low-rank adaptation that differ from vanilla LORA. For example, as shown in Eq. (86), AURORA introduces a non-linear function f_{ANL} into the forward pass, the forward pass of AURORA can be correspondingly expressed as:

$$x_{\text{ANL}} = \text{self.}_\text{ANL}(\text{linear}(\text{dropout}(x_{\text{in}}), A^\top)) \quad (136)$$

$$x_{\Delta W} = s \cdot \text{linear}(x_{\text{ANL}}, B^\top), \quad (137)$$

where `self._ANL()` is a method performing f_{ANL} .

Variants such as PISSA, relying on pretrained weights to initialize low-rank weights, are implemented by modifying the `init_lora_weights` method. In contrast, variants such as LORA-GA, which utilize gradients or activations for initialization, require deactivating the `init_lora_weights` method and executing a variant-specific re-initialization function after computing and storing the gradients or activations.

Sharing-based variants share low-rank weights across modules; the low-rank weights of these variants cannot be directly initialized. For this reason, a variant-specific function `prepare_shared_lora_weights` is required to identify all sets of modules that share low-rank weights and initialize the corresponding shared weights. After all sharing sets and shared weights are prepared, a variant-specific function `update_shared_weights_to_layer` is required to distribute the shared weights.

C. Working Mechanism of LoRAFactory

All LoRA-related hyperparameters within LoRAFactory are parsed via an argument parser and stored in a namespace variable, `args`. Following model initialization, both the model and `args` are passed to the `setup_lora` function. This

function identifies all targeted modules in the model designated for adaptation, and invokes the `switch_to_lora` function. The latter determines the targeted LoRA variant for adaptation and replaces all specified linear modules in the model with corresponding adaptation-class linear modules. Throughout this process, any exceptional cases are automatically managed by these functions. LoRAFactory is natively compatible with modern training strategies, including DeepSpeed ZeRO 3. The model with adapted modules can be trained using custom trainers, such as the Hugging Face Transformers Trainer, or it may employ the toolkits provided within the framework.

IV. EMPIRICAL EVALUATION USING LORAFACtORY

We present a systematic evaluation of 20 representative LoRA variants, which have been published in top-tier venues such as NeurIPS, ICLR, and ICML, within a unified framework implemented in our codebase, **LoRAFactory**. Our benchmark spans three domains: natural language understanding (NLU), natural language generation (NLG), and image classification (IC). A key challenge in comparing LORA variants lies in their sensitivity to hyperparameter choices. While vanilla LORA is known to be highly sensitive to the learning rate [99], [105], the sensitivity profiles of its variants remain largely uncharacterized. To address this, we conduct a comprehensive sensitivity analysis using Llama-3.1-8B-Base as a testbed, varying batch size, LORA dropout rate, training data volume, and learning rate. Our results indicate that learning rate sensitivity is the most salient differentiator, with optimal ranges varying substantially across methods. Consequently, we fix all hyperparameters except the learning rate in the main experiments.

Experimental Protocol. For NLU, we fine-tune RoBERTa-Base [30] on all tasks of the GLUE benchmark [31]. For NLG, we evaluate mathematical reasoning and code generation using Llama-3.1-8B-Base [37]. For IC, we train CLIP-ViT-B/16 [134] on seven image classification datasets: Stanford-Cars [135], DTD [136], EuroSAT [137], GTSRB [138], RE-SISC45 [139], SUN397 [140], and SVHN [141]. Given space limitations and consistent trends observed across domains, we present visualized NLG results in the main text, while full numerical results, including those of NLU and IC, are provided in Appendix C.

Default Configuration. All experiments use rank $r = 8$, scaling coefficient $\alpha = 16$, and no LoRA dropout (except for variants like DENSELORA, where larger r and α are used to maintain comparable trainable parameter counts; see Appendix). We employ the AdamW optimizer [10] with a cosine learning rate schedule. All runs use a fixed random seed; we observe that qualitative trends are robust to initialization.

A. Computational and Memory Overhead Analysis

Figure 8 compares the training time and peak GPU memory usage of LORA variants on Llama-3.1-8B-Base under a defaultly identical hardware and software conditions (single NVIDIA H200 GPU, BF16 precision, sequence length 1024,

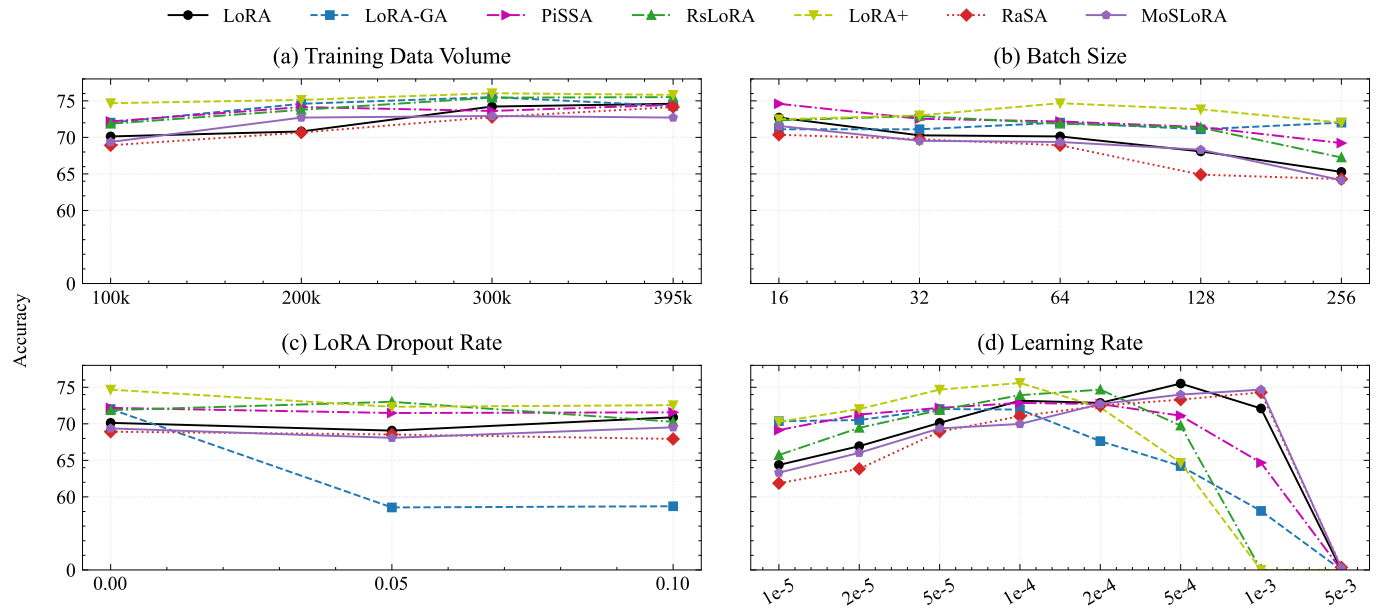


Fig. 6. Performance of LoRA and selected variants with altering distinct hyperparameters.

batch size 1, no activation checkpointing). Variants with negligible overhead (e.g., LORA+) are omitted for clarity. Vanilla LoRA achieves the lowest overhead (4h 42m, 30,067 MB), serving as an efficiency baseline. DORA incurs the highest memory cost (52,847 MB, +75%) due to explicit materialization of low-rank matrices during forward propagation, a cost that can be mitigated via activation checkpointing. LoRAMOE is the slowest (36h 31m, +676.95%) owing to its expert-routing mechanism. ADALORA and RANDLORA exhibit increased runtime due to dynamic rank allocation or full-rank computations. These results underscore a fundamental trade-off: architectural enhancements often come at the expense of computational and memory efficiency (**Finding 1**).

B. Hyperparameter Sensitivity Analysis

We fine-tune Llama-3.1-8B-Base on MetaMathQA [142] and evaluate on GSM8K [143], using a base configuration of 100k samples, batch size 64, 0% dropout, and learning rate 5e-5. In each ablation, only one hyperparameter is varied.

1) *Training Data Volume and Batch Size*: As shown in Figure 6(a), performance generally improves with data volume. Vanilla LORA increases from 70.13 to 74.60 as data grows from 100k to 395k. However, variants like LORA-GA and MoSLoRA saturate earlier. Performance remains roughly stable across batch sizes 16–64 (**Finding 2**), but degrades significantly at larger sizes due to fewer optimization steps. Vanilla LORA drops from 72.71 to 65.28 at batch size 256, whereas LORA-GA maintains robustness, attributable to its gradient-magnitude-enhanced initialization scheme, which reduces reliance on frequent updates. Notably, inter-method performance gaps narrow with more update steps, with a smaller batch size or larger training data volume, suggesting that moderate-scale dataset volumes and update steps are more discriminative for evaluation (**Finding 3**).

2) *LoRA Dropout Rate*: Most variants are insensitive to dropout (**Finding 4**), but LORA-GA suffers severe degradation (from 72.02 to 51.33). This stems from a mismatch

between its initialization (computed without initialized low-rank weights) and training dynamics (with initialized low-rank weights and dropout), which alters input statistics. To ensure fair comparison, we disable dropout in all main experiments.

3) *Learning Rate*: Figure 6(d) reveals pronounced and method-specific learning rate sensitivity (**Finding 5**), with narrow and non-overlapping optimal ranges. This necessitates extensive learning rate sweeps to find out the near-optimal performance of each method we tested, as detailed next.

C. Learning Rate Sweep Results on NLG

1) *Task Settings*: We evaluate mathematical reasoning by fine-tuning on 100k samples from MetaMathQA [142] and testing on GSM8K [143]. For code generation, we train on 100k samples from CodeFeedback [144] and evaluate on HumanEval [145]. To mitigate variance from HumanEval’s small size (163 samples), we average over eight evaluation runs. We sweep eight learning rates (1e-6 to 1e-3) while fixing other settings with the default configurations.

2) *Results and Discussion*: As shown in Figure 7, performance typically rises with learning rate until an optimum, beyond which it declines. Several variants (e.g., ADALORA) converge slower than vanilla LORA, likely due to additional regularization, for example, orthogonality constraints in ADALORA or coupling with pretrained weights (e.g., HiRA, which dampens gradient signals).

Notably, many variants outperform vanilla LORA at low learning rates. On GSM8K at 1e-6, LORA-GA (64.06) surpasses vanilla LORA (52.82) by over 11 points. However, this advantage vanishes at higher rates: the best variant (LORA+, 75.59 at 1e-4) exceeds LORA (75.51 at 1e-4) by only 0.08 points. On HumanEval, only RANDLORA and RASA marginally surpass LORA. At 1e-6, most methods fail to achieve meaningful code generation performance, indicating that stronger update signals are essential for this task.

Surprisingly, LORA exhibits higher performance ceilings than its most evaluated variants on both tasks, a trend also

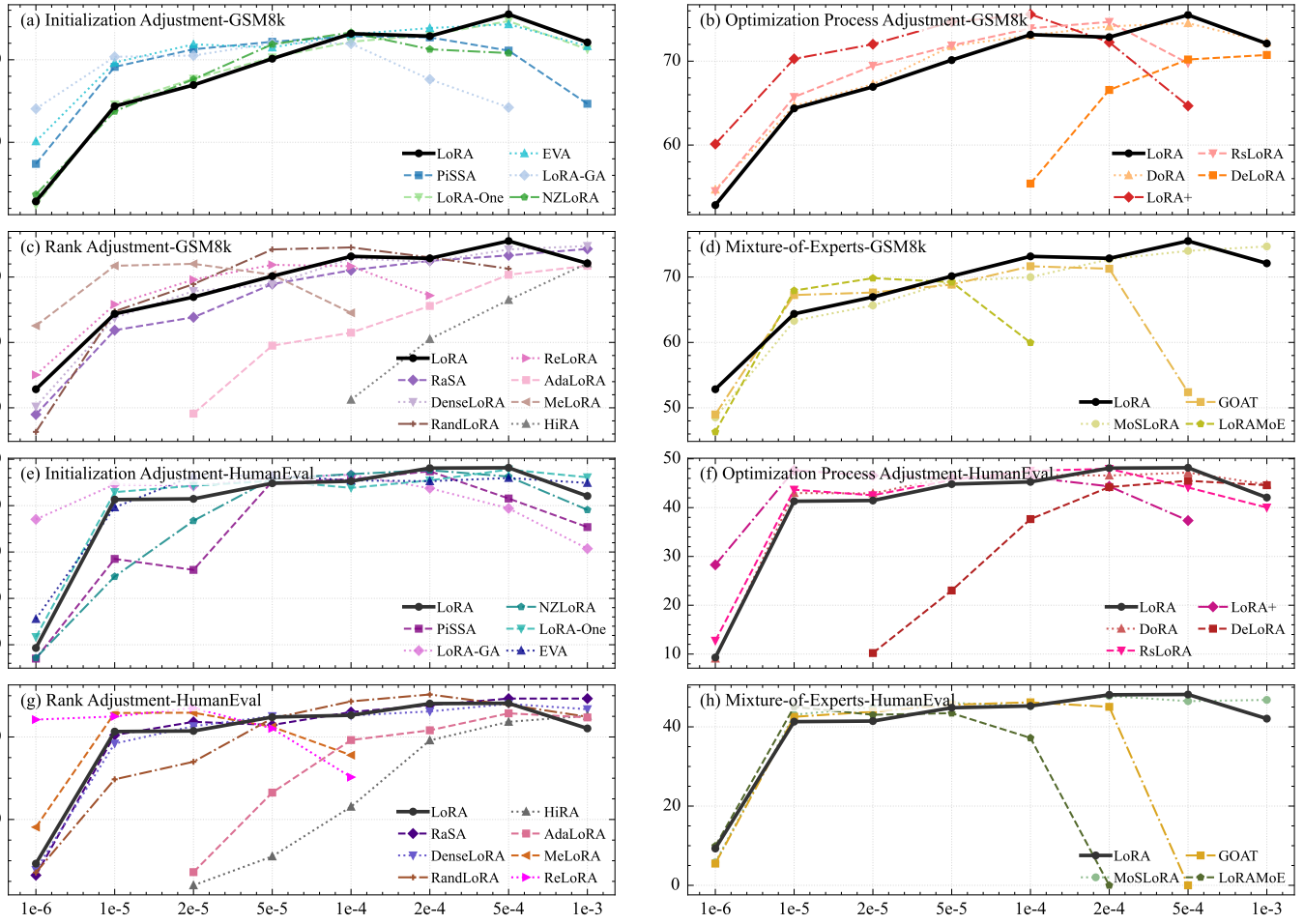


Fig. 7. Performance comparison of LoRA and its variants on GSM8K (accuracy) and HumanEval (pass@1) across a range of learning rates.

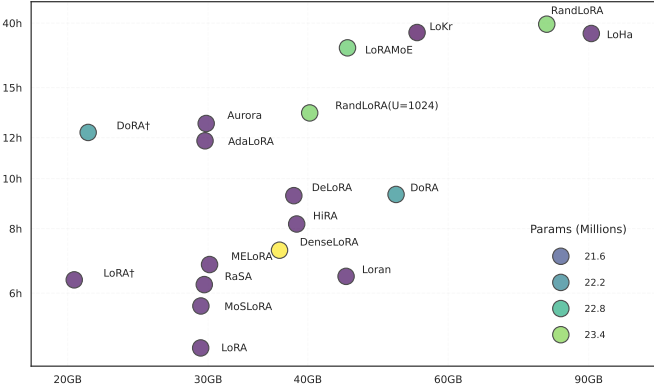


Fig. 8. Computational and memory overhead of LORA variants. \dagger denotes with activation checkpoint, and U is a hyperparameter of RANDLORA.

observed in NLU and IC experiments (**Key Finding**). This phenomenon arises from the *small-gradient issue* in vanilla LORA combined with improper hyperparameter configurations such as small learning rates or scaling factor, limited update steps, its parameter updates are not sufficient, hindering optimization. In contrast, variants like LORA-GA produce initial gradients $\sim 100\times$ larger, enabling effective learning in certain suboptimal hyperparameter regimes. However, when a proper set of hyperparameter configurations is adopted,

compensating for vanilla LORA’s inherent small gradients, thereby neutralizing the relative advantage of these variants.

Our findings suggest that prior studies, which often evaluate the performance using a fixed hyperparameter configuration, may have underestimated the performance of the most important baseline: LORA. Performance gains frequently disappear under comprehensive hyperparameter sweeps, underscoring the necessity of broad hyperparameter exploration for fair and robust evaluation of LORA methods.

V. CONCLUSION

In this work, we conduct a unified study of LORA and its variants. We organize all methods into four categories, establishing a fine-grained and structured taxonomy based on their principal operational axes. Further, we unify them under a review framework of low-rank update dynamics, illuminating their connections. Empirically, we introduce LoRAFactory, a modular and extensible codebase that implements 50+ LORA variants. Through extensive large-scale experiments, several key findings emerge. These results underscore the robust performance of the fundamental baseline, LORA, and emphasize the critical role of hyperparameter tuning, specifically the calibration of the learning rate, in ensuring equitable benchmarking within LORA research. By releasing all code and configurations, we hope this work provides a foundation for more rigorous and transparent evaluation.

REFERENCES

[1] Z. Liang, Y. Xu, Y. Hong, P. Shang, Q. Wang, Q. Fu, and K. Liu, “A survey of multimodel large language models,” in *Proceedings of the 3rd International Conference on Computer, Artificial Intelligence and Control Engineering*, 2024, pp. 405–409.

[2] Z. Li, X. Wu, H. Du, F. Liu, H. Nghiem, and G. Shi, “A survey of state of the art large vision language models: Alignment, benchmark, evaluations and challenges,” *arXiv preprint arXiv:2501.02189*, 2025.

[3] W. X. Zhao, K. Zhou, J. Li, T. Tang, X. Wang, Y. Hou, Y. Min, B. Zhang, J. Zhang, Z. Dong *et al.*, “A survey of large language models,” *arXiv preprint arXiv:2303.18223*, vol. 1, no. 2, 2023.

[4] P. Gao, J. Han, R. Zhang, Z. Lin, S. Geng, A. Zhou, W. Zhang, P. Lu, C. He, X. Yue *et al.*, “Llama-adapter v2: Parameter-efficient visual instruction model,” *arXiv preprint arXiv:2304.15010*, 2023.

[5] X. Liu, K. Ji, Y. Fu, W. L. Tam, Z. Du, Z. Yang, and J. Tang, “P-tuning v2: Prompt tuning can be comparable to fine-tuning universally across scales and tasks,” *arXiv preprint arXiv:2110.07602*, 2021.

[6] E. B. Zaken, S. Ravfogel, and Y. Goldberg, “Bitfit: Simple parameter-efficient fine-tuning for transformer-based masked language-models,” *arXiv preprint arXiv:2106.10199*, 2021.

[7] R. Karimi Mahabadi, J. Henderson, and S. Ruder, “Compacter: Efficient low-rank hypercomplex adapter layers,” *Advances in neural information processing systems*, vol. 34, pp. 1022–1035, 2021.

[8] E. J. Hu, Y. Shen, P. Wallis, Z. Allen-Zhu, Y. Li, S. Wang, L. Wang, W. Chen *et al.*, “Lora: Low-rank adaptation of large language models,” *ICLR*, vol. 1, no. 2, p. 3, 2022.

[9] D. P. Kingma and J. Ba, “Adam: A method for stochastic optimization,” *arXiv preprint arXiv:1412.6980*, 2014.

[10] I. Loshchilov and F. Hutter, “Decoupled weight decay regularization,” *arXiv preprint arXiv:1711.05101*, 2017.

[11] S. Rajbhandari, J. Rasley, O. Ruwase, and Y. He, “Zero: Memory optimizations toward training trillion parameter models,” in *SC20: International Conference for High Performance Computing, Networking, Storage and Analysis*. IEEE, 2020, pp. 1–16.

[12] Y. Zhao, A. Gu, R. Varma, L. Luo, C.-C. Huang, M. Xu, L. Wright, H. Shojanazeri *et al.*, “Pytorch fsdp: experiences on scaling fully sharded data parallel,” *arXiv preprint arXiv:2304.11277*, 2023.

[13] W. Su, Y. Tang, Q. Ai, J. Yan, C. Wang, H. Wang, Z. Ye, Y. Zhou, and Y. Liu, “Parametric retrieval augmented generation,” in *Proceedings of the 48th International ACM SIGIR Conference on Research and Development in Information Retrieval*, 2025, pp. 1240–1250.

[14] A. Zweiger, J. Pari, H. Guo, E. Akyürek, Y. Kim, and P. Agrawal, “Self-adapting language models,” *arXiv preprint arXiv:2506.10943*, 2025.

[15] Y. Wei, Y. Miao, D. Zhou, and D. Hu, “Moka: Multimodal low-rank adaptation for mllms,” *arXiv preprint arXiv:2506.05191*, 2025.

[16] H. Wang, Y. Ye, B. Li, Y. Nie, J. Lu, J. Tang, Y. Wang, and C. Huang, “Vision as lora,” *arXiv preprint arXiv:2503.20680*, 2025.

[17] S. Babakniya, A. R. Elkordy, Y. H. Ezzeldin, Q. Liu, K.-B. Song, M. El-Khamy, and S. Avestimehr, “Slora: Federated parameter efficient fine-tuning of language models,” *arXiv preprint arXiv:2308.06522*, 2023.

[18] J. Qi, Z. Luan, S. Huang, C. Fung, H. Yang, and D. Qian, “Fdlora: Personalized federated learning of large language model via dual lora tuning,” *arXiv preprint arXiv:2406.07925*, 2024.

[19] T. Dettmers, A. Pagnoni, A. Holtzman, and L. Zettlemoyer, “Qlora: Efficient finetuning of quantized llms,” *Advances in neural information processing systems*, vol. 36, pp. 10 088–10 115, 2023.

[20] Y. Li, Y. Yu, C. Liang, P. He, N. Karampatziakis, W. Chen, and T. Zhao, “Loftq: Lora-fine-tuning-aware quantization for large language models,” *arXiv preprint arXiv:2310.08659*, 2023.

[21] V. Lialin, N. Shivagunde, S. Muckatira, and A. Rumshisky, “Relora: High-rank training through low-rank updates,” *URL https://arxiv.org/abs/2307.05695*, 2023.

[22] Q. Zhang, M. Chen, A. Bukharin, N. Karampatziakis, P. He *et al.*, “Adalora: Adaptive budget allocation for parameter-efficient fine-tuning,” *arXiv preprint arXiv:2303.10512*, 2023.

[23] P. Albert, F. Z. Zhang, H. Saratchandran, C. Rodriguez-Opazo, A. v. d. Hengel, and E. Abbasnejad, “Randlora: Full-rank parameter-efficient fine-tuning of large models,” *arXiv preprint arXiv:2502.00987*, 2025.

[24] S. Hayou, N. Ghosh, and B. Yu, “Lora+: Efficient low rank adaptation of large models,” *arXiv preprint arXiv:2402.12354*, 2024.

[25] Z. Wang, J. Liang, R. He, Z. Wang, and T. Tan, “Lora-pro: Are low-rank adapters properly optimized?” in *International Conference on Learning Representations*, 2025.

[26] F. Meng, Z. Wang, and M. Zhang, “Pissa: Principal singular values and singular vectors adaptation of large language models,” in *Advances in Neural Information Processing Systems*, vol. 37, 2024, pp. 121 038–121 072.

[27] S. Wang, L. Yu, and J. Li, “Lora-ga: Low-rank adaptation with gradient approximation,” *Advances in Neural Information Processing Systems*, vol. 37, pp. 54 905–54 931, 2024.

[28] W. Feng, C. Hao, Y. Zhang, Y. Han, and H. Wang, “Mixture-of-loras: An efficient multitask tuning method for large language models,” in *Proceedings of the 2024 Joint International Conference on Computational Linguistics, Language Resources and Evaluation (LREC-COLING 2024)*, 2024, pp. 11 371–11 380.

[29] S. Mangrulkar, S. Gugger, L. Debut, Y. Belkada, S. Paul, B. Bossan, and M. Tietz, “PEFT: State-of-the-art parameter-efficient fine-tuning methods,” *https://github.com/huggingface/peft*, 2022.

[30] Y. Liu, M. Ott, N. Goyal, J. Du, M. Joshi, D. Chen, O. Levy, M. Lewis, L. Zettlemoyer, and V. Stoyanov, “Roberta: A robustly optimized bert pretraining approach,” *arXiv preprint arXiv:1907.11692*, 2019.

[31] A. Wang, A. Singh, J. Michael, F. Hill, O. Levy, and S. R. Bowman, “Glue: A multi-task benchmark and analysis platform for natural language understanding,” *arXiv preprint arXiv:1804.07461*, 2018.

[32] A. Radford, J. Wu, R. Child, D. Luan, D. Amodei, I. Sutskever *et al.*, “Language models are unsupervised multitask learners,” *OpenAI blog*, vol. 1, no. 8, p. 9, 2019.

[33] J. Novikova, O. Dušek, and V. Rieser, “The e2e dataset: New challenges for end-to-end generation,” *arXiv preprint arXiv:1706.09254*, 2017.

[34] T. Brown, B. Mann, N. Ryder, M. Subbiah, J. D. Kaplan, P. Dhariwal, A. Neelakantan, P. Shyam, G. Sastry, A. Askell *et al.*, “Language models are few-shot learners,” *Advances in neural information processing systems*, vol. 33, pp. 1877–1901, 2020.

[35] V. Zhong, C. Xiong, and R. Socher, “Seq2sql: Generating structured queries from natural language using reinforcement learning,” *arXiv preprint arXiv:1709.00103*, 2017.

[36] B. Gliwa, I. Mochol, M. Biesek, and A. Wawer, “Samsum corpus: A human-annotated dialogue dataset for abstractive summarization,” *arXiv preprint arXiv:1911.12237*, 2019.

[37] A. Dubey, A. Jauhri, A. Pandey, A. Kadian, A. Al-Dahle, A. Letman, A. Mathur, A. Schelten, A. Yang, A. Fan *et al.*, “The llama 3 herd of models,” *arXiv e-prints*, pp. arXiv–2407, 2024.

[38] A. Yang, A. Li, B. Yang, B. Zhang, B. Hui, B. Zheng, B. Yu, C. Gao, C. Huang, C. Lv *et al.*, “Qwen3 technical report,” *arXiv preprint arXiv:2505.09388*, 2025.

[39] X. Meng, D. Dai, W. Luo, Z. Yang, S. Wu, X. Wang, P. Wang, Q. Dong, L. Chen, and Z. Sui, “Periodiclora: Breaking the low-rank bottleneck in lora optimization,” *arXiv preprint arXiv:2402.16141*, 2024.

[40] W. Xia, C. Qin, and E. Hazan, “Chain of lora: Efficient finetuning of language models via residual learning,” *arXiv preprint arXiv:2401.04151*, 2024.

[41] Y. Zhang, H. Zhu, A. Liu, H. Yu, P. Koniusz, and I. King, “Less is more: Extreme gradient boost rank-1 adaption for efficient finetuning of llms,” *arXiv preprint arXiv:2410.19694*, 2024.

[42] P. Ren, C. Shi, S. Wu, M. Zhang, Z. Ren, M. de Rijke, Z. Chen, and J. Pei, “Melora: Mini-ensemble low-rank adapters for parameter-efficient fine-tuning,” *arXiv preprint arXiv:2402.17263*, 2024.

[43] N. Hyeon-Woo, M. Ye-Bin, and T.-H. Oh, “Fedpara: Low-rank hadamard product for communication-efficient federated learning,” *arXiv preprint arXiv:2108.06098*, 2021.

[44] S.-Y. Yeh, Y.-G. Hsieh, Z. Gao, B. B. Yang, G. Oh, and Y. Gong, “Navigating text-to-image customization: From lycoris fine-tuning to model evaluation,” in *The Twelfth International Conference on Learning Representations*, 2023.

[45] Q. Huang, T. Ko, Z. Zhuang, L. Tang, and Y. Zhang, “Hira: Parameter-efficient hadamard high-rank adaptation for large language models,” *Advancing Adaptation Techniques for Personalised Dialogue and Conversational AI*, p. 124, 2024.

[46] T. Jiang, S. Huang, S. Luo, Z. Zhang, H. Huang, F. Wei *et al.*, “Mora: High-rank updating for parameter-efficient fine-tuning,” *arXiv preprint arXiv:2405.12130*, 2024.

[47] Y. Song, J. Zhao, I. G. Harris, and S. A. Jyothi, “Sharelora: Parameter efficient and robust large language model fine-tuning via shared low-rank adaptation,” *arXiv preprint arXiv:2406.10785*, 2024.

[48] D. J. Kopiczko, T. Blankevoort, and Y. M. Asano, “Vera: Vector-based random matrix adaptation,” *arXiv preprint arXiv:2310.11454*, 2023.

[49] Z. He, Z. Tu, X. Wang, X. Chen, Z. Wang, J. Xu, T. Liang, W. Jiao, Z. Zhang, and R. Wang, “Rasa: Rank-sharing low-rank adaptation,” *arXiv preprint arXiv:2503.12576*, 2025.

[50] L. Mu, X. Wang, L. Ni, Y. Li, Z. Wu, P. Jin, and Y. Zhang, “Denselora: Dense low-rank adaptation of large language models,” *arXiv preprint arXiv:2505.23808*, 2025.

[51] S. Wang, B. Xue, J. Ye, J. Jiang, L. Chen, L. Kong, and C. Wu, “Prolora: Partial rotation empowers more parameter-efficient lora,” *arXiv preprint arXiv:2402.16902*, 2024.

[52] Y. Zhou, R. Li, C. Zhou, F. Yang, and A. Pan, “Bslora: Enhancing the parameter efficiency of lora with intra-layer and inter-layer sharing,” in *Forty-second International Conference on Machine Learning*.

[53] A. Renduchintala, T. Konuk, and O. Kuchaiev, “Tied-lora: Enhancing parameter efficiency of lora with weight tying,” *arXiv preprint arXiv:2311.09578*, 2023.

[54] Y. Li, S. Han, and S. Ji, “Vb-lora: Extreme parameter efficient fine-tuning with vector banks,” *Advances in Neural Information Processing Systems*, vol. 37, pp. 16742–16751, 2024.

[55] M. Li, P. Ye, J. Ye, H. He, and T. Chen, “E²lora: Efficient and effective low-rank adaptation with entropy-guided adaptive sharing,” in *International Conference on Learning Representations*, 2026.

[56] Y. Hu, Y. Xie, T. Wang, M. Chen, and Z. Pan, “Structure-aware low-rank adaptation for parameter-efficient fine-tuning,” *Mathematics*, vol. 11, no. 20, p. 4317, 2023.

[57] N. Ding, X. Lv, Q. Wang, Y. Chen, B. Zhou, Z. Liu, and M. Sun, “Sparse low-rank adaptation of pre-trained language models,” *arXiv preprint arXiv:2311.11696*, 2023.

[58] R. Zhang, R. Qiang, S. A. Somayajula, and P. Xie, “Autolora: Automatically tuning matrix ranks in low-rank adaptation based on meta learning,” *arXiv preprint arXiv:2403.09113*, 2024.

[59] F. Zhang, L. Li, J. Chen, Z. Jiang, B. Wang, and Y. Qian, “Increlora: Incremental parameter allocation method for parameter-efficient fine-tuning,” *arXiv preprint arXiv:2308.12043*, 2023.

[60] Z. Liu, J. Lyn, W. Zhu, X. Tian, and Y. Graham, “Alora: Allocating low-rank adaptation for fine-tuning large language models,” *arXiv preprint arXiv:2403.16187*, 2024.

[61] R. Qiang, R. Zhang, and P. Xie, “Bilora: A bi-level optimization framework for overfitting-resilient low-rank adaptation of large pre-trained models,” *arXiv preprint arXiv:2403.13037*, 2024.

[62] H. He, P. Ye, Y. Ren, Y. Yuan, L. Zhou, S. Ju, and L. Chen, “Gora: Gradient-driven adaptive low rank adaptation,” in *The Thirty-ninth Annual Conference on Neural Information Processing Systems*, 2025.

[63] J. Ye, H. He, M. Li, F. Han, T. Chen, and P. Ye, “Gradient intrinsic dimensionality alignment: Narrowing the gap between low-rank adaptation and full fine-tuning,” in *International Conference on Learning Representations*, 2026.

[64] F. Paischer, L. Hauzenberger, T. Schmied, B. Alkin, M. P. Deisenroth, and S. Hochreiter, “Parameter efficient fine-tuning via explained variance adaptation,” *arXiv preprint arXiv:2410.07170*, 2024.

[65] D. Kalajdzievski, “A rank stabilization scaling factor for fine-tuning with lora,” *arXiv preprint arXiv:2312.03732*, 2023.

[66] F. Zhang and M. Pilanci, “Riemannian preconditioned lora for fine-tuning foundation models,” *arXiv preprint arXiv:2402.02347*, 2024.

[67] S.-Y. Liu, C.-Y. Wang, H. Yin, P. Molchanov, Y.-C. F. Wang, K.-T. Cheng, and M.-H. Chen, “Dora: Weight-decomposed low-rank adaptation,” in *Forty-first International Conference on Machine Learning*, 2024.

[68] M. Bini, L. Girrbach, and Z. Akata, “Delora: Decoupling angles and strength in low-rank adaptation,” *arXiv preprint arXiv:2503.18225*, 2025.

[69] J. Han, S. Zhang, and K. Zhang, “Dual decomposition of weights and singular value low rank adaptation,” *arXiv preprint arXiv:2505.14367*, 2025.

[70] Y. Hao, Y. Cao, and L. Mou, “Flora: Low-rank adapters are secretly gradient compressors,” *arXiv preprint arXiv:2402.03293*, 2024.

[71] C. Si, X. Wang, X. Yang, Z. Xu, Q. Li, J. Dai, Y. Qiao, X. Yang, and W. Shen, “Flora: Low-rank core space for n-dimension,” *arXiv preprint arXiv:2405.14739*, vol. 10, 2024.

[72] H. Dong, W. Zhu, G. Song, and L. Wang, “Aurora: Breaking low-rank bottleneck of lora with nonlinear mapping,” *arXiv preprint arXiv:2505.18738*, 2025.

[73] Y. Ji, H. Saratchandran, C. Gordon, Z. Zhang, and S. Lucey, “Efficient learning with sine-activated low-rank matrices,” *arXiv preprint arXiv:2403.19243*, 2024.

[74] Y. Li, L. Song, and H. Hou, “Loran: Improved low-rank adaptation by a non-linear transformation,” in *Findings of the Association for Computational Linguistics: EMNLP 2024*, 2024, pp. 3134–3143.

[75] J. Liu, T. Koike-Akino, P. Wang, M. Brand, K. Parsons, and Y. Wang, “Loda: Low-dimensional adaptation of large language models,” in *Enhancing LLM Performance: Efficacy, Fine-Tuning, and Inference Techniques*. Springer, 2025, pp. 67–81.

[76] S. Li, X. Luo, X. Tang, H. Wang, H. Chen, Y. Li, R. Li *et al.*, “Beyond zero initialization: Investigating the impact of non-zero initialization on lora fine-tuning dynamics,” in *Forty-second International Conference on Machine Learning*.

[77] S. Hayou, N. Ghosh, and B. Yu, “The impact of initialization on lora finetuning dynamics,” *Advances in Neural Information Processing Systems*, vol. 37, pp. 117015–117040, 2024.

[78] H. Wang, Y. Li, S. Wang *et al.*, “Milora: Harnessing minor singular components for parameter-efficient llm finetuning,” in *Proceedings of the 2025 Conference of the Nations of the Americas Chapter of the Association for Computational Linguistics: Human Language Technologies (Volume 1: Long Papers)*, 2025, pp. 4823–4836.

[79] C. Lin, L. Li, D. Li, J. Zou, W. Xue, and Y. Guo, “Nora: Nested low-rank adaptation for efficient fine-tuning large models,” *arXiv preprint arXiv:2408.10280*, 2024.

[80] C. Guo, Y. Wu, and Y. Chang, “Nlora: Nystr\” om-initiated low-rank adaptation for large language models,” *arXiv preprint arXiv:2502.14482*, 2025.

[81] Y. Cao and Z. Song, “Sorsa: Singular values and orthonormal regularized singular vectors adaptation of large language models,” *arXiv preprint arXiv:2409.00055*, 2024.

[82] Y. Zhang, F. Liu, and Y. Chen, “Lora-one: One-step full gradient could suffice for fine-tuning large language models, provably and efficiently,” *arXiv preprint arXiv:2502.01235*, 2025.

[83] C. Si, Z. Shi, S. Zhang, X. Yang, H. Pfister, and W. Shen, “Task-specific directions: Definition, exploration, and utilization in parameter efficient fine-tuning,” *arXiv preprint arXiv:2409.01035*, 2024.

[84] Y. Yang, X. Li, Z. Zhou, S. Song, J. Wu *et al.*, “Corda: Context-oriented decomposition adaptation of large language models for task-aware parameter-efficient fine-tuning,” in *Advances in Neural Information Processing Systems*, vol. 37, 2024, pp. 71768–71791.

[85] T. Luo, J. Lei, F. Lei, W. Liu, S. He, J. Zhao, and K. Liu, “Moelora: Contrastive learning guided mixture of experts on parameter-efficient fine-tuning for large language models,” *arXiv preprint arXiv:2402.12851*, 2024.

[86] S. Dou, E. Zhou, Y. Liu, S. Gao, J. Zhao, W. Shen, Y. Zhou, Z. Xi, X. Wang, X. Fan *et al.*, “Loramoe: Alleviate world knowledge forgetting in large language models via moe-style plugin,” *arXiv preprint arXiv:2312.09979*, 2023.

[87] W. Feng, C. Hao, Y. Zhang, Y. Han, and H. Wang, “Mixture-of-loras: An efficient multitask tuning for large language models,” *arXiv preprint arXiv:2403.03432*, 2024.

[88] Z. Liu and J. Luo, “Adamole: Fine-tuning large language models with adaptive mixture of low-rank adaptation experts,” *arXiv preprint arXiv:2405.00361*, 2024.

[89] C. Gao, K. Chen, J. Rao, B. Sun, R. Liu, D. Peng, Y. Zhang, X. Guo, J. Yang, and V. Subrahmanian, “Higher layers need more lora experts,” *arXiv preprint arXiv:2402.08562*, 2024.

[90] C. Fan, Z. Lu, S. Liu, C. Gu, X. Qu, W. Wei, and Y. Cheng, “Make lora great again: Boosting lora with adaptive singular values and mixture-of-experts optimization alignment,” *arXiv preprint arXiv:2502.16894*, 2025.

[91] C. Tian, Z. Shi, Z. Guo, L. Li, and C.-Z. Xu, “Hydralora: An asymmetric lora architecture for efficient fine-tuning,” *Advances in Neural Information Processing Systems*, vol. 37, pp. 9565–9584, 2024.

[92] T. Wu, J. Wang, Z. Zhao, and N. Wong, “Mixture-of-subspaces in low-rank adaptation,” *arXiv preprint arXiv:2406.11909*, 2024.

[93] Y. Wang, Y. Lin, X. Zeng, and G. Zhang, “Multilora: Democratizing lora for better multi-task learning,” *arXiv preprint arXiv:2311.11501*, 2023.

[94] Y. Zhu, N. Wichters, C.-C. Lin, X. Wang, T. Chen, L. Shu, H. Lu, C. Liu, L. Luo, J. Chen *et al.*, “Sira: Sparse mixture of low rank adaptation,” *arXiv preprint arXiv:2311.09179*, 2023.

[95] A. Agiza, M. Neseem, and S. Reda, “Mtlora: Low-rank adaptation approach for efficient multi-task learning,” in *Proceedings of the IEEE/CVF conference on computer vision and pattern recognition*, 2024, pp. 16196–16205.

[96] Y. Yang, P.-T. Jiang, Q. Hou, H. Zhang, J. Chen, and B. Li, “Multi-task dense prediction via mixture of low-rank experts,” in *Proceedings of the IEEE/CVF conference on computer vision and pattern recognition*, 2024, pp. 27927–27937.

[97] S. Chen, Z. Jie, and L. Ma, “Llava-mole: Sparse mixture of lora experts for mitigating data conflicts in instruction finetuning mllms,” *arXiv preprint arXiv:2401.16160*, 2024.

[98] C. Li, H. Farkhoor, R. Liu, and J. Yosinski, “Measuring the intrinsic dimension of objective landscapes,” *arXiv preprint arXiv:1804.08838*, 2018.

[99] D. Biderman, J. Portes, J. J. G. Ortiz, M. Paul, P. Greengard, C. Jennings, D. King, S. Havens, V. Chiley, J. Frankle *et al.*, “Lora learns less and forgets less,” *arXiv preprint arXiv:2405.09673*, 2024.

[100] R. Shuttleworth, J. Andreas, A. Torralba, and P. Sharma, “Lora vs full fine-tuning: An illusion of equivalence,” *arXiv preprint arXiv:2410.21228*, 2024.

[101] L. Zhang, L. Zhang, S. Shi, X. Chu, and B. Li, “Lora-fa: Memory-efficient low-rank adaptation for large language models fine-tuning,” *arXiv preprint arXiv:2308.03303*, 2023.

[102] J. Zhu, K. Greenwald, K. Nadjahi, H. S. D. O. Borde, R. B. Gabrielson, L. Choshen, M. Ghassemi, M. Yurochkin, and J. Solomon, “Asymmetry in low-rank adapters of foundation models,” *arXiv preprint arXiv:2402.16842*, 2024.

[103] S. Ghosh, C. K. R. Evuru, S. Kumar, D. Aneja, Z. Jin, R. Duraiswami, D. Manocha *et al.*, “A closer look at the limitations of instruction tuning,” *arXiv preprint arXiv:2402.05119*, 2024.

[104] M. McCloskey and N. J. Cohen, “Catastrophic interference in connectionist networks: The sequential learning problem,” in *Psychology of learning and motivation*. Elsevier, 1989, vol. 24, pp. 109–165.

[105] J. Schulman and T. M. Lab, “Lora without regret,” *Thinking Machines Lab: Connectionism*, 2025, <https://thinkingmachines.ai/blog/lora/>.

[106] N. Shazeer and M. Stern, “Adafactor: Adaptive learning rates with sublinear memory cost,” in *International Conference on Machine Learning*. PMLR, 2018, pp. 4596–4604.

[107] J. Ren, S. Rajbhandari, R. Y. Aminabadi, O. Ruwase, S. Yang, M. Zhang, D. Li, and Y. He, “{Zero-offload}: Democratizing {billion-scale} model training,” in *2021 USENIX Annual Technical Conference (USENIX ATC 21)*, 2021, pp. 551–564.

[108] M. Frank, P. Wolfe *et al.*, “An algorithm for quadratic programming,” *Naval research logistics quarterly*, vol. 3, no. 1-2, pp. 95–110, 1956.

[109] T. Chen and C. Guestrin, “Xgboost: A scalable tree boosting system,” in *Proceedings of the 22nd ACM SIGKDD international conference on knowledge discovery and data mining*, 2016, pp. 785–794.

[110] A. Edalati, M. Tahaei, I. Kobyzev, V. P. Nia, J. J. Clark, and M. Rezagholizadeh, “Krona: Parameter-efficient tuning with kronecker adapter,” in *Enhancing LLM Performance: Efficacy, Fine-Tuning, and Inference Techniques*. Springer, 2025, pp. 49–65.

[111] M. Dehghani, S. Gouws, O. Vinyals, J. Uszkoreit, and L. Kaiser, “Universal transformers,” *arXiv preprint arXiv:1807.03819*, 2018.

[112] S. Takase and S. Kiyono, “Lessons on parameter sharing across layers in transformers,” *arXiv preprint arXiv:2104.06022*, 2021.

[113] K. Lu, A. Grover, P. Abbeel, and I. Mordatch, “Frozen pretrained transformers as universal computation engines,” in *Proceedings of the AAAI conference on artificial intelligence*, vol. 36, no. 7, 2022, pp. 7628–7636.

[114] M. Schrimpf, I. A. Blank, G. Tuckute, C. Kauf, E. A. Hosseini, N. Kanwisher, J. B. Tenenbaum, and E. Fedorenko, “The neural architecture of language: Integrative modeling converges on predictive processing,” *Proceedings of the National Academy of Sciences*, vol. 118, no. 45, p. e2105646118, 2021.

[115] J. Frankle, D. J. Schwab, and A. S. Mordcos, “Training batchnorm and only batchnorm: On the expressive power of random features in cnns,” *arXiv preprint arXiv:2003.00152*, 2020.

[116] S. Lin, P. Lyu, D. Liu, T. Tang, X. Liang, A. Song, and X. Chang, “Mlp can be a good transformer learner,” in *Proceedings of the IEEE/CVF Conference on Computer Vision and Pattern Recognition*, 2024, pp. 19489–19498.

[117] Y. Mao, K. Huang, C. Guan, G. Bao, F. Mo, and J. Xu, “Dora: Enhancing parameter-efficient fine-tuning with dynamic rank distribution,” *arXiv preprint arXiv:2405.17357*, 2024.

[118] N. Ding, X. Lv, Q. Wang, Y. Chen, B. Zhou, Z. Liu, and M. Sun, “Sparse low-rank adaptation of pre-trained language models,” *arXiv preprint arXiv:2311.11696*, 2023.

[119] H. Rajabzadeh, M. Valipour, T. Zhu, M. Tahaei, H. J. Kwon, A. Ghodsi, B. Chen, and M. Rezagholizadeh, “Qdylora: Quantized dynamic low-rank adaptation for efficient large language model tuning,” *arXiv preprint arXiv:2402.10462*, 2024.

[120] B. Mishra and R. Sepulchre, “Riemannian preconditioning,” *SIAM Journal on Optimization*, vol. 26, no. 1, pp. 635–660, 2016.

[121] M. Bini, K. Roth, Z. Akata, and A. Khoreva, “Ether: Efficient finetuning of large-scale models with hyperplane reflections,” *arXiv preprint arXiv:2405.20271*, 2024.

[122] J. Zhao, Z. Zhang, B. Chen, Z. Wang, A. Anandkumar, and Y. Tian, “Galore: Memory-efficient llm training by gradient low-rank projection,” *arXiv preprint arXiv:2403.03507*, 2024.

[123] C. Si, X. Yang, and W. Shen, “See further for parameter efficient fine-tuning by standing on the shoulders of decomposition,” *arXiv preprint arXiv:2407.05417*, 2024.

[124] K. He, X. Zhang, S. Ren, and J. Sun, “Deep residual learning for image recognition,” in *Proceedings of the IEEE conference on computer vision and pattern recognition*, 2016, pp. 770–778.

[125] G. Montavon, G. Orr, and K.-R. Müller, *Neural networks: tricks of the trade*. Springer, 2012, vol. 7700.

[126] C. Eckart and G. Young, “The approximation of one matrix by another of lower rank,” *Psychometrika*, vol. 1, no. 3, pp. 211–218, 1936.

[127] L. Mirsky, “Symmetric gauge functions and unitarily invariant norms,” *The quarterly journal of mathematics*, vol. 11, no. 1, pp. 50–59, 1960.

[128] S. Azizi, S. Kundu, and M. Pedram, “Lamda: Large model fine-tuning via spectrally decomposed low-dimensional adaptation,” *arXiv preprint arXiv:2406.12832*, 2024.

[129] K. Büyükköyüt, “Olora: Orthonormal low-rank adaptation of large language models,” *arXiv preprint arXiv:2406.01775*, 2024.

[130] K. Lv, Y. Yang, T. Liu, Q. Gao, Q. Guo, and X. Qiu, “Full parameter fine-tuning for large language models with limited resources,” *arXiv preprint arXiv:2306.09782*, 2023.

[131] K. Ponkshe, R. Singhal, E. Gorbunov, A. Tumanov, S. Horvath, and P. Vepakomma, “Initialization using update approximation is a silver bullet for extremely efficient low-rank fine-tuning,” *arXiv preprint arXiv:2411.19557*, 2024.

[132] D. A. Ross, J. Lim, R.-S. Lin, and M.-H. Yang, “Incremental learning for robust visual tracking,” *International journal of computer vision*, vol. 77, no. 1, pp. 125–141, 2008.

[133] N. Halko, P.-G. Martinsson, and J. A. Tropp, “Finding structure with randomness: Probabilistic algorithms for constructing approximate matrix decompositions,” *SIAM review*, vol. 53, no. 2, pp. 217–288, 2011.

[134] A. Radford, J. W. Kim, C. Hallacy, A. Ramesh, G. Goh, S. Agarwal, G. Sastry, A. Askell, P. Mishkin, J. Clark *et al.*, “Learning transferable visual models from natural language supervision,” in *International conference on machine learning*. PMLR, 2021, pp. 8748–8763.

[135] J. Krause, M. Stark, J. Deng, and L. Fei-Fei, “3d object representations for fine-grained categorization,” in *Proceedings of the IEEE international conference on computer vision workshops*, 2013, pp. 554–561.

[136] M. Cimpoi, S. Maji, I. Kokkinos, S. Mohamed, and A. Vedaldi, “Describing textures in the wild,” in *Proceedings of the IEEE conference on computer vision and pattern recognition*, 2014, pp. 3606–3613.

[137] P. Helber, B. Bischke, A. Dengel, and D. Borth, “Eurosat: A novel dataset and deep learning benchmark for land use and land cover classification,” *IEEE Journal of Selected Topics in Applied Earth Observations and Remote Sensing*, vol. 12, no. 7, pp. 2217–2226, 2019.

[138] S. Houben, J. Stallkamp, J. Salmen, M. Schlipsing, and C. Igel, “Detection of traffic signs in real-world images: The german traffic sign detection benchmark,” in *The 2013 international joint conference on neural networks (IJCNN)*. Ieee, 2013, pp. 1–8.

[139] G. Cheng, J. Han, and X. Lu, “Remote sensing image scene classification: Benchmark and state of the art,” *Proceedings of the IEEE*, vol. 105, no. 10, pp. 1865–1883, 2017.

[140] J. Xiao, J. Hays, K. A. Ehinger, A. Oliva, and A. Torralba, “Sun database: Large-scale scene recognition from abbey to zoo,” in *2010 IEEE computer society conference on computer vision and pattern recognition*. IEEE, 2010, pp. 3485–3492.

[141] Y. Netzer, T. Wang, A. Coates, A. Bissacco, B. Wu, A. Y. Ng *et al.*, “Reading digits in natural images with unsupervised feature learning,” in *NIPS workshop on deep learning and unsupervised feature learning*, vol. 2011, no. 2. Granada, 2011, p. 4.

[142] L. Yu, W. Jiang, H. Shi, J. Yu, Z. Liu, Y. Zhang, J. T. Kwok, Z. Li, A. Weller, and W. Liu, “Metamath: Bootstrap your own mathematical questions for large language models,” *arXiv preprint arXiv:2309.12284*, 2023.

[143] K. Cobbe, V. Kosaraju, M. Bavarian, M. Chen, H. Jun, L. Kaiser, M. Plappert, J. Tworek, J. Hilton, R. Nakano *et al.*, “Training verifiers to solve math word problems,” *arXiv preprint arXiv:2110.14168*, 2021.

[144] T. Zheng, G. Zhang, T. Shen, X. Liu, B. Y. Lin, J. Fu, W. Chen, and X. Yue, “Opencodeinterpreter: Integrating code generation with execution and refinement,” *arXiv preprint arXiv:2402.14658*, 2024.

[145] M. Chen, J. Tworek, H. Jun *et al.*, “Evaluating large language models trained on code,” 2021.

- [146] Z. Han, C. Gao, J. Liu, J. Zhang, and S. Q. Zhang, “Parameter-efficient fine-tuning for large models: A comprehensive survey,” *arXiv preprint arXiv:2403.14608*, 2024.
- [147] L. Wang, S. Chen, L. Jiang, S. Pan, R. Cai, S. Yang, and F. Yang, “Parameter-efficient fine-tuning in large models: A survey of methodologies,” *arXiv preprint arXiv:2410.19878*, 2024.
- [148] L. Xu, H. Xie, S.-Z. J. Qin, X. Tao, and F. L. Wang, “Parameter-efficient fine-tuning methods for pretrained language models: A critical review and assessment,” *arXiv preprint arXiv:2312.12148*, 2023.
- [149] Y. Mao, Y. Ge, Y. Fan, W. Xu, Y. Mi, Z. Hu, and Y. Gao, “A survey on lora of large language models,” *Frontiers of Computer Science*, vol. 19, no. 7, p. 197605, 2025.
- [150] M. Yang, J. Chen, Y. Zhang, J. Liu, J. Zhang, Q. Ma, H. Verma, Q. Zhang, M. Zhou, I. King *et al.*, “Low-rank adaptation for foundation models: A comprehensive review,” *arXiv preprint arXiv:2501.00365*, 2024.
- [151] N. Houlsby, A. Giurgiu, S. Jastrzebski, B. Morrone, Q. De Laroussilhe, A. Gesmundo, M. Attariyan, and S. Gelly, “Parameter-efficient transfer learning for nlp,” in *International conference on machine learning*. PMLR, 2019, pp. 2790–2799.
- [152] P. He, X. Liu, J. Gao, and W. Chen, “Deberta: Decoding-enhanced bert with disentangled attention,” *arXiv preprint arXiv:2006.03654*, 2020.
- [153] B. Zi, X. Qi, L. Wang, J. Wang, K.-F. Wong, and L. Zhang, “Delta-lora: Fine-tuning high-rank parameters with the delta of low-rank matrices,” *arXiv preprint arXiv:2309.02411*, 2023.
- [154] C. Raffel, N. Shazeer, A. Roberts, K. Lee, S. Narang, M. Matena, Y. Zhou, W. Li, and P. J. Liu, “Exploring the limits of transfer learning with a unified text-to-text transformer,” *Journal of machine learning research*, vol. 21, no. 140, pp. 1–67, 2020.
- [155] H. Touvron, L. Martin, K. Stone, P. Albert, A. Almahairi, Y. Babaei, N. Bashlykov, S. Batra, P. Bhargava, S. Bhosale *et al.*, “Llama 2: Open foundation and fine-tuned chat models,” *arXiv preprint arXiv:2307.09288*, 2023.
- [156] H. Touvron, T. Lavril, G. Izacard, X. Martinet, M.-A. Lachaux, T. Lacroix, B. Rozière, N. Goyal, E. Hambro, F. Azhar *et al.*, “Llama: Open and efficient foundation language models,” *arXiv preprint arXiv:2302.13971*, 2023.
- [157] G. Team, T. Mesnard, C. Hardin, R. Dadashi, S. Bhupatiraju, S. Pathak, L. Sifre, M. Rivière, M. S. Kale, J. Love *et al.*, “Gemma: Open models based on gemini research and technology,” *arXiv preprint arXiv:2403.08295*, 2024.
- [158] G. Team, M. Rivière, S. Pathak, P. G. Sessa, C. Hardin, S. Bhupatiraju, L. Hussenot, T. Mesnard, B. Shahriari, A. Ramé *et al.*, “Gemma 2: Improving open language models at a practical size, 2024,” *URL https://arxiv.org/abs/2408.00118*, vol. 1, no. 3, 2024.
- [159] G. Team, A. Kamath, J. Ferret, S. Pathak, N. Vieillard, R. Merhej, S. Perrin, T. Matejovicova, A. Ramé, M. Rivière *et al.*, “Gemma 3 technical report,” *arXiv preprint arXiv:2503.19786*, 2025.
- [160] A. Dosovitskiy, L. Beyer, A. Kolesnikov, D. Weissenborn, X. Zhai, T. Unterthiner, M. Dehghani, M. Minderer, G. Heigold, S. Gelly *et al.*, “An image is worth 16x16 words: Transformers for image recognition at scale,” *arXiv preprint arXiv:2010.11929*, 2020.

APPENDIX

A. Related Works

1) *Survey of PEFT and LoRA*: Despite considerable survey attention on PEFT, its most influential method, LoRA, and its proliferating variants receive superficial coverage. Existing surveys treat LoRA as a minor component within broader PEFT taxonomies, offering only cursory lists or brief summaries. For example, Han et al. [146] include a short section on “Reparameterized PEFT” without detailed analysis or mathematical formulations. Wang et al. [147] catalog over 10 LoRA-inspired methods but provide merely enumerative descriptions lacking systematic categorization. Xu et al. [148] list 11 LoRA variants with formulations but do not analyze their underlying mechanisms or comparative advantages. Mao et al. [149] and Yang et al. [150] conduct comprehensive surveys yet still offer lists with brief explanations rather than deeper insights. In summary, while acknowledging LoRA’s popularity, these surveys lack a principled and in-depth examination. This gap motivates our work: a dedicated, systematic, and analytical survey tracing the evolution of LoRA variants, dissecting their innovations, and evaluating their trade-offs.

2) *Evaluation of LoRA and its Variants*: Evaluating LoRA and its variants is complex. The original LoRA paper [8] benchmarks LoRA against PEFT methods including BitFit [6] and adapter tuning [151] on models like RoBERTa [30], DeBERTa [152], GPT-2 [32], and GPT-3-175B [34]. Several follow-up studies [22], [61], [153] adhere to similar pipelines to demonstrate advantages over vanilla LoRA. However, the NLU evaluation pipeline for vanilla LoRA requires intensive hyperparameter grid searches, hindering large-scale comparisons. Its NLG pipeline uses outdated models like GPT-2/GPT-3 on tasks such as WikiSQL [35] and MNLI [31], which are not representative of current frontier models like the Llama3 series [37] or modern NLG scenarios. Recent LoRA variants are also evaluated on vision tasks alongside NLU and NLG. For NLU, the GLUE benchmark with models like RoBERTa, DeBERTa, and T5 [154] is common, with RoBERTa being the most frequent choice. For NLG, LLMs such as the Llama series [37], [155], [156] and Gemma series [157]–[159] are evaluated on commonsense reasoning, chat, mathematical reasoning, and code generation. For vision, ViT [160] and CLIP-ViT are commonly tested on image classification tasks. Considering this, our comprehensive evaluation tests RoBERTa-Base on GLUE for NLU, Llama-3.1-8B-Base on mathematical reasoning and code generation for NLG, and CLIP-ViT-16/B on seven image classification tasks for vision performance.

B. Notations

This section delineates the notations utilized throughout this paper. Unless otherwise indicated, all notations conform to the definitions presented in Table I.

C. Additional Experimental Results

Due to space constraints within the main body of the paper, this section presents supplementary experimental results of significance.

1) *Computational and Memory Overhead Analysis*: Table II presents the numerical training time and peak memory usage of some variants implemented in LoRAFactory (variants such as LORA+, which do not affect the efficiency of LORA, are not presented in this table). To ensure intrinsic efficiency is measured without masking effects from external optimizations, experiments were conducted on a single NVIDIA H200 GPU using the Llama-3.1-8B-Base model (BF16 mixed precision, sequence length 1024, batch size 1) without parallelism, CPU offloading, or activation checkpointing.

Vanilla LORA serves as the foundational baseline, achieving the lowest memory footprint (30,067 MB) and the fastest training time (4h 42m). In contrast, DORA exhibits the highest memory consumption (52,847 MB, +75%), primarily because methods like DORA, HiRA, and LOHA explicitly materialize low-rank matrices (A and B) and their product during the forward pass. Vanilla LoRA avoids this by fusing computation of low-rank weights, a benefit that persists unless activation checkpointing is applied. As the router in each LORAMOE module introduces additional trainable parameters, we compare the computational and memory overhead of LORAMOE with two settings: 8 total experts and 2 activated experts per module; 6 total experts and 2 activated experts per module, each expert with a rank of 1. Therefore, the prior setting has an identical overall rank of 8 with LORA, but it introduces significantly more trainable parameters. The latter setting has a comparable number of trainable parameters with LORA but a smaller overall rank. Both settings of LORAMOE require significantly longer training durations compared to LORA due to the mixture-of-experts architecture, which introduces significant overhead through learnable token routers. While MOSLORA, RASA, and MELORA maintain memory profiles similar to vanilla LoRA with moderate speed trade-offs, methods like ADALORA and RANDLORA suffer from prolonged training times due to dynamic rank allocation or high-rank computation strategies (The official implementation of RANDLORA adopts full-rank computation, which leads to high computational cost. We limit the upper bound of the dimension of random bases of RANDLORA to 1024, denoted as $\text{RANDLORA}_{U=1024}$). These results highlight the inherent tension between expressiveness and efficiency in LoRA extensions.

2) *Learning Rate Sweep Results on NLU Tasks*: **Experimental settings.** We fine-tune RoBERTa-base to evaluate LoRA and its variants on the full GLUE benchmark. We follow standard evaluation metrics for each GLUE sub-task: accuracy for SST-2, MNLI, MRPC, QNLI, and RTE; Pearson correlation for STS-B; F1 for QQP; and Matthews Correlation Coefficient for CoLA. We employ a linear learning rate decay schedule with a warm-up ratio of 0.03. Seven learning rates are tested for all methods, including: [1e-6, 1e-5, 5e-5, 1e-4, 5e-4, 1e-3, 5e-3].

All experimental settings remain consistent across runs. The batch size is 32, weight decay is disabled, and the maximum sequence length is 256 for all GLUE sub-tasks. Both the base model and all LoRA modules operate in FP32 precision without mixed-precision training. Each training run consists of 10 epochs, with the test performance recorded at the end of

TABLE I
LIST OF NOTATIONS

Symbol	Description
$W \in \mathbb{R}^{m \times n}$	Weight matrix of a linear layer.
$\tilde{W} \in \mathbb{R}^{m \times n}$	pretrained weight of W .
ΔW	Update applied to the weight W during fine-tuning.
$A \in \mathbb{R}^{m \times r}, B \in \mathbb{R}^{r \times n}$	Trainable low-rank matrices in the standard LoRA decomposition.
r	Rank hyperparameter of LoRA and its most variants, with $r \ll \min(m, n)$.
α	Scaling hyperparameter of LoRA and its most variants.
γ_r	Scaling factor of LoRA, $\gamma_r \rightarrow 0$ as $r \rightarrow \infty$.
η	Learning rate used for parameter updates.
$\nabla \tilde{W}$	Gradient of the pretrained weight \tilde{W} .
$\nabla A, \nabla B$	Gradients of the low-rank matrices A and B .
W_t	Weight matrix of a linear layer at fine-tuning step t ($W_t = \tilde{W} + \Delta W_t$).
A_t, B_t	Values of the low-rank matrices A and B at fine-tuning step t .
A_0, B_0	Initial values of the low-rank matrices A and B .
$\text{SVD}(M)$	Singular Value Decomposition of matrix M .
$\text{Tr}(M)$	Trace of matrix M .
U, S, V	Matrices from the SVD of a matrix, i.e., $M = USV^\top$.
\odot	Hadamard (element-wise) product of two matrices.
\otimes	Kronecker product of two matrices.
\oplus	Block-diagonal matrix constructor.
$[M_1 M_2 \dots M_n]$	Matrix concatenation operator.
$\mathcal{R}(M)$	Rank of matrix M .
$\ \cdot\ _F$	Frobenius norm of a matrix.
$\mathcal{L}_{\text{task}}$	Primary task-specific loss function (e.g., cross-entropy).
\mathcal{L}_{reg}	Auxiliary regularization loss (e.g., for orthogonality in AdaLoRA).
LoRAFactory	A unified, modular codebase developed in this work for benchmarking LoRA variants.
LLMs	Large Language Models
NLU	Natural Language Understanding.
NLG	Natural Language Generation.
IC	Image Classification.
PEFT	Parameter-Efficient Fine-Tuning.
MoE	Mixture of Experts.

TABLE II
COMPUTATIONAL AND MEMORY USAGE OF LoRA VARIANTS. \dagger DENOTES THE USE OF ACTIVATION CHECKPOINTING.

Method	#Params	Time	Memory
LoRA [8]	20.97M	4h42min	30067MB
LoRA † [8]	20.97M	6h22min	20873MB
DORA [67]	22.35M	9h19min	52847MB
DoRA † [67]	22.35M	12h17min	21729MB
DELoRA [68]	20.97M	9h16min	39343MB
ADALoRA [22]	20.97M	12h10min	30447MB
HIRA [45]	20.97M	8h10min	39669MB
RASA [49]	20.98M	6h14min	30381MB
DENSELoRA [50]	23.99M	7h16min	37751MB
RANDLoRA [23]	23.30M	39h31min	81645MB
RANDLoRA $_{U=1024}$ [23]	23.30M	13h24min	41187MB
MELORA [42]	20.97M	6h49min	30847MB
LoRAMoE $_{e=8}$ [86]	30.93M	36h31min	46425MB
LoRAMoE $_{e=6}$ [86]	23.20M	27h57min	45937MB
MoSLoRA [92]	20.99M	5h50min	30085MB
AURORA [72]	21.00M	12h32min	30549MB
LOHA [43]	20.97M	35h28min	92851MB
LOKR [44]	20.86M	35h53min	56151MB
LORAN [74]	20.97M	6h28min	45747MB

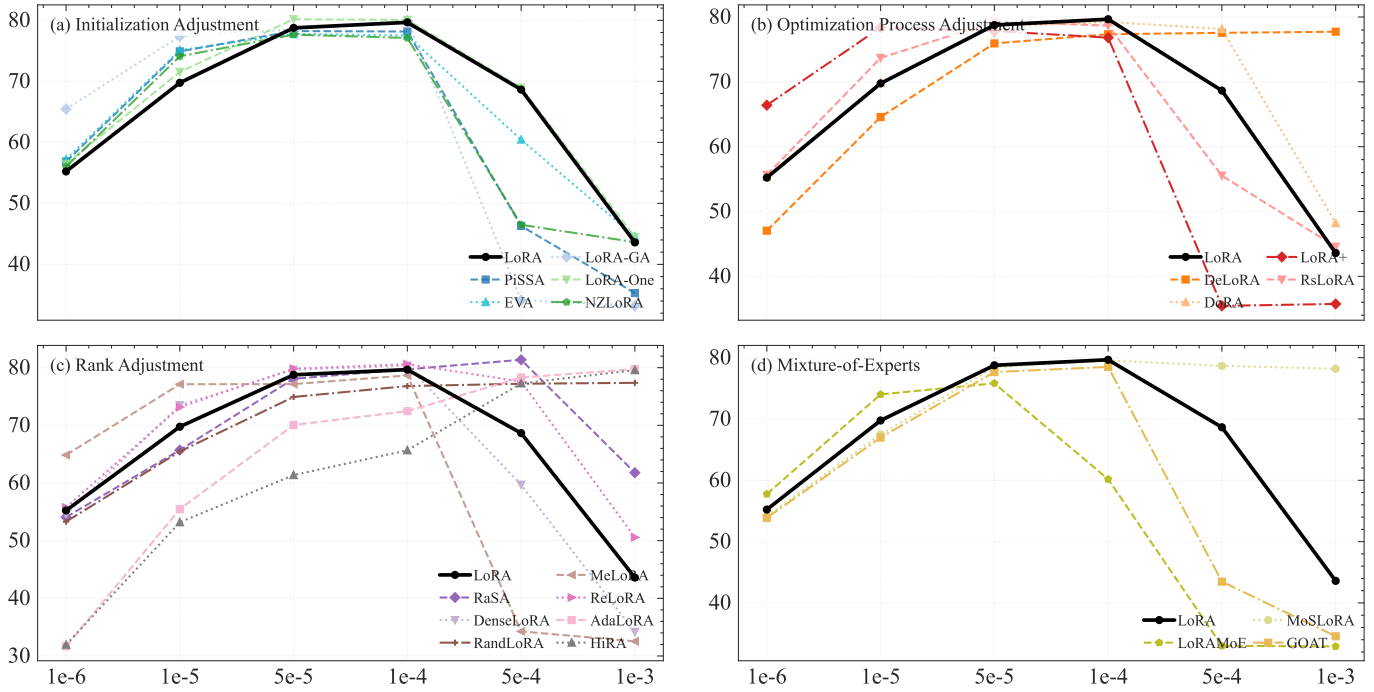


Fig. 9. Performance comparison of various LoRA variants on the GLUE benchmark across different learning rates. Results are grouped by method category as illustrated in Section II. All plots share the same y-axis (averaged numerical score) and x-axis (learning rate).

each epoch; the best test result across all 10 epochs is reported.

Experimental results. Figure 9 shows the average evaluation results on the 9 subsets of the GLUE benchmark. For the detailed numerical results of each subset, please refer to Table IV-X.

The average performance of LoRA attains a relatively modest value of 55.23 at the lowest learning rate examined, with performance progressively increasing to 79.66 as the learning rate rises to 1e-4. Among all tested variants, only RASA significantly exceeds LoRA in peak performance, achieving 81.37 at the learning rate of 5e-4.

All initialization-based LoRA variants significantly enhance gradient flow at small learning rates (e.g., 1e-5), leading to improved performance in such configurations. Similarly, MELORA incorporates a block-diagonal structure, which also amplifies the gradient magnitude in LoRA. However, these enhancements come at a cost: the improved gradient properties hinder convergence at higher learning rates, preventing these methods from reaching or surpassing the peak performance achievable with standard LoRA under such settings. Simultaneously, LoRA+ implements a learning rate decoupling strategy for the low-rank matrices A and B within low-rank adapters. For LoRA+, it is recommended that the learning rate for matrix B be set to 16 times that of matrix A . This approach effectively applies a higher learning rate to matrix B compared to standard LoRA under an equivalent base learning rate, which governs matrix A and other trainable parameters. In practice, while these variants perform well with smaller learning rates, their effectiveness diminishes, occasionally sharply, when larger learning rates are employed.

In contrast, the auxiliary loss in ADALORA, the weight decomposition strategies in DORA and DELORA, and the

Hadamard product operation between low-rank and pretrained weights in HIRA significantly impede convergence at small learning rates. For instance, HIRA achieves only 53.19 at a learning rate of 1e-5, which is 16.6 points lower than LoRA under the same setting. As a result, these methods require learning rates that are about 10 to 1000 times larger than those used by LoRA to achieve comparable performance. It should be noted that LoRA itself typically employs learning rates 10 to 100 times higher than those commonly used in full fine-tuning. Notably, most of these methods do not explicitly state in their original papers that they require such elevated learning rates. This observation highlights the importance of carefully selecting learning rates when applying these methods in practice, as their optimal values may differ significantly from those used in standard fine-tuning approaches.

For Mixture-of-Experts integration based LoRA Variants, both LoRAMoE and GOAT fail to surpass the performance of LoRA on most learning rates we tested, while requiring substantially more training and inference time. One possible reason is that under similar trainable parameter budgets, the inherently sparse structure of MoE-based methods can limit their overall performance. As a non-traditional mixture-of-experts approach, MoSLORA introduces a small intermediate matrix to the low-rank adapter, demonstrating greater stability with respect to learning rate selection than LoRA. Our experiments on NLG and IC also validate this observation.

3) Learning Rate Sweep Results on IC Tasks: Experimental settings For image classification tasks, we fine-tune CLIP-ViT-16/B on seven benchmark datasets: Stanford-Cars [135], DTD [136], EuroSAT [137], GTSRB [138], RESISC45 [139], SUN397 [140], and SVHN [141]. Each method's classification

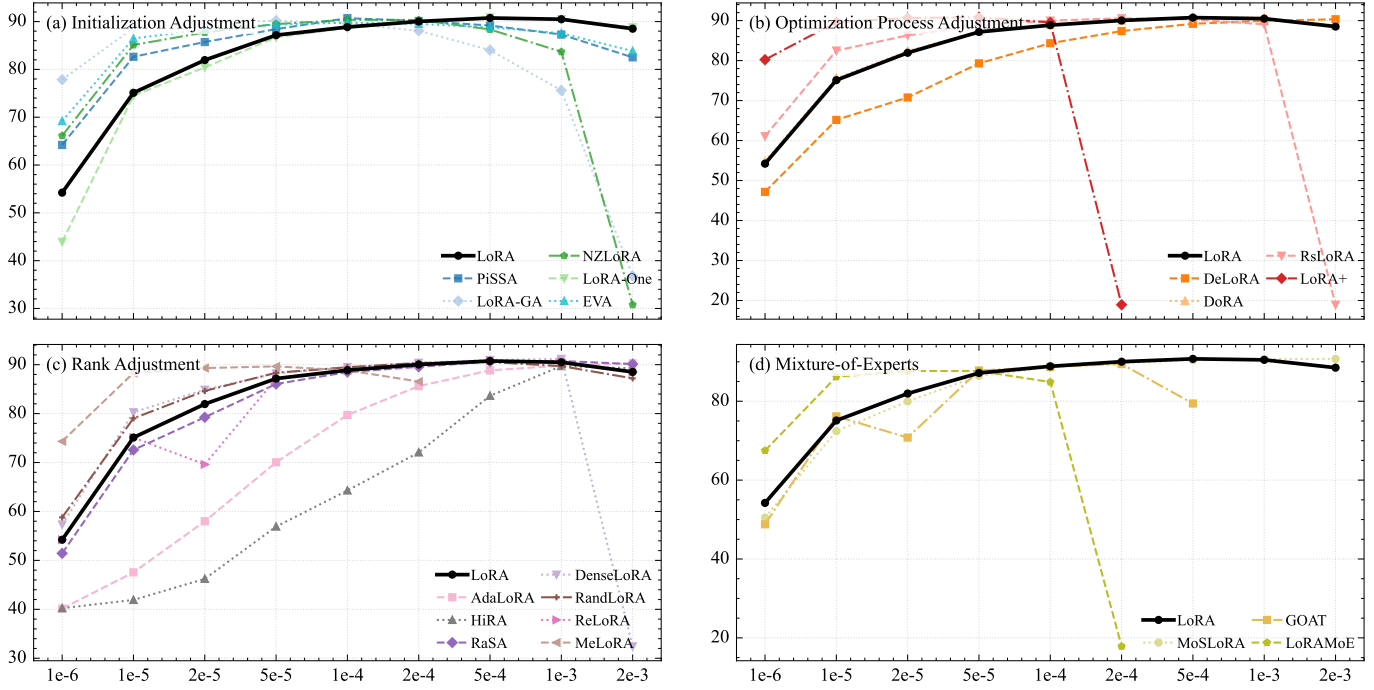


Fig. 10. Performance comparison of LoRA variants on seven image classification tasks across different learning rates. All plots share the same y-axis (accuracy) and x-axis (learning rate).

accuracy is evaluated on the corresponding test set of each task. Experiments are repeated with ten distinct learning rates: [1e-6, 1e-5, 2e-5, 5e-5, 1e-4, 2e-4, 5e-4, 1e-3, 2e-3, 5e-3]. Other experimental settings, including the optimizer (and its configurations), learning rate scheduler (and its configurations), and batch size, remain identical to those used in our NLG experiments and are held constant across all runs.

Experimental results Figure 10 shows the average evaluation results on the 7 subsets of the IC tasks, with LORA and its variants exhibiting a gradual performance improvement as the learning rate increases, consistent with the trends observed in our NLU and NLG experiments; for the results of each subset, please refer to Table XI- XIX. For LORA, average performance rises steadily from 54.22 at a learning rate of 1e-6 to 90.75 at 5e-4. In contrast to our experiments on natural language understanding and generation, LORA and its variants demonstrate greater robustness to variations in learning rates on the information classification tasks examined. Specifically, LORA achieves a performance of 90.03 at a learning rate of 2e-4, with performance remaining approximately stable when the learning rate is slightly reduced to 1e-4 or increased to 5e-4. Most experimental results are similar to those of our experiments on NLU and NLG: variants with enhanced gradient flow (including LORA+, which sets the learning rate of matrix B 16 times the base learning rate) show advantages over vanilla LORA at small learning rates, and the advantages diminish gradually as LORA approaches its peak performance; ADALORA, HiRA, and DELORA show clear disadvantages over other methods at small learning rates for their constraints on the optimization process.

4) Additional Experimental Settings: For LORA variants evaluated in our experiments, we adopt the following variant-specific hyperparameters (we adopt the recommended settings if possible):

- **LoRA-GA:** The number of gradient estimation steps is set to 64; the hyperparameter γ is set to 16.
- **NZLoRA:** Both hyperparameters γ_A and γ_B are set to 16.
- **PiSSA:** The number of fast SVD decomposition iterations PiSSA is set to 64.
- **LORA-ONE:** The number of gradient estimation steps is set to 64; the hyperparameter γ is set to 128.
- **EVA:** The number of the activation estimation steps is set to 64; the convergence threshold of the incremental SVD is set to 0.9.
- **DELORA:** The hyperparameter λ is set to 8. The initialization schemes for A and B are both the Kaiming uniform distribution.
- **LORA+:** The ratio of learning rates used for B and A is set to 16.
- **MELORA:** The number of diagonal blocks is set to 2, resulting in a overall rank of 16 for each adapter.
- **RELORA:** The low-rank weights are merged and reinitialized 3-5 times during each training process; the number of re-warmup steps after each *merge-and-reinit* process is set to 10.
- **ADALORA:** The hyperparameter t_i is set to 100 while t_f is set to 900. The initial rank is set to 12, and the final effective rank is set to 8.
- **RANDLORA:** The rank of low-rank bases is set to 32, ensuring a comparable trainable parameter count to

LoRA; the upper bound of the dimension of all low-rank bases is set to 1024, resulting in a maximum rank of 1024.

- RASA: The shared rank k is set to 1, resulting in an overall rank of $r - 1 + L$ for each adapter.
- DENSELoRA: The rank of each adapter is set to $24 \cdot r = 192$, where r is the rank used for vanilla LoRA. The hyperparameter α is therefore set to $48 \cdot r = 384$. This setting results in a comparable trainable parameter count to LoRA but with a much higher overall rank.
- LoRAMoE and GOAT: The number of experts is set to 8, each expert with a rank of 1, resulting in a total rank of 8; the number of activated experts for each token is set to 2.
- HiRA: No extra hyperparameters.
- MOSLoRA: No extra hyperparameters.
- RSLoRA: No extra hyperparameters.
- DoRA: No extra hyperparameters.

5) *Learning Rate Sweep Results on High-rank Settings:* To systematically investigate the high-rank performance of LoRA and its variants, we select one representative variant from each major category of LoRA extensions and evaluate their behavior under a high-rank setting. Specifically, we benchmark four variants: LoRA-GA, RSLoRA, MELORA, and LoRAMoE, against vanilla LoRA. All experimental configurations are kept identical to those used in our main NLG experiments, except that the LoRA rank is uniformly set to 128 across all methods. As noted in Section II, it is common practice to set the scaling hyperparameter α to twice the LoRA rank. To isolate and assess the impact of this convention, particularly in contrast to variants like RSLoRA, which inherently adjust scaling, we also evaluate vanilla LoRA with $\alpha = 256$ (i.e., 2×128) as a controlled baseline.

The experimental results under the high-rank setting are summarized in Table III. On GSM8K, Vanilla LoRA achieves the best performance among all evaluated methods, reaching 76.57 (an improvement of +1.07 over LoRA with $r = 8$) with a learning rate of 1e-4 and $\alpha = 256$. Notably, LoRA with $\alpha = 16$ also attains a competitive accuracy of 76.12 on GSM8K when using a relatively high learning rate of 5e-4. This suggests that, in our experimental setup, a larger learning rate can partially compensate for the effect of a small fixed α . These trends differ from those reported in Figure S3 of Biderman et al. [99], which may be due to differences in learning-rate tuning or task selection across studies. Furthermore, the empirical findings from Kalajdzievski et al. [65] indicate that the gradient norm of LoRA tends to collapse as the rank increases. Our results demonstrate that this issue can be mitigated through several strategies: applying the rank-stabilizing scaling of RSLoRA; setting $\alpha = 2r$ as empirical studies suggested; adopting LoRA variants with enhanced gradient flow such as LoRA-GA, or using a larger learning rate. On HumanEval, Vanilla LoRA ($\alpha = 256$) and LoRA-GA both achieve peak performance of 51.30, which is 3.28 points higher than the peak performance of LoRA with $r = 8$, at learning rates of 1e-4 and 5e-4, respectively. The substantial improvements on both GSM8k and HumanEval

highlight the effectiveness of increasing LoRA's rank when training settings are appropriately configured.

TABLE III

PERFORMANCE OF LoRA AND ITS VARIANTS UNDER A HIGH-RANK SETTING ACROSS LEARNING RATES ON GSM8K AND HUMAN EVAL. WE USE \dagger AND \ddagger TO DENOTE LoRA WITH $\alpha = 256$ AND $\alpha = 16$, RESPECTIVELY.

Method	GSM8K						HumanEval					
	1e-5	2e-5	5e-5	1e-4	2e-4	5e-4	1e-5	2e-5	5e-5	1e-4	2e-4	5e-4
LoRA \dagger	72.02	72.40	74.98	76.57	74.30	1.29	46.88	46.80	48.70	51.30	51.07	41.31
LoRA \ddagger	61.87	66.49	72.86	71.65	73.01	76.12	40.02	41.84	43.90	46.11	47.09	48.63
LoRA-GA	70.66	72.48	75.74	75.82	74.60	71.42	41.16	46.49	51.30	50.99	51.07	48.48
RsLoRA	68.34	71.72	74.91	75.66	74.75	1.52	44.51	45.66	50.00	51.14	51.60	46.27
MELoRA	71.42	72.02	74.60	72.63	69.90	57.32	48.09	48.78	50.53	48.40	43.14	32.70

TABLE IV
PERFORMANCE COMPARISON ON THE GLUE BENCHMARK WITH A LEARNING RATE OF 1E-6.

Method	SST-2	CoLA	MNLI	MRPC	QNLI	QQP	RTE	STS-B	WNLI	Avg
LoRA	89.45	0.00	78.69	66.38	82.70	79.43	47.65	13.37	39.44	55.23
Rank Adjustment Based LoRA Variants										
HiRA	49.08	0.96	32.74	65.83	49.13	0.00	47.65	2.71	39.44	31.95
RaSA	88.76	0.00	76.95	66.38	80.59	78.64	48.38	6.20	40.85	54.08
AdaLoRA	49.08	0.00	32.77	65.71	48.92	0.00	47.65	2.64	39.44	31.66
MELoRA	92.55	0.00	84.10	66.38	88.82	83.33	50.54	78.53	39.44	64.85
DenseLoRA	91.51	0.00	81.29	66.38	86.02	81.30	48.74	0.00	36.62	54.58
RandLoRA	84.29	0.00	71.93	66.38	80.08	78.10	47.65	11.85	39.44	53.30
ReLoRA	89.22	0.00	77.47	66.38	81.85	82.31	48.38	15.48	40.85	55.77
Optimization Process Adjustment Based LoRA Variants										
DoRA	89.56	0.00	78.70	66.38	82.93	79.48	47.65	13.88	39.44	55.34
RsLoRA	91.97	0.00	81.83	66.38	86.14	81.24	49.10	6.17	38.03	55.65
LoRA+	93.23	0.00	84.64	66.38	89.76	84.04	49.10	81.13	49.30	66.40
DeLoRA	50.92	0.00	66.85	66.38	63.18	77.35	48.74	9.24	40.85	47.05
Initialization Adjustment Based LoRA Variants										
EVA	91.63	0.00	81.57	66.38	86.75	80.95	49.46	20.34	38.03	57.23
PiSSA	90.94	0.00	82.01	66.38	85.68	81.48	49.10	18.05	38.03	56.85
LoRAGA	92.55	0.00	84.51	66.38	89.97	83.61	53.79	80.34	38.03	65.46
LoRA-One	89.11	0.00	78.18	66.38	83.29	78.60	47.29	9.15	56.34	56.48
NZLoRA	90.94	0.00	82.04	66.38	86.56	81.27	49.46	9.38	38.03	56.01
Mixture-of-Experts Integration Based Variants										
GOAT	87.16	0.00	76.17	66.38	69.73	78.49	52.35	5.34	49.30	53.88
MoSLoRA	88.42	0.00	77.32	66.38	81.48	78.62	48.38	6.26	40.85	54.19
LoRAMoE	91.86	0.00	82.82	66.38	87.20	82.02	49.46	22.07	38.03	57.76

TABLE V
PERFORMANCE COMPARISON ON THE GLUE BENCHMARK WITH A LEARNING RATE OF 1E-5.

Method	SST-2	CoLA	MNLI	MRPC	QNLI	QQP	RTE	STS-B	WNLI	AVG
LoRA	93.35	32.91	85.59	66.38	90.47	84.91	49.10	82.88	42.25	69.76
Rank Adjustment Based LoRA Variants										
HiRA	86.12	0.00	76.76	66.26	79.62	78.65	47.65	4.22	39.44	53.19
RaSA	93.23	0.00	85.28	66.38	90.24	84.48	49.82	81.12	40.85	65.71
AdaLoRA	90.37	0.00	82.29	66.38	85.97	81.31	47.65	5.69	39.44	55.46
MELoRA	94.38	53.18	86.70	84.08	91.97	86.57	68.95	88.87	39.44	77.13
DenseLoRA	94.04	50.99	86.15	66.38	91.70	85.59	49.46	86.41	50.70	73.49
RandLoRA	92.66	0.00	84.88	66.38	89.12	84.03	51.99	80.68	39.44	65.46
ReLoRA	93.46	52.74	85.09	66.38	89.89	87.23	49.46	83.39	50.70	73.15
Optimization Process Adjustment Based LoRA Variants										
DoRA	93.23	32.03	85.73	66.38	90.60	84.90	49.10	82.89	43.66	69.84
RsLoRA	94.27	48.15	86.51	68.58	91.45	85.96	54.15	86.16	47.89	73.68
LoRA+	94.38	56.06	87.31	84.81	92.44	87.58	71.12	89.53	42.25	78.39
DeLoRA	91.86	0.00	84.66	66.38	89.08	83.22	49.10	76.11	40.85	64.58
Initialization Adjustment Based LoRA Variants										
EVA	94.38	51.11	86.06	75.96	91.83	85.57	61.01	86.38	43.66	75.11
PiSSA	93.12	50.70	86.42	73.03	91.51	86.23	58.48	86.68	47.89	74.90
LoRAGA	94.61	54.87	87.09	85.72	92.44	86.97	69.68	88.30	36.62	77.37
LoRA-One	93.23	35.74	85.79	66.38	90.68	84.91	48.01	82.91	56.34	71.55
NZLoRA	93.58	50.87	86.42	67.85	91.55	85.76	60.29	85.52	45.07	74.10
Mixture-of-Experts Integration Based Variants										
GOAT	93.12	0.00	85.64	66.38	90.41	85.33	51.26	81.28	49.30	66.97
MoSLoRA	93.35	18.30	85.58	66.38	90.62	84.73	49.10	81.44	38.03	67.50
LoRAMoE	93.35	48.07	85.63	69.49	92.02	86.06	66.06	88.75	36.62	74.01

TABLE VI
PERFORMANCE COMPARISON ON THE GLUE BENCHMARK WITH A LEARNING RATE OF 5E-5.

Method	SST-2	CoLA	MNLI	MRPC	QNLI	QQP	RTE	STS-B	WNLI	AVG
LoRA	94.38	55.25	87.67	85.60	92.35	87.37	67.51	89.37	49.30	78.76
Rank Adjustment Based LoRA Variants										
HiRA	92.09	0.00	84.36	66.38	88.93	83.58	48.38	47.79	40.85	61.37
RaSA	93.92	54.32	87.76	84.38	92.44	87.15	66.79	89.48	46.48	78.08
AdaLoRA	93.23	40.03	86.11	66.38	90.45	85.12	47.65	82.10	39.44	70.06
MELoRA	93.46	56.25	85.89	84.93	91.19	86.67	75.81	90.57	29.58	77.15
DenseLoRA	94.38	58.05	87.81	86.70	92.61	87.88	69.68	90.30	49.30	79.63
RandLoRA	92.89	48.94	87.09	81.70	92.27	86.82	62.45	86.94	35.21	74.92
ReLoRA	94.61	55.08	87.07	85.17	92.06	89.48	70.04	88.62	56.34	79.83
Optimization Process Adjustment Based LoRA Variants										
DoRA	94.38	52.44	87.73	85.36	92.39	87.37	68.23	89.42	49.30	78.51
RsLoRA	94.61	54.98	87.67	85.72	92.73	88.07	72.92	90.39	46.48	79.29
LoRA+	94.95	60.57	87.28	86.52	92.39	87.89	74.73	90.82	25.35	77.83
DeLoRA	93.92	52.37	86.57	83.53	91.59	86.14	59.57	84.65	45.07	75.93
Initialization Adjustment Based LoRA Variants										
EVA	94.04	56.02	87.42	85.23	92.42	87.46	72.92	90.53	33.80	77.76
PiSSA	93.92	57.29	87.38	86.21	92.08	87.75	70.40	89.73	39.44	78.24
LoRAGA	93.35	59.07	87.34	86.33	92.73	87.27	76.17	90.29	33.80	78.48
LoRA-One	94.15	55.79	87.77	84.62	92.71	87.35	70.76	89.28	59.15	80.18
NZLoRA	94.27	56.58	87.07	85.85	92.40	87.74	74.01	89.95	30.99	77.65
Mixture-of-Experts Integration Based Variants										
GOAT	94.04	55.23	86.83	83.71	92.46	87.43	56.68	88.91	53.52	77.65
MoSLoRA	94.27	53.82	87.47	85.17	92.20	87.24	70.04	89.12	46.48	78.42
LoRAMoE	93.00	53.91	85.55	85.72	91.72	86.02	70.76	90.37	25.35	75.82

TABLE VII
PERFORMANCE COMPARISON ON THE GLUE BENCHMARK WITH A LEARNING RATE OF 1E-4.

Method	SST-2	CoLA	MNLI	MRPC	QNLI	QQP	RTE	STS-B	WNLI	AVG
LoRA	94.27	55.99	87.70	86.58	92.75	88.17	73.29	90.29	47.89	79.66
Rank Adjustment Based LoRA Variants										
HiRA	93.23	0.00	85.72	66.38	90.64	85.14	49.82	80.68	39.44	65.67
RaSA	93.81	57.27	87.74	85.60	92.42	87.83	73.29	90.11	49.30	79.71
AdaLoRA	93.81	49.69	87.27	66.38	92.14	86.68	49.82	86.94	39.44	72.46
MELoRA	92.43	53.38	85.11	84.38	91.13	85.22	69.68	90.24	56.34	78.66
DenseLoRA	93.81	59.57	87.47	87.00	92.78	88.64	75.45	90.59	47.89	80.36
RandLoRA	93.81	51.71	87.35	85.23	92.46	87.70	68.95	88.83	35.21	76.81
ReLoRA	94.72	58.35	87.67	87.19	92.69	87.50	71.12	89.88	56.34	80.61
Optimization Process Adjustment Based LoRA Variants										
DoRA	94.15	56.29	87.63	86.39	92.58	88.13	72.56	90.33	45.07	79.24
RsLoRA	94.27	57.78	87.25	85.30	92.46	88.27	73.65	91.04	38.03	78.67
LoRA+	93.58	61.82	86.56	86.58	92.40	86.01	52.71	90.87	40.85	76.82
DeLoRA	94.38	52.42	87.11	85.30	92.29	86.95	66.79	87.13	43.66	77.34
Initialization Adjustment Based LoRA Variants										
EVA	94.15	58.81	87.51	85.48	92.29	88.18	75.09	90.75	25.35	77.51
PiSSA	93.92	59.81	87.24	86.70	92.37	88.10	76.90	90.27	28.17	78.16
LoRAGA	92.55	57.54	86.16	85.66	91.70	86.77	72.56	90.25	56.34	79.95
LoRA-One	94.38	55.51	87.89	85.42	92.86	87.91	74.37	90.17	52.11	80.07
NZLoRA	94.04	59.05	87.27	86.15	91.93	87.77	72.20	90.20	25.35	77.11
Mixture-of-Experts Integration Based Variants										
GOAT	94.04	53.64	86.99	85.72	92.10	87.25	69.31	89.56	47.89	78.50
MoSLoRA	94.95	55.49	87.62	86.82	92.67	87.88	72.56	90.22	47.89	79.57
LoRAMoE	91.97	56.25	32.74	84.26	90.24	0.00	71.84	90.39	23.94	60.18

TABLE VIII
PERFORMANCE COMPARISON ON THE GLUE BENCHMARK WITH A LEARNING RATE OF 5E-4.

Method	SST-2	CoLA	MNLI	MRPC	QNLI	QQP	RTE	STS-B	WNLI	AVG
LoRA	93.23	61.58	87.12	86.15	92.23	0.00	78.34	91.00	28.17	68.65
Rank Adjustment Based LoRA Variants										
HiRA	94.04	55.47	87.15	84.81	92.58	87.79	64.98	87.77	40.85	77.27
RaSA	94.04	60.32	87.11	86.94	92.42	88.50	75.81	90.88	56.34	81.37
AdaLoRA	93.35	58.06	87.25	87.19	92.76	88.26	70.76	90.31	36.62	78.29
MELoRA	50.92	0.00	32.74	66.38	50.63	0.00	52.71	0.00	56.34	34.26
DenseLoRA	93.35	60.82	31.82	87.37	92.08	0.00	52.71	91.01	28.17	59.70
RandLoRA	94.15	57.53	86.82	87.00	92.35	88.15	75.81	90.53	22.54	77.21
ReLoRA	93.58	55.48	84.49	86.09	91.83	86.83	52.71	91.05	56.34	77.60
Optimization Process Adjustment Based LoRA Variants										
DoRA	93.58	62.35	86.56	87.25	92.42	85.52	76.53	90.94	28.17	78.15
RsLoRA	50.92	60.58	32.74	84.81	50.63	0.00	72.92	90.85	56.34	55.53
LoRA+	50.92	0.00	32.74	66.38	49.37	0.00	52.71	10.57	56.34	35.45
DeLoRA	94.27	59.05	87.50	86.64	92.42	87.97	72.20	89.81	28.17	77.56
Initialization Adjustment Based LoRA Variants										
EVA	92.66	59.05	86.81	84.81	91.63	0.00	52.71	90.72	56.34	68.30
PiSSA	50.92	0.00	32.74	83.89	50.63	0.00	52.71	89.49	56.34	46.30
LoRAGA	50.92	0.00	31.82	66.38	49.37	0.00	47.29	5.15	56.34	34.14
LoRA-One	93.69	62.07	86.95	87.37	92.01	0.00	78.34	90.65	29.58	68.96
NZLoRA	50.92	0.00	32.74	85.42	50.63	0.00	52.71	89.66	56.34	46.49
Mixture-of-Experts Integration Based Variants										
GOAT	50.92	0.00	32.74	85.17	49.37	0.00	52.71	89.29	30.99	43.47
MoSLoRA	93.23	59.56	87.00	85.36	92.12	88.29	76.53	90.72	35.21	78.67
LoRAMoE	50.92	0.00	32.74	66.38	49.37	0.00	52.71	1.29	43.66	33.01

TABLE IX
PERFORMANCE COMPARISON ON THE GLUE BENCHMARK WITH A LEARNING RATE OF 1E-3.

Method	SST-2	CoLA	MNLI	MRPC	QNLI	QQP	RTE	STS-B	WNLI	AVG
LoRA	50.92	0.00	32.74	86.33	49.37	0.00	52.71	89.35	30.99	43.60
Rank Adjustment Based LoRA Variants										
HiRA	93.69	57.27	86.89	86.94	92.23	88.52	72.92	89.76	47.89	79.57
RaSA	93.00	0.00	87.27	86.46	92.25	0.00	77.98	90.90	28.17	61.78
AdaLoRA	93.81	61.57	87.33	86.76	92.12	88.27	76.53	90.53	40.85	79.75
MELoRA	50.92	0.00	31.82	66.38	49.37	0.00	52.71	0.00	43.66	32.55
DenseLoRA	50.92	0.00	32.74	66.38	50.63	0.00	52.71	0.00	56.34	34.18
RandLoRA	93.58	56.50	86.59	87.37	91.19	87.13	77.98	90.65	25.35	77.37
ReLoRA	50.92	15.54	35.45	66.38	50.63	38.72	52.71	88.51	56.34	50.58
Optimization Process Adjustment Based LoRA Variants										
DoRA	50.92	58.83	32.74	66.38	50.63	0.00	52.71	89.39	32.39	48.22
RsLoRA	50.92	0.00	35.45	66.38	49.37	0.00	52.71	89.94	56.34	44.57
LoRA+	50.92	0.00	32.74	66.38	49.37	0.00	52.71	13.26	56.34	35.75
DeLoRA	93.81	61.09	87.72	86.58	92.50	88.23	68.95	89.74	30.99	77.73
Initialization Adjustment Based LoRA Variants										
EVA	50.92	0.00	35.45	66.38	49.37	0.00	52.71	89.70	56.34	44.54
PiSSA	50.92	0.00	32.74	66.38	50.63	0.00	52.71	7.96	56.34	35.30
LoRAGA	50.92	0.00	31.82	66.38	49.37	0.00	47.29	0.00	56.34	33.20
LoRA-One	50.92	0.00	32.74	85.91	49.37	0.00	52.71	90.79	38.03	44.50
NZLoRA	50.92	0.00	32.74	66.38	50.63	0.00	47.29	88.46	56.34	43.64
Mixture-of-Experts Integration Based Variants										
GOAT	50.92	0.00	32.74	66.38	49.37	0.00	52.71	2.65	56.34	34.57
MoSLoRA	94.04	60.07	87.32	86.39	92.33	87.76	52.71	89.55	53.52	78.19
LoRAMoE	50.92	0.00	32.74	66.38	49.37	0.00	52.71	0.40	43.66	32.91

TABLE X
PERFORMANCE COMPARISON ON THE GLUE BENCHMARK WITH A LEARNING RATE OF 5E-3.

Method	SST-2	CoLA	MNLI	MRPC	QNLI	QQP	RTE	STS-B	WNLI	AVG
LoRA	50.92	0.00	32.74	66.38	49.37	0.00	52.71	0.00	56.34	34.18
Rank Adjustment Based LoRA Variants										
HiRA	90.37	59.12	32.74	86.82	49.37	0.00	79.78	90.69	23.94	56.98
RaSA	50.92	0.00	32.74	66.38	50.63	0.00	52.71	0.00	43.66	32.73
AdaLoRA	50.92	60.08	32.74	86.03	50.63	0.00	52.71	0.00	54.93	42.99
MELoRA	50.92	0.00	32.74	66.38	49.37	0.00	52.71	0.10	56.34	34.28
DenseLoRA	50.92	0.00	31.82	66.38	49.37	0.00	52.71	0.23	56.34	34.20
RandLoRA	50.92	0.00	31.82	66.38	50.63	0.00	52.71	0.00	56.34	33.21
ReLoRA	50.92	62.40	35.45	66.38	50.63	38.72	52.71	2.52	56.34	46.23
Optimization Process Adjustment Based LoRA Variants										
DoRA	50.92	0.00	32.74	66.38	49.37	0.00	52.71	0.00	43.66	32.82
RsLoRA	50.92	0.00	32.74	66.38	49.37	0.00	52.71	0.34	43.66	32.90
LoRA+	50.92	0.00	32.74	66.38	49.37	0.00	52.71	1.23	43.66	33.00
DeLoRA	94.15	0.00	87.07	66.38	92.63	88.24	47.29	0.00	56.34	58.71
Initialization Adjustment Based LoRA Variants										
EVA	50.92	0.00	32.74	66.38	49.37	0.00	52.71	0.00	56.34	34.18
PiSSA	50.92	0.00	32.74	66.38	49.37	0.00	52.71	0.00	43.66	32.62
LoRAGA	50.92	0.00	32.74	66.38	49.37	0.00	52.71	2.97	43.66	33.19
LoRA-One	50.92	0.00	35.45	66.38	49.37	0.00	52.71	2.89	43.66	33.49
NZLoRA	50.92	0.00	32.74	66.38	49.37	0.00	52.71	0.98	43.66	32.97
Mixture-of-Experts Integration Based Variants										
GOAT	50.92	0.00	35.45	66.38	49.37	0.00	52.71	1.60	43.66	33.34
MoSLoRA	50.92	0.00	32.74	66.38	49.37	0.00	52.71	0.00	56.34	34.27
LoRAMoE	50.92	0.00	32.74	66.38	50.63	0.00	52.71	0.80	56.34	34.50

TABLE XI
PERFORMANCE ON THE SEVEN IMAGE CLASSIFICATION TASKS WITH A LEARNING RATE OF 1E-6.

Method	Cars	DTD	EuroSAT	GTSRB	RESISC45	SUN397	SVHN	Avg
LoRA	65.58	47.39	73.69	44.00	65.16	65.30	62.01	54.22
Rank Adjustment Based LoRA Variants								
HiRA	63.96	42.87	40.74	69.00	56.71	62.76	13.91	40.23
RaSA	65.25	46.54	66.72	36.00	63.32	64.87	53.01	51.44
AdaLoRA	63.89	42.87	40.44	69.00	56.63	62.75	13.75	40.15
MELoRA	71.60	63.30	96.93	39.59	86.27	69.90	92.75	74.33
DenseLoRA	66.24	50.00	79.13	69.00	67.52	66.65	71.05	57.33
RandLoRA	66.70	49.95	84.31	1.18	69.03	65.79	74.47	58.78
ReLoRA	65.44	46.60	70.44	0.39	63.98	64.91	55.38	52.45
Optimization Process Adjustment Based LoRA Variants								
DoRA	65.64	47.93	74.94	48.00	65.51	65.46	63.82	54.83
RsLoRA	67.35	52.13	87.39	3.06	70.87	67.30	79.54	61.09
LoRA+	74.31	70.64	97.39	63.65	89.30	71.83	94.48	80.23
DeLoRA	64.92	44.79	59.07	37.00	60.94	63.73	36.37	47.17
Initialization Adjustment Based LoRA Variants								
EVA	69.53	58.35	94.89	22.64	81.17	68.71	89.02	69.19
PiSSA	67.83	53.94	92.19	8.84	75.33	67.89	83.42	64.21
LoRA-GA	73.50	68.03	97.26	53.33	88.35	70.83	93.73	77.86
LoRA-One	18.70	46.65	61.65	2.47	51.97	62.66	63.39	43.93
NZLoRA	68.69	55.59	94.20	12.73	78.22	67.90	85.57	66.13
Mixture-of-Experts Integration Based Variants								
GOAT	63.11	44.04	60.04	44.00	59.46	61.94	52.57	48.80
MoSLoRA	65.27	45.80	64.28	36.00	62.59	64.62	50.50	50.49
LoRAMoE	69.37	55.21	94.93	16.94	79.05	67.89	89.07	67.49

TABLE XII
PERFORMANCE ON THE SEVEN IMAGE CLASSIFICATION TASKS WITH A LEARNING RATE OF 1E-5.

Method	Cars	DTD	EuroSAT	GTSRB	RESISC45	SUN397	SVHN	Avg
LoRA	71.79	66.28	96.93	40.40	86.37	70.59	93.38	75.11
Rank Adjustment Based LoRA Variants								
HiRA	64.35	43.35	44.81	58.00	57.89	63.04	19.40	41.92
RaSA	70.73	63.03	96.22	29.46	84.56	69.89	92.29	72.31
AdaLoRA	64.64	45.32	50.83	44.00	60.33	63.88	47.41	47.55
MELoRA	80.74	75.05	98.35	96.85	94.75	76.16	96.29	88.31
DenseLoRA	74.38	71.76	97.28	63.28	89.25	71.82	94.12	80.27
RandLoRA	74.06	67.82	97.61	60.03	88.87	70.84	94.01	79.03
ReLoRA	70.39	62.34	96.13	29.06	84.41	69.71	92.38	72.06
Optimization Process Adjustment Based LoRA Variants								
DoRA	72.18	66.44	97.06	42.59	86.81	70.73	93.48	75.61
RsLoRA	75.60	71.70	97.80	74.34	90.59	72.59	94.89	82.50
LoRA+	83.32	77.66	98.50	98.17	95.22	77.56	96.91	89.62
DeLoRA	68.09	54.89	93.37	11.46	76.54	67.37	84.50	65.17
Initialization Adjustment Based LoRA Variants								
EVA	78.51	74.79	98.06	91.71	92.56	73.97	95.72	86.47
PiSSA	75.36	69.52	97.83	76.98	91.03	72.72	95.06	82.64
LoRA-GA	82.33	75.53	98.52	96.96	94.70	76.01	96.49	88.65
LoRA-One	70.50	67.39	96.11	39.07	85.84	70.28	92.41	74.51
NZLoRA	77.70	72.82	98.26	85.82	92.25	73.36	95.55	85.11
Mixture-of-Experts Integration Based Variants								
GOAT	71.40	66.65	96.48	48.87	87.49	69.36	92.91	76.17
MoSLoRA	70.69	63.09	96.09	30.37	84.48	69.92	92.36	72.43
LoRAMoE	78.72	72.02	98.15	91.92	92.70	74.26	95.62	86.20

TABLE XIII
PERFORMANCE ON THE SEVEN IMAGE CLASSIFICATION TASKS WITH A LEARNING RATE OF 2E-5.

Method	Cars	DTD	EuroSAT	GTSRB	RESISC45	SUN397	SVHN	Avg
LoRA	75.29	71.44	97.63	71.57	90.41	72.43	94.90	81.95
Rank Adjustment Based LoRA Variants								
HiRA	64.83	44.68	53.80	40.00	60.19	63.69	35.93	46.22
RaSA	73.91	69.31	97.33	59.29	88.97	71.71	94.26	79.25
AdaLoRA	66.14	51.06	77.07	50.00	67.76	67.46	75.92	57.99
MELoRA	82.35	76.44	98.57	98.25	95.59	77.12	96.83	89.31
DenseLoRA	77.84	73.56	98.04	83.28	91.81	74.21	95.39	84.88
RandLoRA	77.50	73.62	98.20	83.22	91.75	72.79	95.31	84.63
ReLoRA	73.45	69.41	97.33	59.98	88.49	71.26	94.19	79.16
Optimization Process Adjustment Based LoRA Variants								
DoRA	75.59	71.81	97.80	73.37	90.56	72.61	94.98	82.39
RsLoRA	78.97	74.26	98.13	89.09	92.79	74.92	95.91	86.30
LoRA+	85.95	79.68	98.76	98.77	95.71	78.45	97.28	90.66
DeLoRA	69.73	60.16	95.83	27.21	83.00	68.54	90.98	70.78
Initialization Adjustment Based LoRA Variants								
EVA	81.05	76.17	98.37	96.75	94.30	75.43	96.34	88.34
PiSSA	77.95	71.17	98.30	89.37	92.90	74.52	95.91	85.73
LoRA-GA	84.17	77.13	98.52	98.34	95.63	76.89	96.85	89.65
LoRA-One	73.39	72.77	97.26	63.67	89.56	72.01	94.29	80.42
NZLoRA	80.13	74.47	98.41	95.42	94.11	75.48	96.17	87.74
Mixture-of-Experts Integration Based Variants								
GOAT	76.48	72.34	97.54	78.95	91.30	72.21	6.70	70.79
MoSLoRA	74.05	70.05	97.19	63.17	89.27	71.81	94.25	79.97
LoRAMoE	79.42	74.26	98.20	95.86	94.29	75.75	96.01	87.68

TABLE XIV
PERFORMANCE ON THE IMAGE CLASSIFICATION TASKS WITH A LEARNING RATE OF 5E-5.

Method	Cars	DTD	EuroSAT	GTSRB	RESISC45	SUN397	SVHN	Avg
LoRA	80.08	74.52	98.07	92.15	93.49	75.68	96.15	87.16
Rank Adjustment Based LoRA Variants								
HiRA	65.89	50.64	77.04	53.00	67.22	66.16	70.83	56.90
RaSA	78.72	74.63	98.09	87.57	92.68	74.82	95.83	86.05
AdaLoRA	69.39	64.47	95.00	17.81	82.87	69.22	91.61	70.05
MELoRA	83.16	77.13	98.80	98.71	96.11	76.52	97.15	89.65
DenseLoRA	81.63	74.79	98.41	95.61	94.19	76.57	96.32	88.22
RandLoRA	81.61	75.74	98.54	95.99	94.48	75.71	96.40	88.35
ReLoRA	78.10	74.68	98.04	86.92	92.19	73.98	95.63	85.65
Optimization Process Adjustment Based LoRA Variants								
DoRA	80.25	74.68	98.11	92.80	93.48	75.87	96.19	87.34
RsLoRA	82.08	75.74	98.35	97.11	94.81	77.10	96.62	88.83
LoRA+	87.30	79.04	98.70	98.90	96.41	78.11	97.36	90.83
DeLoRA	73.24	68.51	97.15	62.95	88.73	70.76	93.85	79.31
Initialization Adjustment Based LoRA Variants								
EVA	82.42	77.55	98.44	98.59	95.37	76.50	96.77	89.38
PiSSA	81.22	74.20	98.57	96.92	94.84	76.57	96.63	88.42
LoRA-GA	85.93	77.87	98.61	98.96	95.81	77.28	97.02	90.21
LoRA-One	78.46	75.43	98.11	91.14	92.89	75.11	95.89	86.72
NZLoRA	82.55	76.60	98.61	98.60	95.71	77.39	96.87	89.48
Mixture-of-Experts Integration Based Variants								
GOAT	81.06	75.37	98.06	94.53	93.97	75.59	96.00	87.80
MoSLoRA	79.06	74.36	98.04	89.83	92.79	75.22	95.85	86.45
LoRAMoE	80.11	73.30	98.43	95.50	94.63	75.94	95.68	87.66

TABLE XV
PERFORMANCE ON SEVEN IMAGE CLASSIFICATION TASKS WITH A LEARNING RATE OF 1E-4.

Method	Cars	DTD	EuroSAT	GTSRB	RESISC45	SUN397	SVHN	Avg
LoRA	82.22	75.85	98.41	97.08	94.67	77.18	96.58	88.86
Rank Adjustment Based LoRA Variants								
HiRA	68.08	56.06	89.80	5.91	76.21	68.12	85.80	64.28
RaSA	81.52	76.01	98.26	96.36	94.11	76.79	96.36	88.49
AdaLoRA	73.29	74.31	97.06	58.87	88.51	71.76	94.21	79.72
MELoRA	82.66	74.84	98.57	98.68	95.59	74.59	96.98	88.84
DenseLoRA	83.80	77.18	98.43	97.87	95.22	77.37	96.75	89.52
RandLoRA	83.04	76.81	98.65	98.37	95.51	77.08	96.85	89.47
ReLoRA	81.18	76.44	98.30	95.56	93.92	76.04	96.31	88.25
Optimization Process Adjustment Based LoRA Variants								
DoRA	82.20	76.01	98.41	97.22	94.70	77.27	96.64	88.92
RsLoRA	83.78	78.40	98.63	98.85	95.51	77.85	96.98	90.00
LoRA+	87.40	72.71	98.70	98.84	95.54	76.61	96.91	89.53
DeLoRA	76.53	72.77	97.94	83.49	91.68	72.78	95.22	84.34
Initialization Adjustment Based LoRA Variants								
EVA	83.99	77.45	98.33	98.74	95.79	77.07	97.07	89.78
PiSSA	83.34	77.66	98.67	98.27	95.63	77.10	97.00	89.67
LoRA-GA	85.04	75.74	98.61	98.80	95.57	76.49	96.94	89.60
LoRA-One	81.30	76.38	98.43	97.01	94.38	76.82	96.41	88.68
NZLoRA	84.77	78.72	98.72	99.07	96.00	78.20	97.09	90.37
Mixture-of-Experts Integration Based Variants								
GOAT	82.43	75.59	98.26	96.53	95.03	76.82	96.25	88.70
MoSLoRA	81.81	76.01	98.35	96.56	94.32	76.75	96.39	88.60
LoRAMoE	77.85	72.23	97.26	89.53	92.06	73.31	91.88	84.87

TABLE XVI
PERFORMANCE ON THE SEVEN IMAGE CLASSIFICATION TASKS WITH A LEARNING RATE OF 2E-4.

Method	Cars	DTD	EuroSAT	GTSRB	RESISC45	SUN397	SVHN	Avg
LoRA	84.07	78.62	98.57	98.50	95.52	77.90	97.02	90.03
Rank Adjustment Based LoRA Variants								
HiRA	70.87	66.06	95.69	24.93	84.62	69.76	92.49	72.06
RaSA	83.17	77.50	98.50	98.11	95.29	77.63	96.73	89.56
AdaLoRA	78.12	75.05	97.65	86.07	91.94	74.75	95.72	85.61
MELoRA	79.34	70.00	98.37	98.14	94.14	69.75	96.12	86.55
DenseLoRA	85.75	78.40	98.70	98.45	95.90	78.35	97.08	90.38
RandLoRA	85.24	78.19	98.61	99.15	96.25	78.03	97.05	90.36
ReLoRA	82.84	78.46	98.44	97.80	94.98	77.06	96.78	89.48
Optimization Process Adjustment Based LoRA Variants								
DoRA	84.12	77.77	98.65	98.76	95.59	77.88	97.06	89.98
RsLoRA	85.92	78.88	98.63	99.19	96.14	78.02	97.30	90.58
LoRA+	1.12	4.84	70.54	23.14	10.21	3.15	19.59	18.94
DeLoRA	79.69	74.47	98.37	94.96	93.52	74.80	95.95	87.39
Initialization Adjustment Based LoRA Variants								
EVA	83.92	76.22	98.56	98.53	95.81	76.63	96.98	89.52
PiSSA	85.09	78.30	98.83	98.69	95.73	77.22	97.07	90.13
LoRA-GA	82.74	71.44	98.43	98.72	94.81	73.43	96.96	88.08
LoRA-One	83.11	78.83	98.61	98.48	95.29	77.64	96.90	89.84
NZLoRA	85.66	77.98	98.80	98.82	96.22	77.52	97.36	90.34
Mixture-of-Experts Integration Based Variants								
GOAT	83.46	77.45	98.56	97.18	95.32	77.39	96.62	89.43
MoSLoRA	83.34	77.39	98.46	98.12	95.46	77.75	96.86	89.63
LoRAMoE	1.41	9.26	56.19	20.92	16.17	1.43	19.59	17.85

TABLE XVII
PERFORMANCE ON THE SEVEN IMAGE CLASSIFICATION TASKS WITH A LEARNING RATE OF 5E-4.

Method	Cars	DTD	EuroSAT	GTSRB	RESISC45	SUN397	SVHN	Avg
LoRA	86.78	78.62	98.74	98.93	96.27	78.68	97.20	90.75
Rank Adjustment Based LoRA Variants								
HiRA	76.46	73.88	97.65	78.80	90.60	73.19	94.86	83.63
RaSA	86.36	78.62	98.59	98.94	96.05	78.68	97.16	90.63
AdaLoRA	81.77	76.86	98.48	96.99	94.16	77.08	96.53	88.84
MELoRA	2.46	11.06	74.24	39.00	38.25	6.01	20.44	27.35
DenseLoRA	87.10	78.72	98.83	99.17	96.32	79.01	97.41	90.94
RandLoRA	86.38	77.93	98.70	99.22	96.25	77.79	97.41	90.53
ReLoRA	85.59	79.31	98.67	98.49	95.90	77.82	97.07	90.41
Optimization Process Adjustment Based LoRA Variants								
DoRA	86.72	78.94	98.61	99.06	96.05	78.82	97.27	90.78
RsLoRA	87.19	76.28	98.72	98.90	96.24	77.68	97.25	90.32
LoRA+	1.11	3.24	33.13	9.90	9.44	1.23	19.72	11.11
DeLoRA	82.03	76.76	98.59	98.08	95.40	76.87	96.65	89.20
Initialization Adjustment Based LoRA Variants								
EVA	83.17	73.62	98.41	98.40	95.62	75.15	97.13	88.79
PiSSA	85.10	73.67	98.48	98.77	95.56	75.53	97.15	89.18
LoRA-GA	77.12	60.53	97.52	98.20	93.17	65.33	96.44	84.04
LoRA-One	86.66	79.63	98.59	99.14	96.38	78.54	97.33	90.90
NZLoRA	83.92	71.54	98.57	98.74	95.54	73.31	96.83	88.35
Mixture-of-Experts Integration Based Variants								
GOAT	84.33	77.23	98.28	96.30	94.86	76.38	28.61	79.43
MoSLoRA	85.23	78.56	98.63	98.75	96.06	78.31	97.10	90.38
LoRAMoE	87.00	4.41	59.41	6.98	11.98	1.02	19.59	14.89

TABLE XVIII
PERFORMANCE ON THE SEVEN IMAGE CLASSIFICATION TASKS WITH A LEARNING RATE OF 1E-3.

Method	Cars	DTD	EuroSAT	GTSRB	RESISC45	SUN397	SVHN	Avg
LoRA	87.41	77.07	98.74	99.03	96.19	77.71	97.27	90.49
Rank Adjustment Based LoRA Variants								
HiRA	80.94	75.64	98.24	93.79	93.33	75.85	96.05	87.69
RaSA	87.71	77.93	98.69	98.92	96.35	78.35	97.30	90.75
AdaLoRA	83.73	78.51	98.46	98.11	95.14	77.86	96.77	89.80
MELoRA	1.79	11.76	72.09	27.47	33.59	2.69	31.39	25.83
DenseLoRA	88.15	80.21	98.74	98.92	96.41	78.65	97.26	91.19
RandLoRA	86.03	74.57	98.70	99.30	96.14	75.84	97.39	89.71
ReLoRA	85.66	77.34	98.61	98.82	95.84	76.62	97.08	90.00
Optimization Process Adjustment Based LoRA Variants								
DoRA	88.07	77.71	98.69	98.92	96.43	77.73	97.35	90.70
RsLoRA	86.46	72.29	98.57	98.50	95.57	75.52	96.52	89.06
LoRA+	99.00	3.35	37.30	11.03	8.14	30.00	19.59	11.53
DeLoRA	83.83	78.03	98.65	98.73	95.92	77.34	97.07	89.94
Initialization Adjustment Based LoRA Variants								
EVA	83.97	66.76	98.22	98.15	94.86	74.21	96.88	87.58
PiSSA	83.40	67.61	98.41	98.38	94.73	71.77	96.75	87.29
LoRA-GA	58.91	44.95	96.57	95.15	89.60	48.79	95.29	75.61
LoRA-One	87.53	77.29	98.69	98.52	96.38	78.03	97.19	90.52
NZLoRA	77.13	59.47	97.46	97.97	92.94	65.55	95.33	83.69
Mixture-of-Experts Integration Based Variants								
GOAT	1.06	6.28	69.50	11.47	8.84	67.34	32.97	28.21
MoSLoRA	86.94	78.72	98.63	98.92	95.95	78.50	97.34	90.71
LoRAMoE	92.00	4.31	19.02	13.71	6.51	38.00	19.59	9.21

TABLE XIX
PERFORMANCE ON THE SEVEN IMAGE CLASSIFICATION TASKS WITH A LEARNING RATE OF 2E-3.

Method	Cars	DTD	EuroSAT	GTSRB	RESISC45	SUN397	SVHN	AVG
LoRA	86.01	69.95	98.59	98.53	95.22	75.09	96.20	88.51
Rank Adjustment Based LoRA Variants								
HiRA	83.16	77.07	98.39	97.46	94.71	77.35	96.70	89.26
RaSA	87.36	74.89	98.57	98.80	96.16	77.75	97.30	90.12
AdaLoRA	85.05	78.35	98.80	98.65	95.70	78.44	96.90	90.27
MELoRA	1.58	8.62	61.13	24.15	17.40	1.26	22.17	19.47
DenseLoRA	55.00	3.14	98.70	98.74	5.54	72.00	19.59	32.43
RandLoRA	82.37	67.82	98.28	99.18	95.06	70.66	97.03	87.20
ReLoRA	82.30	69.26	97.98	98.32	94.44	71.15	96.27	87.10
Optimization Process Adjustment Based LoRA Variants								
DoRA	86.66	70.43	98.48	98.93	94.98	75.32	96.70	88.79
RsLoRA	1.83	5.32	56.26	22.32	14.03	65.00	32.10	18.93
LoRA+	66.00	2.13	35.69	7.95	2.24	25.00	19.59	9.79
DeLoRA	85.00	78.78	98.70	98.76	95.86	78.06	97.19	90.34
Initialization Adjustment Based LoRA Variants								
EVA	80.00	57.39	97.28	94.82	92.90	70.24	94.23	83.84
PiSSA	77.99	54.68	96.91	96.72	92.60	64.44	94.33	82.52
LoRA-GA	2.72	13.72	83.43	49.11	50.32	4.59	53.62	36.79
LoRA-One	86.47	71.65	98.30	98.48	95.32	75.50	95.95	88.81
NZLoRA	2.50	12.02	67.85	41.00	41.37	4.29	46.39	30.77
Mixture-of-Experts Integration Based Variants								
GOAT	83.00	3.30	40.72	9.94	3.98	31.00	19.63	11.24
MoSLoRA	87.20	77.93	98.70	99.11	96.33	78.68	97.15	90.73
LoRAMoE	88.00	2.39	25.39	7.18	5.35	38.00	19.55	8.73

TABLE XX
PERFORMANCE ON IMAGE CLASSIFICATION TASKS WITH A LEARNING RATE OF 5E-3.

Method	Cars	DTD	EuroSAT	GTSRB	RESISC45	SUN397	SVHN	AVG
LoRA	1.24	4.57	50.63	14.43	6.06	79.00	19.59	13.90
Rank Adjustment Based LoRA Variants								
HiRA	85.45	79.10	98.67	98.73	96.19	78.78	97.28	90.60
RaSA	72.00	4.73	27.61	11.58	20.67	2.27	19.60	12.45
AdaLoRA	85.60	79.15	98.63	98.67	96.06	78.31	97.04	90.49
MELoRA	1.31	8.35	49.65	12.95	13.06	1.10	28.53	16.42
DenseLoRA	92.00	4.79	45.63	11.80	7.98	73.00	19.59	13.06
RandLoRA	70.51	51.65	97.19	98.50	91.35	55.24	95.77	80.03
ReLoRA	1.09	4.04	44.91	6.91	7.95	1.74	19.59	12.32
Optimization Process Adjustment Based LoRA Variants								
DoRA	86.00	2.55	50.76	14.82	7.13	1.90	19.59	13.94
RsLoRA	72.00	5.80	31.15	10.93	13.44	34.00	22.60	12.14
LoRA+	81.00	2.13	11.30	48.00	2.24	30.00	19.59	5.26
DeLoRA	86.25	79.36	98.78	98.60	96.13	78.51	97.36	90.71
Initialization Adjustment Based LoRA Variants								
EVA	91.00	4.10	41.96	10.97	19.57	1.26	19.62	14.06
PiSSA	1.14	5.21	49.93	19.82	7.49	1.21	38.00	17.54
LoRA-GA	1.82	10.96	59.17	25.63	16.32	1.48	35.63	21.57
LoRA-One	67.00	5.59	48.48	5.98	8.43	72.00	27.11	13.85
NZLoRA	95.00	5.48	57.37	13.08	11.60	69.00	33.16	17.48
Mixture-of-Experts Integration Based Variants								
GOAT	88.00	2.45	24.76	6.12	3.46	30.00	19.59	8.22
MoSLoRA	95.00	6.54	57.85	15.85	9.44	74.00	32.67	17.72
LoRAMoE	88.00	2.93	23.35	9.91	4.19	27.00	19.59	8.73

TABLE XXI
PERFORMANCE ON GSM8K.

Method	1e-6	1e-5	2e-5	5e-5	1e-4	2e-4	5e-4	1e-3
LoRA	52.84	64.37	66.94	70.13	73.16	72.86	75.51	72.10
Rank Adjustment Based LoRA Variants								
HiRA	6.44	7.44	30.02	49.73	54.81	62.09	66.49	72.10
RaSA	48.98	61.87	63.84	68.92	71.04	72.48	73.31	74.30
AdaLoRA	5.84	34.65	49.32	59.51	61.49	65.58	70.35	71.72
MELoRA	62.55	71.72	72.02	70.36	64.52	57.01	1.74	2.05
DenseLoRA	50.19	63.76	67.85	68.84	72.86	72.33	74.22	74.75
RandLoRA	46.32	64.75	68.92	74.22	74.53	75.59	71.27	65.43
ReLoRA	55.04	65.81	69.6	71.87	71.65	67.17	41.93	1.52
Optimization Process Adjustment Based LoRA Variants								
DoRA	54.69	64.67	67.25	71.80	73.09	74.15	74.53	72.25
RsLoRA	54.51	65.73	69.45	71.87	73.92	74.68	69.75	67.55
LoRA+	60.12	70.28	72.02	74.68	75.59	72.25	64.67	1.59
DeLoRA	30.86	39.68	42.34	49.22	66.57	70.20	70.74	72.02
Initialization Adjustment Based LoRA Variants								
EVA	60.12	69.67	71.87	71.49	73.09	73.84	74.30	71.65
PiSSA	57.39	69.14	71.27	72.18	72.86	72.71	71.11	64.67
LoRA-GA	64.06	70.36	70.51	72.02	71.95	67.63	64.22	48.45
LoRA-One	52.39	64.59	67.70	70.28	72.18	73.01	74.68	71.27
NZLoRA	53.68	63.76	67.63	71.87	73.31	71.27	70.81	64.22
Mixture-of-Experts Integration Based Variants								
GOAT	48.98	67.25	67.63	68.84	71.65	71.27	52.39	2.12
MoSLoRA	48.52	63.31	66.03	69.37	69.98	72.71	74.00	74.68
LoRAMoE	46.32	67.93	69.83	69.22	59.97	34.60	1.67	1.52

TABLE XXII
PERFORMANCE ON HUMAN-EVAL.

Method	1e-6	1e-5	2e-5	5e-5	1e-4	2e-4	5e-4	1e-3
LoRA	9.30	41.31	41.46	44.82	45.27	48.09	48.17	42.07
Rank Adjustment Based LoRA Variants								
HiRA	0.00	3.20	4.04	11.05	23.09	39.18	43.67	45.12
RaSA	6.48	40.47	43.67	42.91	46.04	47.71	49.31	49.31
AdaLoRA	0.08	4.19	7.24	26.52	39.25	41.62	45.73	44.74
MELoRA	18.14	45.81	45.88	42.45	35.59	26.45	0.00	0.00
DenseLoRA	7.77	38.41	42.61	45.05	45.20	46.19	48.02	46.72
RandLoRA	7.16	29.73	33.99	44.51	48.63	50.30	47.79	44.89
ReLoRA	44.21	44.97	47.03	42.07	30.26	10.44	1.07	0.00
Optimization Process Adjustment Based LoRA Variants								
DoRA	9.07	42.99	42.91	46.34	46.72	46.57	47.18	44.74
RsLoRA	12.73	43.67	42.53	45.66	47.56	47.94	44.13	40.02
LoRA+	28.28	47.64	46.57	46.04	46.19	44.36	37.35	0.00
DeLoRA	4.88	7.01	10.21	23.02	37.65	44.21	45.50	44.59
Initialization Adjustment Based LoRA Variants								
EVA	15.55	39.63	46.42	46.49	45.43	45.20	45.96	44.89
PiSSA	7.01	28.51	26.14	45.20	45.66	47.41	41.54	35.37
LoRA-GA	37.04	44.59	44.28	45.96	46.65	43.75	39.41	30.72
LoRA-One	11.66	42.91	44.28	45.35	43.83	45.43	47.79	46.11
NZLoRA	7.16	24.70	36.74	45.81	46.80	47.64	46.27	39.10
Mixture-of-Experts Integration Based Variants								
GOAT	5.49	42.53	43.83	45.58	46.19	45.05	0.00	0.00
MoSLoRA	5.79	43.06	44.97	46.04	45.27	47.79	46.49	46.80
LoRAMoE	9.91	45.05	43.05	43.45	37.20	0.00	0.00	0.00